PLATFORM MOTION DISTURBANCES DECOUPLING BY MEANS OF INERTIAL SENSORS FOR A MOTION STABILIZED GIMBAL

A THESIS SUBMITTED TO
THE GRADUATE SCHOOL OF NATURAL AND APPLIED SCIENCES
OF
MIDDLE EAST TECHNICAL UNIVERSITY

BY

DENİZ MUTLU

IN PARTIAL FULFILLMENT OF THE REQUIREMENTS
FOR
THE DEGREE OF MASTER OF SCIENCE
IN
MECHANICAL ENGINEERING

DECEMBER 2015

Approval of the thesis:

PLATFORM MOTION DISTURBANCES DECOUPLING BY MEANS OF INERTIAL SENSORS FOR A MOTION STABILIZED GIMBAL

submitted by **DENİZ MUTLU** in partial fulfillment of the requirements for the degree of **Master of Science in Mechanical Engineering Department, Middle East Technical University** by,

Prof. Dr. Gülbin Dural Ünver _____
Dean, Graduate School of **Natural and Applied Sciences**

Prof. Dr. Tuna Balkan _____
Head of Department, **Mechanical Engineering**

Prof. Dr. Tuna Balkan _____
Supervisor, **Mechanical Engineering Dept., METU**

Prof. Dr. Bülent E. Platin _____
Co-Supervisor, **Mechanical Engineering Dept., METU**

Examining Committee Members:

Prof. Dr. Y. Samim Ünlüsoy _____
Mechanical Engineering Dept., METU

Prof. Dr.Tuna Balkan _____
Mechanical Engineering Dept., METU

Assoc. Prof. Dr.Yiğit Yazıcıoğlu _____
Mechanical Engineering Dept., METU

Assoc. Prof. Dr. S. Çağlar Başlamışlı _____
Mechanical Engineering Dept., Hacettepe University

Asst. Prof. Dr. Kıvanç Azgın _____
Mechanical Engineering Dept., METU

Date: **11/12/2015**

I hereby declare that all information in this document has been obtained and presented in accordance with academic rules and ethical conduct. I also declare that, as required by these rules and conduct, I have fully cited and referenced all material and results that are not original to this work.

Name, Last name: Deniz MUTLU

Signature:

ABSTRACT

PLATFORM MOTION DISTURBANCES DECOUPLING BY MEANS OF INERTIAL SENSORS FOR A MOTION STABILIZED GIMBAL

Mutlu, Deniz

M.Sc., Department of Mechanical Engineering

Supervisor: Prof. Dr. Tuna Balkan

Co-Supervisor: Prof. Dr. Bülent E. Platin

December 2015, 119 pages

In this study, a method is developed to overcome platform motion based disturbances resulting from kinematic and dynamic interactions between platform and gimbal system. The method is confined to using underlying non-linear relations in order to increase performance of the system in nearly all of its motion envelope. Sensor requirements and measurements methods are also stated for the developed method. In order to simulate real system conditions, an identification procedure is applied on the system whose outputs are later integrated into system mode. After development of the proposed disturbance rejection algorithm, wide range of simulations are performed to assess its performance with realistic data obtained from an intended base vehicle. Remarkable increases in disturbance rejection in different scenarios are obtained through simulations which indicates promising results for real life application.

Keywords: motion stabilization, target tracking, disturbance decoupling, disturbance rejection

ÖZ

STABİLİZE BİR GİMBAL İÇİN ATALETSEL SENSÖRLER YARDIMI İLE PLATFORM HAREKETİ KAYNAKLI BOZUCU ETKİLERİN GİDERİLMESİ

Mutlu, Deniz

Yüksek Lisans, Makina Mühendisliği Bölümü

Tez Yöneticisi: Prof. Dr. Tuna Balkan

Ortak Tez Yöneticisi: Prof. Dr. Bülent E. Platin

Aralık 2015, 119 sayfa

Bu çalışmada, bir gimbal sistemi üzerinde platform ve kardan sistemi arasındaki kinematik ve dinamik etkileşimler sonucu oluşan bozucu etkilerin giderilmesi için bir yöntem geliştirilmiştir. Geliştirilen yöntemin gimbal sisteminin neredeyse tüm hareket zarfı içerisindeki performansını arttırabilmesi için yöntemin tasarımı doğrusal olmayan bu ilişkilerin direk kullanımı ile sınırlandırılmıştır. Yöntem için gerekli algılayıcı seçimleri ve ölçüm metodları belirtilmiştir. Yöntemin gerçek sistem koşullarına yakın değerlendirmesinin yapılabilmesi için gimbal sistemi üzerinde bir sistem tanımlama süreci sonrası elde edilen veriler ile sistem modeli güncellenmiştir. Bozucu etki giderme algoritmasının geliştirilmesinden sonra performansını değerlendirme amacıyla gerçek hareketli platform verisini kullananılarak benzetim yoluyla geniş kapsamlı denemeler gerçekleştirilmiştir. Farklı senaryolar dahilinde koşturulan benzetimler sonucunda bozucu etki giderimi açısından kayda değer sonuçlar elde edilmiştir, bu durum gerçek uygulama için umut vermektedir.

Anahtar Kelimeler: hareket stabilizasyonu, hedef takibi, bozucu etki dekuplajı, bozucu etki giderimi

To my beloved country

may we find the long lost hope

"...bulacak bir gün elbet
yatağını bu nehir
durulup dinginleşecek
birgün elbet bu nehir
ve çocuklar oynaşacak mutlu çocuklar
anacan sularında bu mutlu nehrin!..."

Hasan Hüseyin Korkmazgil

ACKNOWLEDGMENTS

First of all, I would like to express my deepest gratitude to my supervisor Prof. Dr. Tuna Balkan and my co-supervisor Prof. Dr. Bülent E. Platin, for their guidance, encouragements, and above all their everlasting hope on me.

I would like to thank to my colleagues Mr. Furkan Lüleci, Mr. Gökhan Özyurt and Mr. Hayrettin Ulaş Akova. Our discussions on the topic greatly helped this study.

I would like to express my appreciations to my manager Mr. Burak Gürcan and my design team leader Mr. Eray Özçelik at ASELSAN Inc. for their endless support.

I would also like to thank to ASELSAN Inc. for its support on my graduate education.

Finally, I would like to express my sincerest thanks to my dear friend Mr. Erman Çağan Özdemir, and love of my life Berrin, who were my closest allies against any kind of trouble I faced in the duration of this study.

TABLE OF CONTENTS

LIST OF TABLES

LIST OF FIGURES

LIST OF SYMBOLS AND ABBREVIATIONS

SYMBOLS

$\overline{R}$	:	Rotational Transformation
$\vec{\omega}$	:	Angular Velocity Vector
$\vec{\alpha}$	:	Angular Acceleration Vector
$\vec{a}$	:	Linear Acceleration Vector
$\vec{r}$	:	Position Vector in Cartesian Coordinates
x	:	Unit Vector
$\vec{v}_B^{(A)}$	:	Vector v' related to body/frame B, resolved in frame A
$\overline{J}$	:	Inertia Tensor
$\overline{W}$	:	Angular Velocity Tensor

ABBREVIATIONS

LOS	:	Line of Sight
TRA	:	Outer Traverse Axis of Gimbal
ELV	:	Inner Elevation Axis of Gimbal
STAB	:	Stabilization
PID	:	Proportional Integral Derivative
FF	:	Feed forward
DC	:	Decoupling Controller

CHAPTER 1

INTRODUCTION

1.1. Motivation

Ever increasing capabilities of airborne assault systems through the years creates a continuous demand of increased performance for air defense systems. In the case of low altitude defense systems where target acquisition and tracking are mostly accomplished by movable sensors, most of the burden is on the shoulders of gimbal assemblies serving the purpose of directing these sensors with utmost precision. Such gimbal assemblies are designed for the purposes of target identification, kill assessment and steering gun systems toward target where top-notch tracking precision is required. An example of a gimbal system designed for the purpose of target identification and kill assessment can be seen in Figure 1-1.

Figure 1-1: 2-An example gimbal system used for aerial target identification and kill assessment (Photo courtesy of ASELSAN Inc.)

Aerial defense systems mounted on mobile platforms also require means to isolate platform motion from the sensor in order to render target acquisition possible and

facilitate target tracking under stochastic platform motion. Such means to stabilize the target sensors from base motion can be achieved by a control system composed of inertial motion sensors attached to target sensors, actuators attached to the gimbal axes and a control algorithm that works as a regulator to keep the outputs of inertial sensors as close to zero as possible so to ensure that the payload is kept motionless in the axes measured by inertial sensors. Gimbal system investigated in this study is also designed to operate on a mobile platform serving the purpose of steering an anti-aircraft gun mounted on the same platform. The gimbal system and conceptual drawing of the aerial defense system can be seen in Figure 1-2 and Figure 1-3 respectively.

Figure 1-2: Target tracking gimbal system investigated in this study (Photo courtesy of ASELSAN Inc.)

Figure 1-3: Low altitude air defense system mounted on a tracked vehicle (Photo courtesy of ASELSAN Inc.)

For the system examined in this study, the choice of inertial sensors are two rate gyroscopes placed orthogonally with each other and target tracking sensor's line of sight (LOS), a vector coincident with sensor's field of view cone's symmetry axis. With this choice of inertial sensors, the regulator control algorithm achieves stabilization by minimizing rotational rates of LOS vector. Thus the orientation of LOS vector is kept constant in three dimensional space so that field of view of tracking sensors are kept over the same point in space regardless of base motion. One important point for such a stabilization method is that only the "yaw" and "pitch" rates of the LOS are controlled and there is no control over the "roll" rate of the tracking sensor. The control of roll rate of the sensor under base motion disturbance with outer yaw axis - inner pitch axis of the gimbal assembly is not possible as there is no actuator, so algorithms implemented in tracking sensor are constructed accordingly to be immune to rotation of target's projection in sensing element.

After successful rate stabilization is achieved, target tracking is performed by using outputs of tracking sensors as commands to the controller so that the same controller

works both as a regulator and a servo controller. A schematics for a motion stabilized target tracking gimbal system can be found in Figure 1-4.

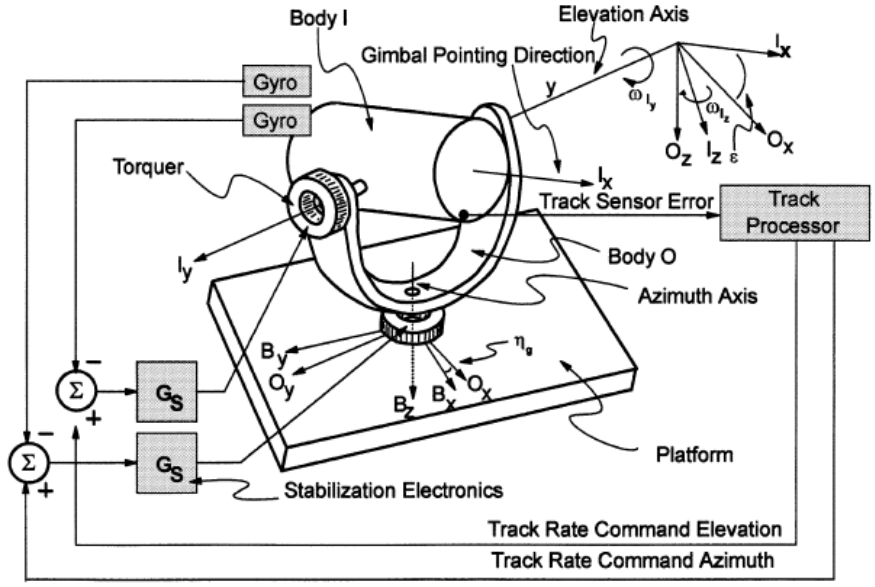

Figure 1-4: Schematics of a motion stabilized target tracking gimbal [1]

1.2. State of The Art

Target tracking systems used in mobile defense systems are destined to endure many different disturbances acting on them in their harsh operating environments. These disturbances have a very wide range of causes ranging from gimbal systems own construction deficits to forces of nature. A nearly complete chart of disturbance sources can be found in Figure 1-5.

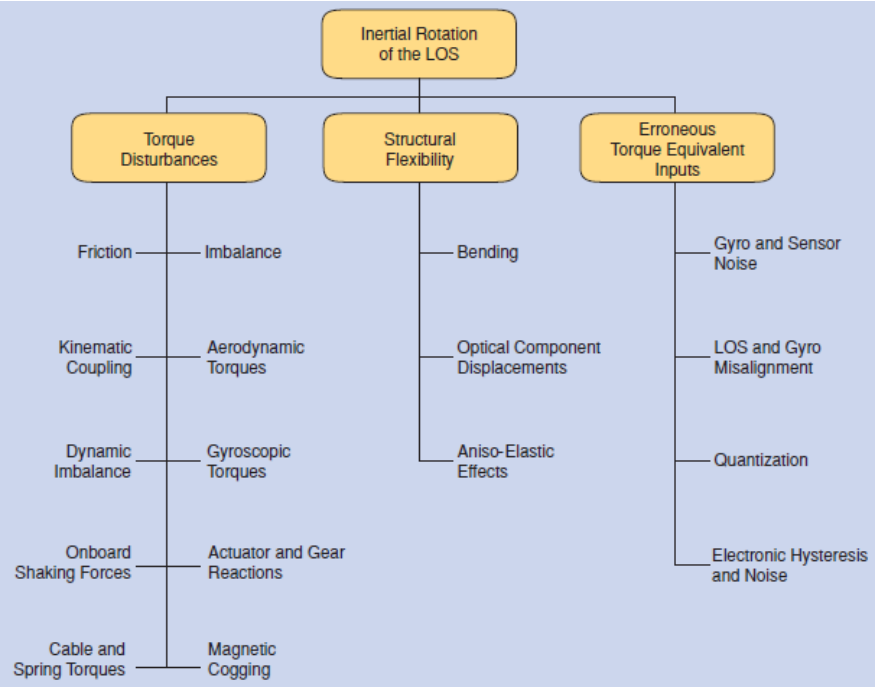

Figure 1-5: Sources of disturbances for LOS stabilization [2]

Platform motion manifests itself in LOS stabilization through different sources; namely onboard shaking forces, friction, kinematic coupling, gyroscopic torques, imbalance and dynamic imbalance [2]. The scope of this study is limited in understanding and overcoming kinematic coupling, gyroscopic torques and dynamic imbalance which occur due to interactions between gimbal and platform kinematics, and resultant dynamic effects. So in this study, the phrase "platform motion disturbances" is used to refer this segment of wide range disturbances resulting from platform motion. Also, disturbances resulting from dynamic imbalance and gyroscopic torques are referred as a "geometric coupling" in total, a term used in one of the very first publications on the topic [3].

A variety of studies on kinematic and geometric coupling effects can be found in the literature. Starting with a previously mentioned early publication in the field [3], the effects of kinematic and geometric coupling for a outer yaw inner pitch gimbal assembly are defined in terms of kinematic and dynamic variables of platform and gimbal without providing each explicit relation, and represented in the form of a block diagram, which can be found in Figure 1-6. The main drawback of the proposed method is using simplifying assumption of purely diagonal inertia tensors for both gimbal bodies. In addition, torque relations and coupling terms for a half-

angle mirror assembly are explicitly given. The most critical hypothesis of this reference is that the defined kinematic and geometric coupling effects must be considered while determining whole design requirements in order to have a successful implementation. A similar study including off-diagonal inertia terms in the definitions of coupling effects can be found in [4].

A comprehensive survey on the topic of kinematic relationships between base platform and gimbal assembly can be found in [5]. This publication combines kinematics of all possible two axis gimbal arrangements which paves the path for studies regarding two axis motion stabilized gimbals.

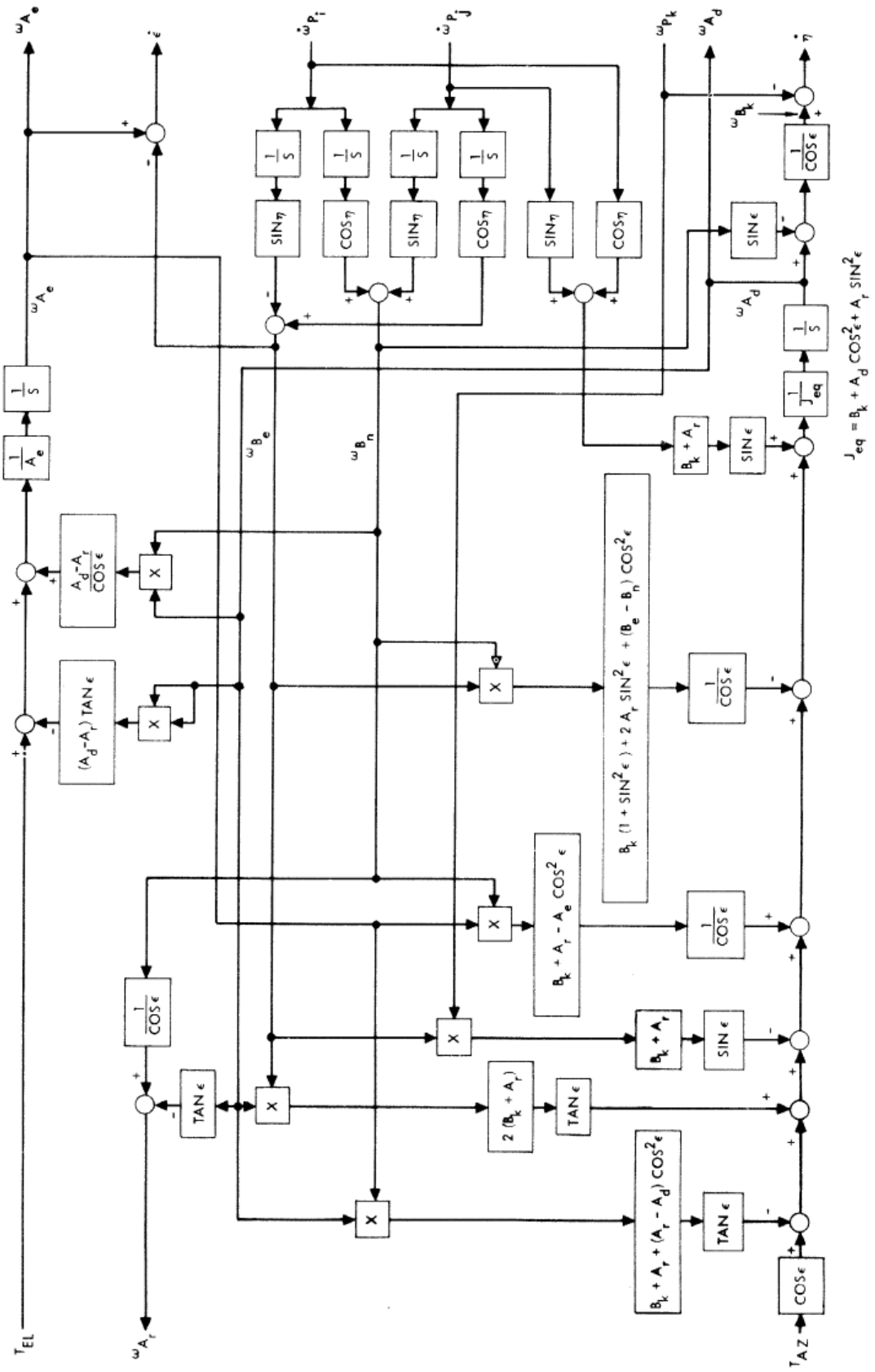

Figure 1-6: Torque relations for an outer yaw inner pitch gimbal [3]

In another investigation about comparison of different placements for LOS inertial sensors, geometric coupling effect is identified as increased torque requirements resulting from gimbal axes interactions and the authors managed to decouple part of it related to angular velocity interactions without using angular acceleration relations [1].

In one previously mentioned study, the description of kinematic coupling is provided as manifestation of gimbal lock phenomena, which consequently increases torque requirements as the gimbal assembly approaches gimbal lock condition, and provides a simplified mathematical representation with only roll motion of the platform [2].

To cope with disturbances acting on a system, one can choose to completely rely on disturbance rejection capabilities of conventional feedback control methods. But the nature of conventional feedback control methods being "inherently reactive" [6], they require error build-up to take action limiting their disturbance rejection performance. In order to increase disturbance rejection capabilities of conventional feedback controllers, one can alter parameters or whole structure of the controller but with the expense of considerable changes in command tracking characteristics. An improved linear feedback controller can be found in [7], which proposes a PI^2 controller to increase command tracking and disturbance rejection. Although not stated in the referenced publication, obtaining a stable closed loop system may be problematic in different system characteristics due to increase in type number of the overall system. An illustration of torque disturbance rejection characteristics applied for a motion stabilized gimbal with conventional P, PI and PID controllers can be found in Figure 1-7. In order to increase disturbance rejection performance, additional means of control are required to aid or replace conventional controllers without tampering command tracking performance.

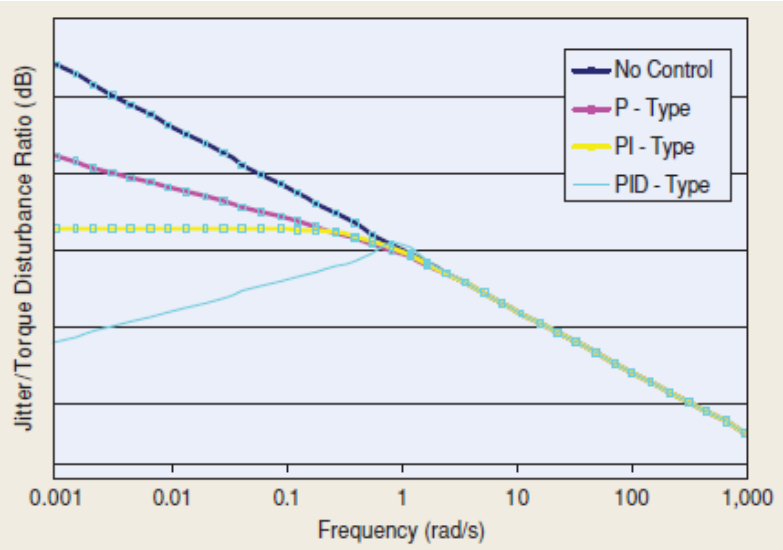

Figure 1-7: Torque disturbance rejection characteristics of conventional controllers [8]

To increase disturbance rejection characteristics of motion stabilized gimbal systems, a considerable number of methods exist in literature. In the scope of this study, presentation of them is limited to generic methods not specifically designed to counteract coupling effects but stated to have corrective effect on them, and methods especially designed to suppress these effects.

A simple example to the generic methods is to use single state disturbance observers for both axes which produce additional torque values as system response drifts from output of a pure inertia due to acting disturbances [9].

Another observer based method utilizes an extended state observer and non-linear state feedback in order to increase disturbance rejection characteristics which is also demonstrated to outperform classical PID method [10].

Studies of adaptive control methods applied to LOS stabilization and their effects on disturbance rejection can be found in [11] and [12]. In the context of adaptive and optimal control methods, a study stands out, which utilizes linearized equations of motion obtained through Euler-Lagrange formulations to construct a linear quadratic regulator used with fuzzy gain scheduling [13]. The objective of the referenced study is to increase disturbance rejection performance against a wide range of disturbances like mechanical resonance and change of electric parameters, and up to

certain extent of immunity is provided from coupling effects by utilization of non-linear equations of motion. Before mentioning control methods specifically designed to overcome coupling effects, mechanical design improvements to moderately lower these effects should be mentioned. One design method is to use increased number of axes rather than two which is theoretically adequate to obtain any required LOS orientation in space. Unfortunately, increasing number of axes comes with the price of additional size and weight with increased effects of structural flexibility [2]. One example of such configuration can be seen in Figure 1-8, which is a naval target tracking system using four separate motion axes.

Figure 1-8: SASS InfraRed search and track system by Selex ES Ltd. [14]

Another gimbal design method is to tilt the base mount accordingly to align gimbal system to experience minimal coupling effect which even allows operation at zenith point. However, this method is only viable if gimbal system is not required to have a full horizontal coverage. An example of this construction can be seen in Figure 1-9 which is a naval close in weapon system designed to protect ships from incoming missiles.

Figure 1-9: Sea Zenith CIWS by Oerlikon Contraves Defence [15]

An estranged design method proposed in [16] is to add an additional inner "deroll" axis to outer yaw inner pitch configuration. This obliquely placed axis with very limited motion envelope is originally proposed to correct image roll without handicaps of using increased number of axes due to its compactness, it is stated that this configuration can also be utilized to overcome coupling effects. A schematic of the gimbal system with "deroll" axis can be seen in Figure 1-10.

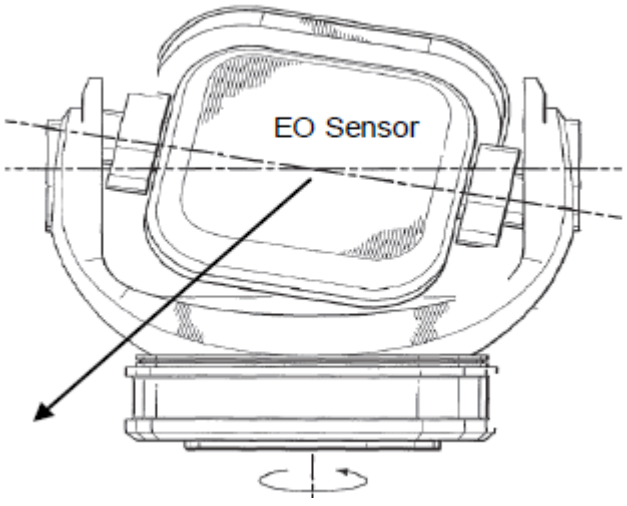

Figure 1-10: Two axis gimbal system with additional "deroll" axis [16]

Control methods addressing kinematic and geometric coupling effects focus on two fundamental methods. First one is based on developing a direct method to decouple the effects using governing equations which is also the adopted method in this study;

the other fundamental method is the inverse system method which is based on feedback linearization.

A study utilizing direct approach can be found in [17], where coupling effects on a half angle mirror system are tried to be suppressed via base motion measurements. The lacking aspect of this study is missing decoupling action for kinematic coupling which is due to only measurements available for the platform motion being angular velocity components.

A different direct approach proposal can be found in [18], where coupling effects on a inner yaw(only to correct imaging sensor roll, no effect on LOS direction), middle pitch, outer roll gimbal assembly are minimized using a three axis base angular velocity sensor. Even though geometric coupling effects are defined with simplifying assumption of diagonal inertia tensors and kinematic coupling is not considered, successful results are obtained due to tests being performed at orientations where kinematic coupling is minimal. The potential pitfall in the given study is that the forward kinematic relations are utilized requiring use of axis relative velocity values obtained as derivatives of axis encoder measurements which may be problematic for some applications.

Studies regarding inverse system method [19] and [20] employed this approach as an additional error based feedback method aiding existing PID controllers with one exception of [21] where a sliding mode control method is also added. The result of these studies are only presented at the working points where linearizations of system dynamics are performed producing difficulty in evaluating outcomes.

1.3. Aim of The Study

The aim of this study is to develop a direct control method to suppress platform motion coupling effects for a two axis gimbal system in order to enhance stabilization and target tracking performance. In addition, developed method is limited to only enhance disturbance rejection capability of the system and not to alter command tracking characteristics beyond what is obtainable when platform motion is not present. The control method is required to rapidly generate additional motor torques to overcome coupling effects before they induce considerable amounts of errors in system outputs. This requirement restricts the construction of

control method to be composed of direct calculations rather than error based methods to obtain required additional control outputs. For this purpose, kinematic and dynamic relations for the gimbal system are examined to completely identify non-linear nature of coupling effects.

1.4. Outline of The Study

In Chapter 2, complete kinematic relations of a two axis gimbal mounted on a moving platform are presented with different cases of stabilization and target tracking, and kinematic coupling effect is defined in terms of kinematic quantities. Additional sensor requirements for the developed method are also presented in this chapter.

In Chapter 3, internal dynamics in the form of Newton-Euler equations of a two axis gimbal system is presented with definition of geometric coupling disturbances, also a system identification procedure to match original system and developed system model is included.

In Chapter 4, details of feedback controllers for command tracking and developed controller to overcome coupling effects are presented.

In Chapter 5, the simulation results are presented to exhibit the performance of developed control method in different scenarios.

In Chapter 6, the study is finalized with summary and conclusion.

CHAPTER 2

Kinematics of Motion Stabilized 2-Axis Target Tracking Gimbal

2.1. Introduction

Understanding kinematic relations of a 2-axis gimbal assembly with outer yaw gimbal and inner pitch gimbal is the first fundamental step in understanding the overall dynamics of gimbal system. At a first glance, one may underestimate the kinematic relations for a 2-axis gimbal since it is only composed of two rotational axes placed orthogonally. But with addition of base motion and constraints imposed on the system by LOS stabilization, kinematic equations become coupled and must be solved accordingly in order to later utilize them in a controller architecture aimed to overcome kinematic and dynamic disturbances due to 2-axis interconnected motion. In this chapter, kinematic relations with LOS rate stabilization constraint and target tracking commands, kinematic coupling of base motion to outer yaw gimbal are presented including their MATLAB Simulink realizations for simulation purposes. In addition, verification of findings are cross-checked with two different MATLAB SimMechanics models which incorporate LOS rate stabilization and target tracking to a kinematic gimbal model by means of additional kinematic joints.

2.2. Kinematic Equations

In following sections, kinematic relations are presented in a manner of starting from the base motion and moving towards the payload motion so that effects of base motion on each element of gimbal assembly can be represented clearly. Later on, rate stabilization is imposed on equations as a kinematic constraint as zero angular rates at two orthogonal axes of sensor coordinate system.

2.2.1. Kinematic Definitions

The kinematic equations involve three distinct bodies; namely Hull (base body representing moving platform), Traverse Axis (outer yaw gimbal body) and Elevation Axis (inner pitch gimbal body). In Figure 2-1 coordinate axes related to different bodies are shown with orientation of individual axes. The positive directions for axis angles (θ: Traverse Axis Angle, ψ elevation axis angle) are also incorporated into the figure.

The orientations of coordinate axes are selected so as to match with the axis selection of the reference target tracking system.

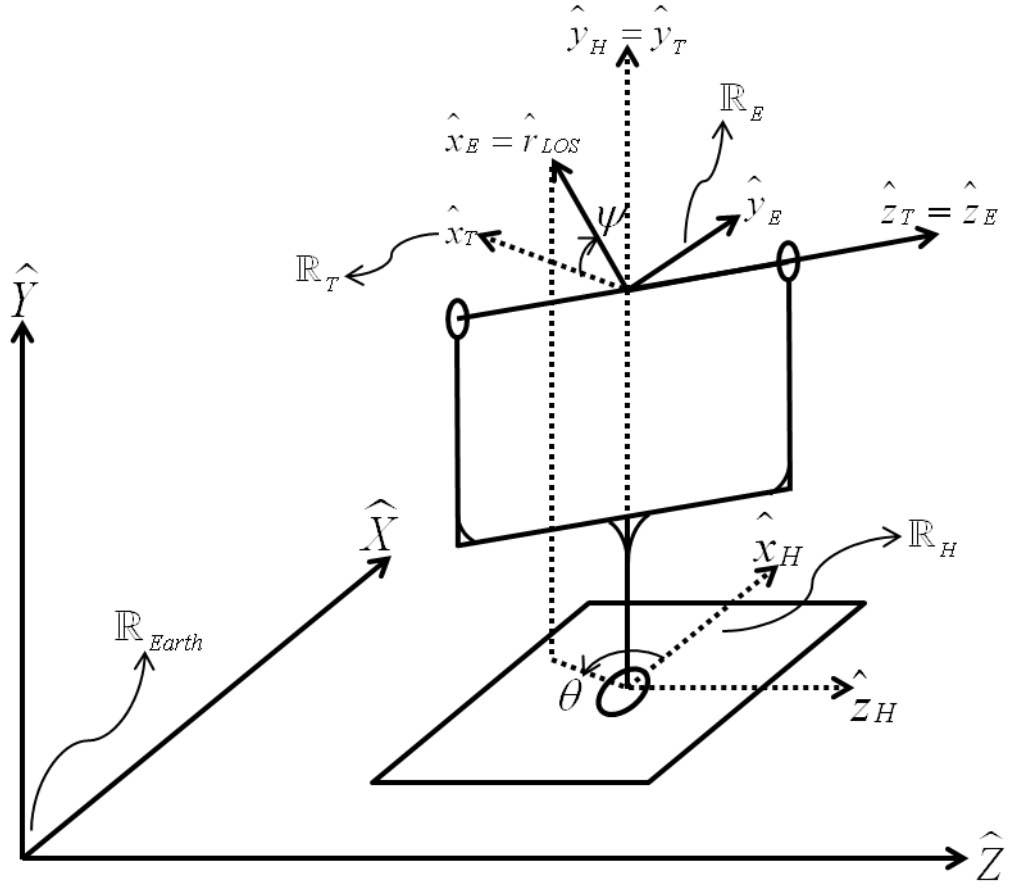

Figure 2-1: 2-axis gimbal system coordinate axes

Angular orientation of each individual body with respect to Earth coordinate frame are represented as three distinct Euler transformation matrices: $\overline{R_H}$, $\overline{R_T}$ and $\overline{R_E}$.

Where $\overline{R_E}$ designates the tracking sensor group's orientation as well, and x axis of $\overline{R_E}$ is also coincident with LOS vector $\hat{r}_{LOS}$.

Angular velocity and acceleration variables for the traverse and elevation bodies are expressed in their respective body coordinates in order to use them directly in kinetic equations, i.e. Euler torque equations. The same quantities for hull body is expressed in its body coordinates as well since the constructed control architecture utilizes strapdown sensors attached to hull body to overcome torque disturbances. More detail on these topics is presented in related chapters.

Angular kinematic quantities for all three bodies can be listed as:

- Hull: Base platform representing the tracked vehicle

  $\overline{R}_H$: 3x3 Euler transformation matrix representing Hull orientation w.r.t. Earth

  $\vec{\omega}_H^{(H)}$: Angular velocity of Hull body resolved in Hull frame

  $\vec{\alpha}_H^{(H)}$: Angular acceleration of Hull body resolved in Hull frame
- Traverse: Traverse body representing the outer yaw gimbal frame

  $\overline{R}_T$: 3x3 Euler transformation matrix representing Traverse orientation w.r.t. Earth

  $\vec{\omega}_T^{(T)}$: Angular velocity of Traverse body resolved in Traverse frame

  $\vec{\alpha}_T^{(T)}$: Angular acceleration of Traverse body resolved in Traverse frame
- Elevation: Elevation body representing the inner pitch gimbal / tracking sensor frame

  $\overline{R}_E$: 3x3 Euler transformation matrix representing Elevation orientation w.r.t. Earth

  $\vec{\omega}_E^{(E)}$: Angular velocity of Elevation body resolved in Elevation frame

  $\vec{\alpha}_T^{(T)}$: Angular acceleration of Elevation body resolved in Elevation frame.

Angular kinematic quantities for rotation axes can be listed as:

- Traverse Axis:

  θ : Traverse axis relative angle

  $\dot{\theta}$: Traverse axis relative angular velocity

  $\ddot{\theta}$: Traverse axis relative angular acceleration

- Elevation Axis:

  ψ : Elevation axis relative angle

  $\dot{\psi}$: Elevation axis relative angular velocity

  $\ddot{\psi}$: Elevation axis relative angular acceleration

Linear kinematic variables and relations between them are taken out of the scope of this study since linear motion of the base does not inflict a disturbance torque on the gimbal axes for the specific system chosen for this study. The reasoning behind this is explained in the chapter for dynamics of the gimbal assembly.

2.2.2. Angular Orientation, Velocity and Acceleration Kinematic Relations

In this section, relations between angular quantities are represented as matrix equations starting with a known base angular motion state, representing states of the other two bodies accordingly and imposing constraints of rate stabilization and target tracking on these states.

At this step, base angular orientation, velocity and acceleration quantities are assumed to be known, how these quantities are calculated or measured is presented in the chapter involving platform motion.

Since rate stabilization and target tracking impose constraints on the system through orientation, velocity and acceleration of LOS vector, these states are also taken to be known.

2.2.2.1. Angular Orientation Relations

With base angular orientation $\overline{R}_H$ known, traverse and elevation angular orientations can be found with the help of axis relative positions θ and ψ.

Since the traverse frame is equal to base frame rotated in $y_H = y_T$ axis by θ amount, orientation of traverse frame can be written as a body fixed rotation:

$$\overline{R}_T = \overline{R}_\theta \overline{R}_H \tag{2.1}$$

Where $\overline{R}_\theta$ is a 3x3 Euler transformation matrix in the form:

$$\overline{R}_\theta = \begin{bmatrix} \cos\theta & 0 & -\sin\theta \\ 0 & 1 & 0 \\ \sin\theta & 0 & \cos\theta \end{bmatrix} \tag{2.2}$$

And the elevation frame is equal to traverse frame rotated in $\hat{z}_T = \hat{z}_E$ axis by ψ amount, orientation of elevation frame can be written as a body fixed rotation:

$$\overline{R}_E = \overline{R}_\psi \overline{R}_T \tag{2.3}$$

Where $\overline{R}_\psi$ is a 3x3 Euler transformation matrix in the form:

$$\overline{R}_\psi = \begin{bmatrix} \cos\psi & \sin\psi & 0 \\ -\sin\psi & \cos\psi & 0 \\ 0 & 0 & 1 \end{bmatrix} \tag{2.4}$$

Combining these two equations, the elevation frame's angular orientation with respect to Earth frame can be stated as:

$$\overline{R}_E = \overline{R}_\psi \overline{R}_T = \overline{R}_\psi \overline{R}_\theta \overline{R}_H \tag{2.5}$$

In expanded form:

$$\overline{R}_E = \begin{bmatrix} \cos\theta & \sin\psi & -\sin\theta\cos\psi \\ -\cos\theta\sin\psi & \cos\psi & \sin\theta\sin\psi \\ \sin\theta & 0 & \cos\theta \end{bmatrix} \overline{R}_H \tag{2.6}$$

The LOS vector in Earth frame resolution can also be expressed in terms of axis angles and hull orientation utilizing equation (2.5):

$$\hat{r}_{LOS}^{(E)} = \overline{R}_E \hat{r}_{LOS}^{(Earth)} \tag{2.7}$$

$$\hat{r}_{LOS}^{(E)} = \begin{bmatrix} \cos\theta & \sin\psi & -\sin\theta\cos\psi \\ -\cos\theta\sin\psi & \cos\psi & \sin\theta\sin\psi \\ \sin\theta & 0 & \cos\theta \end{bmatrix} \overline{R}_H \hat{r}_{LOS}^{(Earth)} \tag{2.8}$$

LOS vector is coincident with x_E, so its resolution in Elevation frame can be utilized in the same equation as:

$$\hat{r}_{LOS}^{(E)} = \begin{bmatrix} 1 \\ 0 \\ 0 \end{bmatrix} = \begin{bmatrix} \cos\theta & \sin\psi & -\sin\theta\cos\psi \\ -\cos\theta\sin\psi & \cos\psi & \sin\theta\sin\psi \\ \sin\theta & 0 & \cos\theta \end{bmatrix} \overline{R}_H \hat{r}_{LOS}^{(Earth)} \tag{2.9}$$

And one can arrange this equation easily using orthonormality principle of Euler transformation matrices as:

$$\overline{R}_H \hat{r}_{LOS}^{(Earth)} = \begin{bmatrix} \cos\theta & \sin\psi & -\sin\theta\cos\psi \\ -\cos\theta\sin\psi & \cos\psi & \sin\theta\sin\psi \\ \sin\theta & 0 & \cos\theta \end{bmatrix}^T \begin{bmatrix} 1 \\ 0 \\ 0 \end{bmatrix}$$
$$= \begin{bmatrix} \cos\theta & -\cos\theta\sin\psi & \sin\theta \\ \sin\psi & \cos\psi & 0 \\ -\sin\theta\cos\psi & \sin\theta\sin\psi & \cos\theta \end{bmatrix} \begin{bmatrix} 1 \\ 0 \\ 0 \end{bmatrix} \tag{2.10}$$

If hull orientation and LOS vector in resolved in Earth frame are known quantities, one can represent left hand side of this equation as a known unit vector and find an expression for traverse and elevation axis angles as:

$$\overline{R}_H \hat{r}_{LOS}^{(Earth)} = \begin{bmatrix} x_{LOS} \\ y_{LOS} \\ z_{LOS} \end{bmatrix} = \begin{bmatrix} \cos\theta\cos\psi \\ \sin\psi \\ -\sin\theta\cos\psi \end{bmatrix} \tag{2.11}$$

Which can be solved for θ and ψ uniquely considering theoretical limits for these angles as; $-\pi < \theta < \pi, -\pi/2 < \psi < \pi/2$. (Solutions outside these limits have identical counterparts inside the limits, so they are excluded.)

The solution for gimbal angles;

$$\theta = \arctan 2\left(\frac{-z_{LOS}}{\sqrt{1-y_{LOS}^2}}, \frac{x_{LOS}}{\sqrt{1-y_{LOS}^2}} \right),\ \psi = \arctan 2\left(y_{LOS}, \sqrt{1-y_{LOS}^2} \right) \tag{2.12}$$

which has four trivial solutions for unit vectors in $\pm x$ and $\pm z$ directions on each axis, also asymptotical solutions exist for $\psi = \pm\pi/2$ which represent gimbal lock condition.

The found solutions for gimbal angles are constructed as MATLAB Simulink blocks for further use in simulations and control algorithm. These can be seen in Figure 2-2, Figure 2-3 and Figure 2-4.

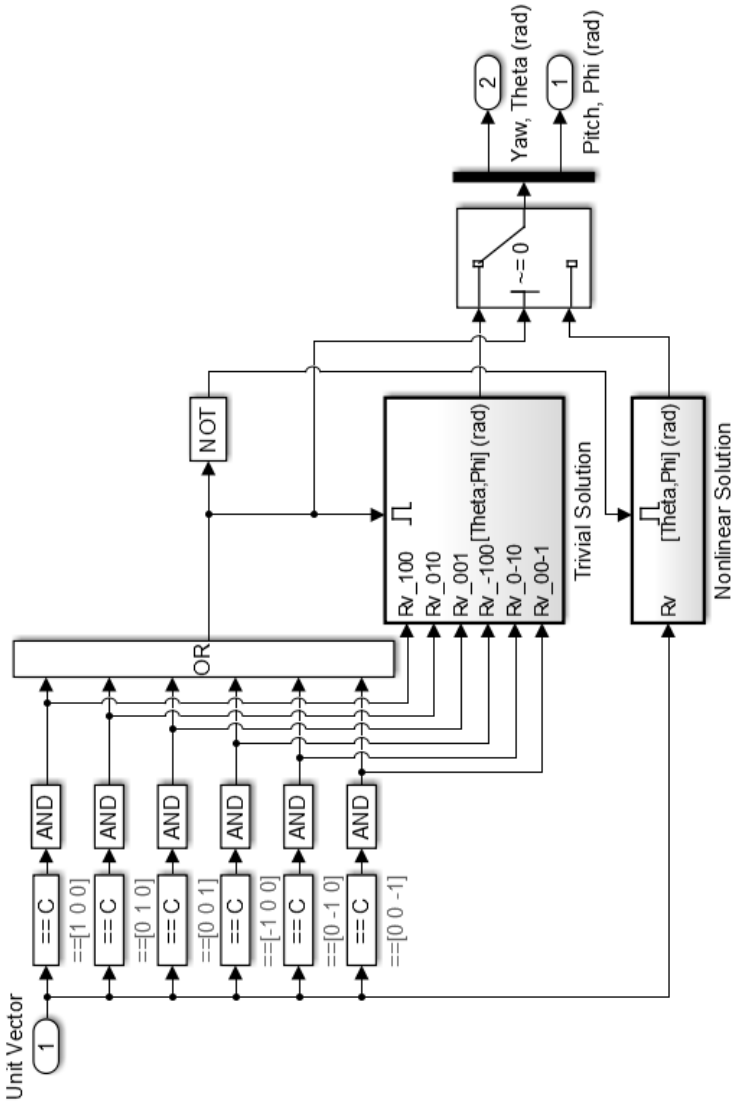

Figure 2-2: Gimbal angles inverse solution model in Simulink

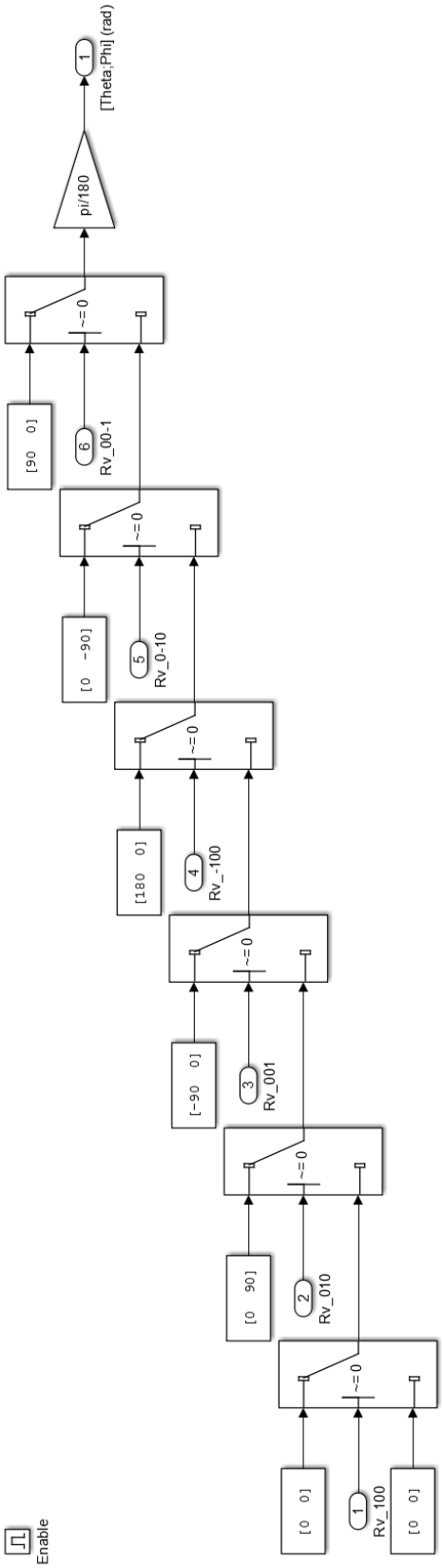

Figure 2-3: Gimbal angles inverse solution, trivial solution subsystem

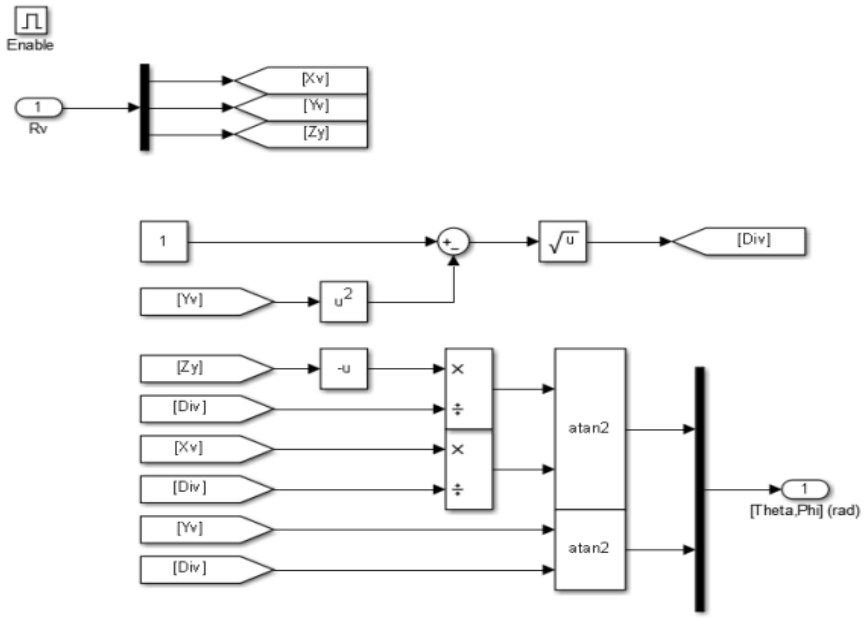

Figure 2-4: Gimbal axis angles inverse solution, nonlinear solution subsystem

2.2.2.2. Angular Velocity Relations

To implement dynamic equations and compute required gimbal axis torque values to stabilize the LOS vector or aid target tracking, respective body angular velocity and acceleration components must be computed beforehand. Angular velocity components in terms can be computed through a set of calculations performed on findings of equation pairs (2.5) and (2.12), but this approach involves derivate operations at certain stages. Using outcomes of a discrete derivative process would inject large amounts of noise into the control system, so one must avoid such a method. One another way to obtain angular velocity components is to measure hull body angular velocity by a rate gyroscope triad and utilize findings of equation pairs (2.5) and (2.12) in axis transformations.

Using the mentioned method, angular velocity relations can easily be derived by simple vector summation as long as all velocity components are in the same resolution frame. The traverse and elevation frame angular velocities can be derived as:

$$\begin{aligned}\vec{\omega}_T^{(H)} &= \vec{\omega}_H^{(H)} + \dot{\theta} y_H \\ \vec{\omega}_E^{(T)} &= \vec{\omega}_T^{(T)} + \dot{\psi} \hat{z}_T\end{aligned} \tag{2.13}$$

At the beginning of this chapter, it is mentioned that angular velocity and acceleration quantities should be calculated in their corresponding body frames to easily incorporate them into dynamic equations, so these angular velocity components must also be transformed into their corresponding body frames which can be achieved by utilizing each individual axis' transformation matrices as:

$$\begin{aligned}\vec{\omega}_T^{(T)} &= \overline{R}_\theta \vec{\omega}_T^{(H)} = \overline{R}_\theta \left(\vec{\omega}_H^{(H)} + \dot{\theta} y_H^{(H)} \right) \\ \vec{\omega}_E^{(E)} &= \overline{R}_\psi \vec{\omega}_E^{(T)} = \overline{R}_\psi \left(\vec{\omega}_T^{(T)} + \dot{\psi} \hat{z}_H^{(H)} \right)\end{aligned} \tag{2.14}$$

In expanded form, these equations can be written as:

$$\begin{aligned}\vec{\omega}_T^{(T)} &= \begin{bmatrix} \cos\theta & 0 & -\sin\theta \\ 0 & 1 & 0 \\ \sin\theta & 0 & \cos\theta \end{bmatrix} \left(\vec{\omega}_H^{(H)} + \begin{bmatrix} 0 \\ \dot{\theta} \\ 0 \end{bmatrix} \right) \\ \vec{\omega}_E^{(E)} &= \begin{bmatrix} \cos\psi & \sin\psi & 0 \\ -\sin\psi & \cos\psi & 0 \\ 0 & 0 & 1 \end{bmatrix} \left(\vec{\omega}_T^{(T)} + \begin{bmatrix} 0 \\ 0 \\ \dot{\psi} \end{bmatrix} \right)\end{aligned} \tag{2.15}$$

To obtain the elevation frame angular velocity in terms of base angular velocity components and gimbal angles; these two equations is combined into one, also hull body velocity vectors resolved in their body frames are represented as its Cartesian components.

$$\vec{\omega}_H^{(H)} = \begin{bmatrix} \omega_{Hx} \\ \omega_{Hy} \\ \omega_{Hz} \end{bmatrix}, \ \vec{\omega}_T^{(T)} = \begin{bmatrix} \omega_{Tx} \\ \omega_{Ty} \\ \omega_{Tz} \end{bmatrix} \text{ and } \vec{\omega}_E^{(E)} = \begin{bmatrix} \omega_{Ex} \\ \omega_{Ey} \\ \omega_{Ez} \end{bmatrix} \tag{2.16}$$

$$\begin{bmatrix} \omega_{Ex} \\ \omega_{Ey} \\ \omega_{Ez} \end{bmatrix} = \begin{bmatrix} \cos\psi & \sin\psi & 0 \\ -\sin\psi & \cos\psi & 0 \\ 0 & 0 & 1 \end{bmatrix} \left(\begin{bmatrix} \cos\theta & 0 & -\sin\theta \\ 0 & 1 & 0 \\ \sin\theta & 0 & \cos\theta \end{bmatrix} \begin{bmatrix} \omega_{Hx} \\ \omega_{Hy} + \dot{\theta} \\ \omega_{Hz} \end{bmatrix} + \begin{bmatrix} 0 \\ 0 \\ \dot{\psi} \end{bmatrix} \right) \tag{2.17}$$

In expanded form;

$$\begin{bmatrix} \omega_{Ex} \\ \omega_{Ey} \\ \omega_{Ez} \end{bmatrix} = \begin{bmatrix} \omega_{Hx}\cos\psi\cos\theta - \omega_{Hz}\cos\psi\sin\theta + \omega_{Hy}\sin\psi + \dot{\theta}\sin\psi \\ -\omega_{Hx}\sin\psi\cos\theta + \omega_{Hz}\sin\psi\sin\theta + \omega_{Hy}\cos\psi + \dot{\theta}\cos\psi \\ \omega_{Hx}\sin\theta + \omega_{Hz}\cos\theta + \dot{\psi} \end{bmatrix} \tag{2.18}$$

Elevation frame represents LOS frame, so one can also write:

$$\begin{aligned} \vec{\omega}_E^{(E)} &= \begin{bmatrix} \omega_{Ex} \\ \omega_{Ey} \\ \omega_{Ez} \end{bmatrix} = \vec{\omega}_{LOS}^{(LOS)} = \begin{bmatrix} \omega_{LOSx} \\ \omega_{LOSy} \\ \omega_{LOSz} \end{bmatrix} \\ &= \begin{bmatrix} \omega_{Hx}\cos\psi\cos\theta - \omega_{Hz}\cos\psi\sin\theta + \omega_{Hy}\sin\psi + \dot{\theta}\sin\psi \\ -\omega_{Hx}\sin\psi\cos\theta + \omega_{Hz}\sin\psi\sin\theta + \omega_{Hy}\cos\psi + \dot{\theta}\cos\psi \\ \omega_{Hx}\sin\theta + \omega_{Hz}\cos\theta + \dot{\psi} \end{bmatrix} \end{aligned} \tag{2.19}$$

It is also stated that rate stabilization is performed by minimizing yaw and pitch rates of LOS frame when base motion is present and target tracking is achieved by obtaining certain levels of angular rates for these same axes by means of rotational actuators. This fact gives considerable amount of importance to second and third rows of the given equation since they represent quantities that are to be controlled to achieve stabilization and target tracking. The first row has no specific importance than being an expression of roll rate of LOS frame which is not controlled.

$$\begin{aligned} \omega_{LOSy} &= \omega_{LOSyaw} = -\omega_{Hx}\sin\psi\cos\theta + \omega_{Hz}\sin\psi\sin\theta + \omega_{Hy}\cos\psi + \dot{\theta}\cos\psi \\ \omega_{LOSz} &= \omega_{LOSpitch} = \omega_{Hx}\sin\theta + \omega_{Hz}\cos\theta + \dot{\psi} \end{aligned} \tag{2.20}$$

These two equations can be solved for axis angular rates as:

$$\begin{aligned} \dot{\theta} &= \frac{\omega_{LOSyaw} + \omega_{Hx}\sin\psi\cos\theta - \omega_{Hy}\cos\psi - \omega_{Hz}\sin\psi\sin\theta}{\cos\psi} \\ \dot{\psi} &= \omega_{LOSpitch} - \omega_{Hx}\sin\theta - \omega_{Hz}\cos\theta \end{aligned} \tag{2.21}$$

For rate stabilization, LOS frame angular rates should be taken as: $\omega_{LOSyaw} = \omega_{LOSpitch} = 0$

For target tracking, LOS frame angular rates should be taken as required by target and base motions; which is thoroughly discussed in the section for target motion kinematic resolution.

At the final stage of angular velocity calculations, obtaining traverse and elevation frames body angular rates is as simple as to input findings of equation pair (2.21) and (2.12) into equation pair (2.15)

Equation pairs (2.21) and (2.15) are constructed as MATLAB Simulink blocks for further use in simulations and control algorithm.

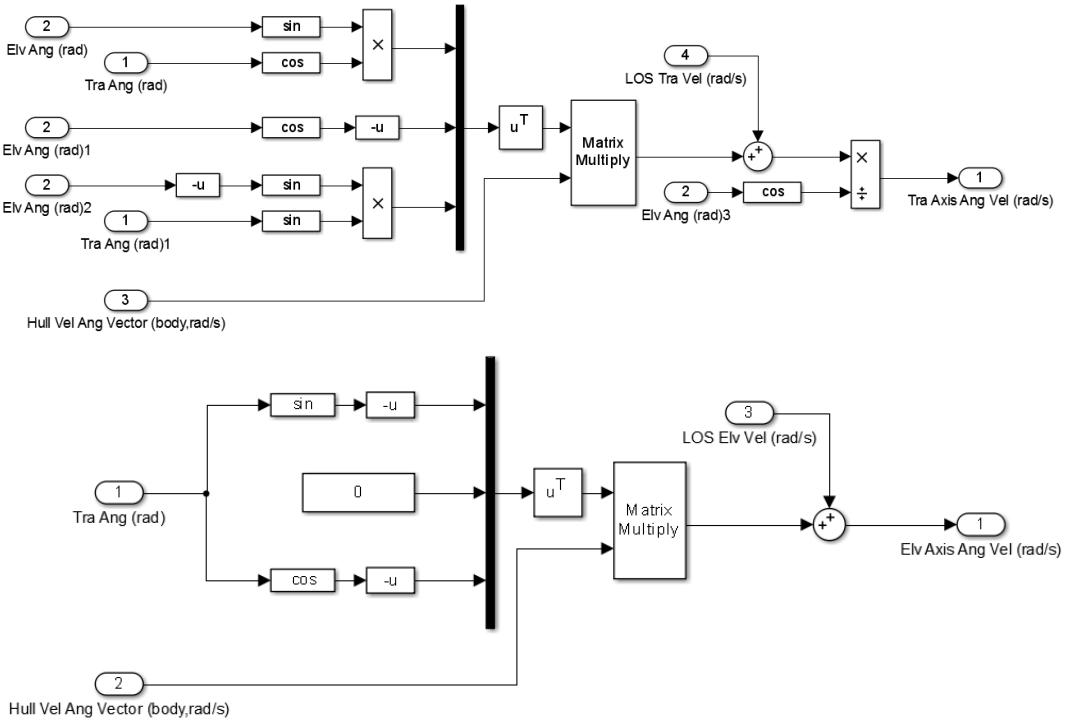

Figure 2-5: Gimbal axis angular velocity solutions model in Simulink

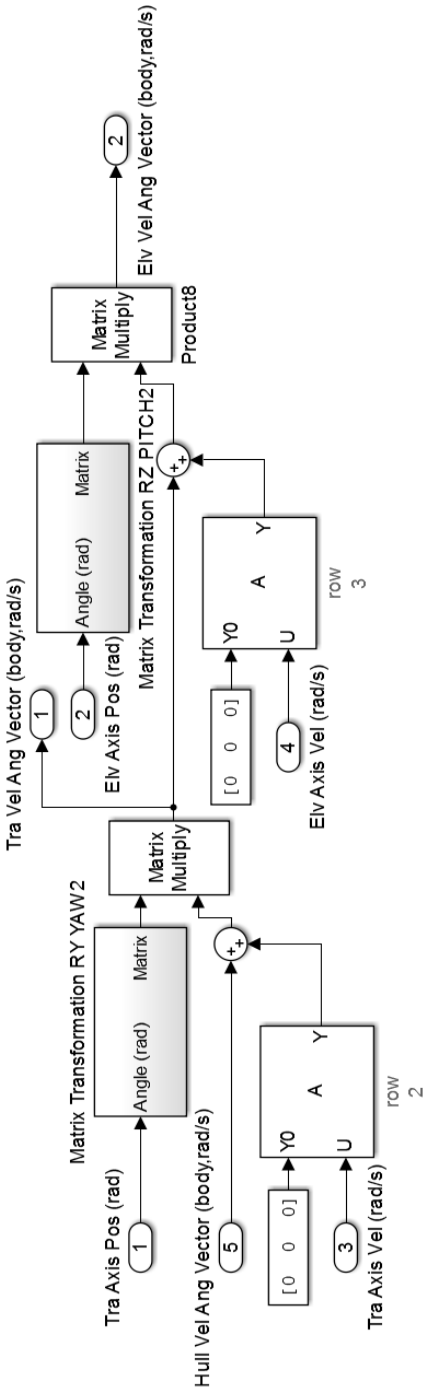

Figure 2-6: Body angular velocity solutions model in Simulink

2.2.2.3. Angular Acceleration Relations

Another requirement than body angular velocity components to utilize dynamic equations is to obtain required body angular acceleration values as stated which can easily be achieved by taking derivative of the findings of equation (2.15), but due to

increased signal noise with a discrete derivation operation would render such an approach unfeasible. So respective body angular acceleration components are chosen to be computed through applying known kinematic quantities to hull body acceleration components which are to be measured via additional sensors; namely group of linear accelerometers placed in a configuration to also give rotational acceleration values; placed on hull body itself.

Angular acceleration relations can be expressed as the following equations written in hull and traverse resolution frames:

$$\begin{aligned} \vec{\alpha}_T^{(H)} &= \vec{\alpha}_H^{(H)} + \ddot{\theta}\, y_H^{(H)} + \dot{\theta}\left(\vec{\omega}_H^{(H)} \times y_H^{(H)}\right) \\ \vec{\alpha}_E^{(T)} &= \vec{\alpha}_T^{(T)} + \ddot{\psi}\, \hat{z}_T^{(T)} + \ddot{\psi}\left(\vec{\omega}_T^{(T)} \times \hat{z}_T^{(T)}\right) \end{aligned} \tag{2.22}$$

At the beginning of this chapter, it is mentioned that angular velocity and acceleration quantities should be calculated in their corresponding body frames to easily incorporate them into dynamic equations, so these angular acceleration components must also be transformed into their corresponding body frames which can be achieved by utilizing each individual axis' transformation matrices as:

$$\begin{aligned} \vec{\alpha}_T^{(T)} &= \overline{R}_\theta \vec{\alpha}_T^{(H)} = \overline{R}_\theta \left(\vec{\alpha}_H^{(H)} + \ddot{\theta}\, y_H^{(H)} + \dot{\theta}\left(\vec{\omega}_H^{(H)} \times y_H^{(H)}\right)\right) \\ \vec{\alpha}_E^{(E)} &= \overline{R}_\psi \vec{\alpha}_E^{(T)} = \overline{R}_\psi \left(\vec{\alpha}_T^{(T)} + \ddot{\psi}\, \hat{z}_T^{(T)} + \ddot{\psi}\left(\vec{\omega}_T^{(T)} \times \hat{z}_T^{(T)}\right)\right) \end{aligned} \tag{2.23}$$

These equations can be expanded using Cartesian components of vector quantities and axis transformation matrices as:

$$\vec{\alpha}_H^{(H)} = \begin{bmatrix} \alpha_{Hx} \\ \alpha_{Hy} \\ \alpha_{Hz} \end{bmatrix},\ \vec{\alpha}_T^{(T)} = \begin{bmatrix} \alpha_{Tx} \\ \alpha_{Ty} \\ \alpha_{Tz} \end{bmatrix} \text{ and } \vec{\alpha}_E^{(E)} = \begin{bmatrix} \alpha_{Ex} \\ \alpha_{Ey} \\ \alpha_{Ez} \end{bmatrix} \tag{2.24}$$

$$\begin{aligned}
\vec{\alpha}_T^{(T)} &= \begin{bmatrix} \alpha_{Tx} \\ \alpha_{Ty} \\ \alpha_{Tz} \end{bmatrix} = \overline{R}_\theta \vec{\alpha}_T^{(H)} = \begin{bmatrix} \cos\theta & 0 & -\sin\theta \\ 0 & 1 & 0 \\ \sin\theta & 0 & \cos\theta \end{bmatrix} \begin{bmatrix} \alpha_{Hx} - \dot{\theta}\omega_{Hz} \\ \alpha_{Hy} + \ddot{\theta} \\ \alpha_{Hz} + \dot{\theta}\omega_{Hx} \end{bmatrix} \\
\vec{\alpha}_E^{(E)} &= \begin{bmatrix} \alpha_{Ex} \\ \alpha_{Ey} \\ \alpha_{Ez} \end{bmatrix} = \overline{R}_\psi \vec{\alpha}_E^{(T)} = \begin{bmatrix} \cos\psi & \sin\psi & 0 \\ -\sin\psi & \cos\psi & 0 \\ 0 & 0 & 1 \end{bmatrix} \left(\vec{\alpha}_T^{(T)} + \begin{bmatrix} \dot{\psi}\omega_{Ty} \\ -\dot{\psi}\omega_{Tx} \\ \ddot{\psi} \end{bmatrix} \right)
\end{aligned} \tag{2.25}$$

Similar to angular velocity equations, to obtain the elevation frame angular acceleration in terms of base angular velocity and acceleration components, body angular velocity components, gimbal axes angles, rates and accelerations; these two equations is combined into one.

$$\begin{aligned}
\vec{\alpha}_E^{(E)} &= \begin{bmatrix} \alpha_{Ex} \\ \alpha_{Ey} \\ \alpha_{Ez} \end{bmatrix} = \overline{R}_\psi \vec{\alpha}_E^{(T)} \\
&= \begin{bmatrix} \cos\psi & \sin\psi & 0 \\ -\sin\psi & \cos\psi & 0 \\ 0 & 0 & 1 \end{bmatrix} \left(\begin{bmatrix} \cos\theta & 0 & -\sin\theta \\ 0 & 1 & 0 \\ \sin\theta & 0 & \cos\theta \end{bmatrix} \begin{bmatrix} \alpha_{Hx} - \dot{\theta}\omega_{Hz} \\ \alpha_{Hy} + \ddot{\theta} \\ \alpha_{Hz} + \dot{\theta}\omega_{Hx} \end{bmatrix} + \begin{bmatrix} \dot{\psi}\omega_{Ty} \\ -\dot{\psi}\omega_{Tx} \\ \ddot{\psi} \end{bmatrix} \right)
\end{aligned} \tag{2.26}$$

Previously given equation gives explicit definitions for LOS frame angular acceleration components when expanded as:

$$\begin{aligned}
\vec{\alpha}_E^{(E)} &= \vec{\alpha}_{LOS}^{(LOS)} = \begin{bmatrix} \alpha_{LOSx} \\ \alpha_{LOSy} \\ \alpha_{LOSz} \end{bmatrix} \\
&= \begin{bmatrix} \ddot{\theta}\sin\psi + \alpha_{Hy}\sin\psi + \alpha_{Hx}\cos\psi\cos\theta - \alpha_{Hz}\cos\psi\sin\theta \\ \ddot{\theta}\cos\psi + \alpha_{Hy}\cos\psi - \alpha_{Hx}\cos\theta\sin\psi + \alpha_{Hz}\sin\psi\sin\theta \\ \ddot{\psi} + \alpha_{Hz}\cos\theta + \alpha_{Hx}\sin\theta \end{bmatrix} \\
&\begin{bmatrix} +\dot{\psi}\omega_{Ty}\cos\psi - \dot{\psi}\omega_{Tx}\sin\psi - \dot{\theta}\omega_{Hz}\cos\psi\cos\theta - \dot{\theta}\omega_{Hx}\cos\psi\sin\theta \\ -\dot{\psi}\omega_{Tx}\cos\psi - \dot{\psi}\omega_{Ty}\sin\psi + \dot{\theta}\omega_{Hz}\cos\theta\sin\psi + \dot{\theta}\omega_{Hx}\sin\psi\sin\theta \\ +\dot{\theta}\omega_{Hx}\cos\theta - \dot{\theta}\omega_{Hz}\sin\theta \end{bmatrix}
\end{aligned} \tag{2.27}$$

Similar to angular velocity equations, last two rows of LOS is of special importance since they represent angular acceleration of controlled axes. The first row represents the uncontrolled roll acceleration of LOS frame.

$$
\begin{aligned}
&\alpha_{LOSy} = \alpha_{LOSy} = \ddot{\theta}\cos\psi + \alpha_{Hy}\cos\psi - \alpha_{Hx}\cos\theta\sin\psi + \alpha_{Hz}\sin\psi\sin\theta \\
&-\dot{\psi}\omega_{Tx}\cos\psi - \dot{\psi}\omega_{Ty}\sin\psi + \dot{\theta}\omega_{Hz}\cos\theta\sin\psi + \dot{\theta}\omega_{Hx}\sin\psi\sin\theta \\
&\alpha_{LOSz} = \alpha_{LOSpitch} = \ddot{\psi} + \alpha_{Hz}\cos\theta + \alpha_{Hx}\sin\theta \\
&+\dot{\theta}\omega_{Hx}\cos\theta - \dot{\theta}\omega_{Hz}\sin\theta
\end{aligned}
\tag{2.28}
$$

The last two rows can be solved to get gimbal axes relative angular acceleration quantities as:

$$
\begin{aligned}
&\ddot{\theta} = \frac{\alpha_{LOSy} + \sin\psi\left[\cos\theta\left(\alpha_{Hx} - \dot{\theta}\omega_{Hz}\right) - \sin\theta\left(\alpha_{Hz} + \dot{\theta}\omega_{Hx}\right) + \dot{\psi}\omega_{Ty}\right]}{\cos\psi} \\
&-\left(\alpha_{Hy} - \dot{\psi}\omega_{Tx}\right) \\
&\ddot{\psi} = \alpha_{LOSz} - \cos\theta\left(\alpha_{Hz} + \dot{\theta}\omega_{Hx}\right) - \sin\theta\left(\alpha_{Hx} - \dot{\theta}\omega_{Hz}\right)
\end{aligned}
\tag{2.29}
$$

For a successful stabilization of LOS vector, angular acceleration components of LOS frame orthogonal to LOS vector should be minimized, giving: $\alpha_{LOSyaw} = \alpha_{LOSpitch} = 0$ For target tracking purposes; these angular acceleration components should be set accordingly to target trajectory requirements.

Remark that the gimbal traverse axis angular acceleration component includes components of traverse axis angular velocity also, which requires equation pair (2.15) must be solved before dealing with angular acceleration components.

$$
\vec{\omega}_T^{(T)} = \begin{bmatrix} \cos\theta & 0 & -\sin\theta \\ 0 & 1 & 0 \\ \sin\theta & 0 & \cos\theta \end{bmatrix} \left(\vec{\omega}_H^{(H)} + \begin{bmatrix} 0 \\ \dot{\theta} \\ 0 \end{bmatrix} \right) = \begin{bmatrix} \omega_{Hx}\cos\theta - \omega_{Hz}\sin\theta \\ \dot{\theta} + \omega_{Hy} \\ \omega_{Hz}\cos\theta + \omega_{Hx}\sin\theta \end{bmatrix} \tag{2.30}
$$

At the final stage of angular acceleration calculations, required gimbal body angular acceleration components can be calculated by inserting outputs of equation pair(2.29) back into equation pair (2.25).

These equation pairs (2.29) and (2.25) are also constructed as MATLAB Simulink blocks for further use in simulations and control algorithm.

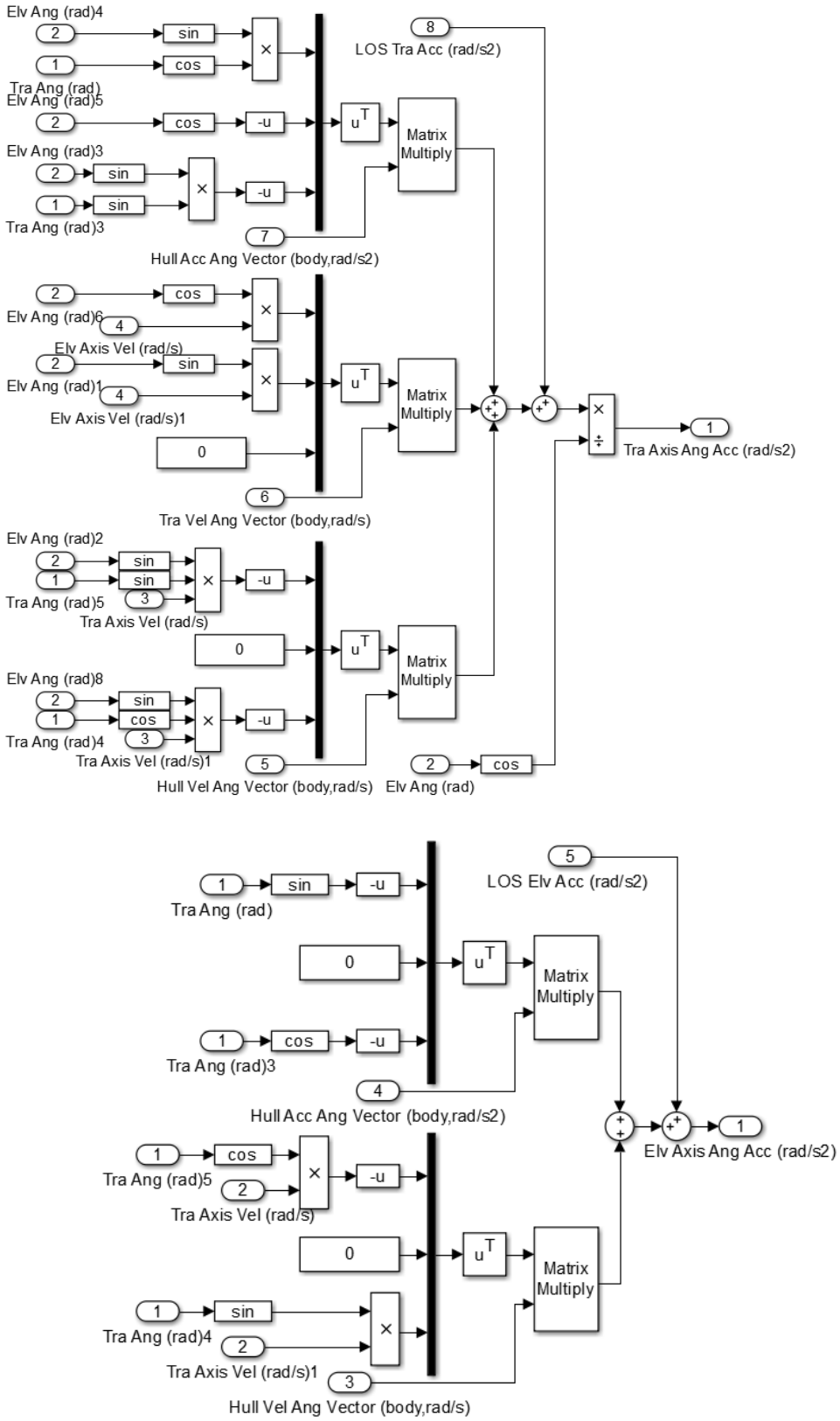

Figure 2-7: Gimbal axes angular acceleration solutions models in MATLAB Simulink

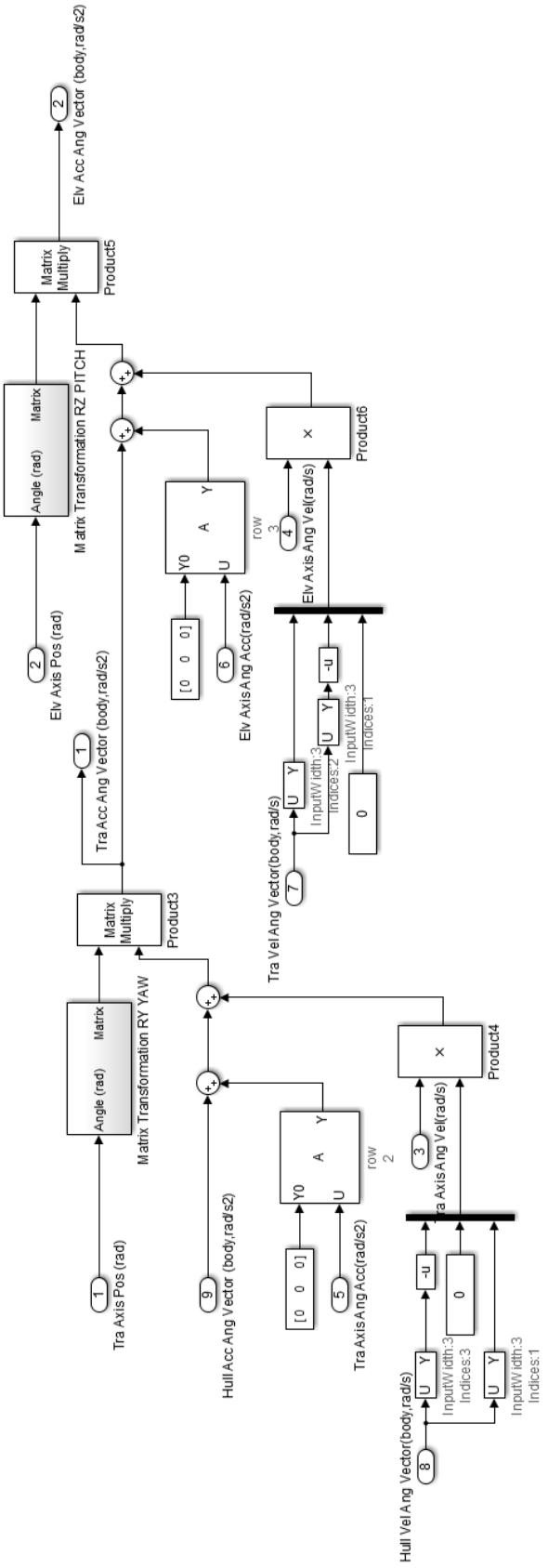

Figure 2-8: Body angular acceleration solutions in MATLAB Simulink

Obtaining body angular acceleration components in addition to angular velocity with known body angular acceleration and velocity components of the platform and gimbal angles finalizes the step of obtaining kinematic quantities that are to be used in disturbance decoupling control structure. But to simulate complete kinematics of the gimbal system one should follow a more complicated path using previously given calculations, and the order of execution of these calculations is crucial since it would not be possible to obtain required kinematic components unless the order given below is not followed:

Known quantities:

$\overline{R}_H$: Angular orientation of tracked vehicle

$\vec{\omega}_H^{(H)}$: Angular velocity vector of tracked vehicle

$\vec{\alpha}_H^{(H)}$: Angular acceleration of tracked vehicle

$\hat{r}_{LOS}^{(Earth)}$: Required LOS orientation unit vector dictated by stabilization or target tracking

$\vec{\omega}_{LOS}^{(LOS)}$: Required LOS angular velocity vector dictated by stabilization or target tracking

$\vec{\alpha}_{LOS}^{(LOS)}$: Required LOS angular acceleration vector dictated by stabilization or target tracking

Calculation Steps:

1. Calculate required gimbal axis angles using equation pair(2.12):

$$\theta = \arctan 2\left(\frac{-z_{LOS}}{\sqrt{1-y_{LOS}^2}}, \frac{x_{LOS}}{\sqrt{1-y_{LOS}^2}} \right),\ \psi = \arctan 2\left(y_{LOS}, \sqrt{1-y_{LOS}^2} \right)$$

2. Calculate required gimbal axis angular velocity values using equation pair (2.21):

$$\dot{\theta} = \frac{\omega_{LOSyaw} + \omega_{Hx}\sin\psi\cos\theta - \omega_{Hy}\cos\psi - \omega_{Hz}\sin\psi\sin\theta}{\cos\psi}$$

$$\dot{\psi} = \omega_{LOSpitch} - \omega_{Hx}\sin\theta - \omega_{Hz}\cos\theta$$

3. Calculate required traverse and elevation frames' body angular velocity vectors using equation pair (2.15):

$$\vec{\omega}_T^{(T)} = \begin{bmatrix} \cos\theta & 0 & -\sin\theta \\ 0 & 1 & 0 \\ \sin\theta & 0 & \cos\theta \end{bmatrix} \left(\vec{\omega}_H^{(H)} + \begin{bmatrix} 0 \\ \dot{\theta} \\ 0 \end{bmatrix} \right)$$

$$\vec{\omega}_E^{(E)} = \begin{bmatrix} \cos\psi & \sin\psi & 0 \\ -\sin\psi & \cos\psi & 0 \\ 0 & 0 & 1 \end{bmatrix} \left(\vec{\omega}_T^{(T)} + \begin{bmatrix} 0 \\ 0 \\ \dot{\psi} \end{bmatrix} \right)$$

4. Calculate required gimbal axis angular acceleration values using equation pair (2.29):

$$\ddot{\theta} = \frac{\alpha_{LOSy} + \sin\psi \left[\cos\theta \left(\alpha_{Hx} - \dot{\theta}\omega_{Hz} \right) - \sin\theta \left(\alpha_{Hz} + \dot{\theta}\omega_{Hx} \right) + \dot{\psi}\omega_{Ty} \right] - \cos\psi \left(\alpha_{Hy} - \dot{\psi}\omega_{Tx} \right)}{\cos\psi}$$

$$\ddot{\psi} = \alpha_{LOSz} - \cos\theta \left(\alpha_{Hz} + \dot{\theta}\omega_{Hx} \right) - \sin\theta \left(\alpha_{Hx} - \dot{\theta}\omega_{Hz} \right)$$

5. Calculate required traverse and elevation frames' body angular acceleration vectors using equation pair (2.25):

$$\vec{\alpha}_T^{(T)} = \begin{bmatrix} \alpha_{Tx} \\ \alpha_{Ty} \\ \alpha_{Tz} \end{bmatrix} = \overline{R}_\theta \vec{\alpha}_T^{(H)} = \begin{bmatrix} \cos\theta & 0 & -\sin\theta \\ 0 & 1 & 0 \\ \sin\theta & 0 & \cos\theta \end{bmatrix} \begin{bmatrix} \alpha_{Hx} - \dot{\theta}\omega_{Hz} \\ \alpha_{Hy} + \ddot{\theta} \\ \alpha_{Hz} + \dot{\theta}\omega_{Hx} \end{bmatrix}$$

$$\vec{\alpha}_E^{(E)} = \begin{bmatrix} \alpha_{Ex} \\ \alpha_{Ey} \\ \alpha_{Ez} \end{bmatrix} = \overline{R}_\psi \vec{\alpha}_E^{(T)} = \begin{bmatrix} \cos\psi & \sin\psi & 0 \\ -\sin\psi & \cos\psi & 0 \\ 0 & 0 & 1 \end{bmatrix} \left(\vec{\alpha}_T^{(T)} + \begin{bmatrix} \dot{\psi}\omega_{Ty} \\ -\dot{\psi}\omega_{Tx} \\ \ddot{\psi} \end{bmatrix} \right)$$

2.3. Kinematic Coupling

Previous section presents a method to obtain required body angular acceleration and velocity rates that can be used in dynamic equations to calculate torque requirements of the gimbal undergoing a certain scenario. But the method represented so far fails at the point of explicitly depicting the overall relationship between base motion and stabilization since the aim up to this point is to introduce a method to numerically calculate required kinematic quantities from measured inputs. In this section, equations presented in previous sections are carried one step forward to show the relations in a more explicit manner. To define clearly, the last additional step is to

obtain body angular velocity and acceleration vectors explicitly in terms of hull, traverse and elevation axis quantities.

First, LOS vector stabilization conditions; $\omega_{LOSroll} = \omega_{LOSpitch} = 0$ and $\alpha_{LOSroll} = \alpha_{LOSpitch} = 0$; are applied to equation pairs (2.21) and (2.25) giving:

$$\begin{aligned} \dot{\theta} &= \frac{\omega_{Hx}\sin\psi\cos\theta - \omega_{Hy}\cos\psi - \omega_{Hz}\sin\psi\sin\theta}{\cos\psi} \\ \dot{\psi} &= -\omega_{Hx}\sin\theta - \omega_{Hz}\cos\theta \end{aligned} \tag{2.31}$$

$$\begin{aligned} \ddot{\theta} &= \frac{\sin\psi\left[\cos\theta\left(\alpha_{Hx} - \dot{\theta}\omega_{Hz}\right) - \sin\theta\left(\alpha_{Hz} + \dot{\theta}\omega_{Hx}\right) + \dot{\psi}\omega_{Ty}\right]}{\cos\psi} \\ &\quad -\left(\alpha_{Hy} - \dot{\psi}\omega_{Tx}\right) \\ \ddot{\psi} &= -\cos\theta\left(\alpha_{Hz} + \dot{\theta}\omega_{Hx}\right) - \sin\theta\left(\alpha_{Hx} - \dot{\theta}\omega_{Hz}\right) \end{aligned} \tag{2.32}$$

Now to obtain angular velocity components of body frames equation pair (2.31) is inserted into equation pair (2.15) giving:

$$\begin{aligned} \vec{\omega}_T^{(T)} &= \begin{bmatrix} \omega_{Hx}\cos\theta - \omega_{Hz}\sin\theta \\ \tan\psi\left(\omega_{Hx}\cos\theta - \omega_{Hz}\sin\theta\right) \\ \omega_{Hz}\cos\theta + \omega_{Hx}\sin\theta \end{bmatrix} \\ \vec{\omega}_E^{(E)} &= \vec{\omega}_{LOS}^{(LOS)} = \begin{bmatrix} \omega_{LOSroll} \\ \omega_{LOSpitch} \\ \omega_{LOSyaw} \end{bmatrix} = \begin{bmatrix} \dfrac{\omega_{Hx}\cos\theta - \omega_{Hz}\sin\theta}{\cos\psi} \\ 0 \\ 0 \end{bmatrix} \end{aligned} \tag{2.33}$$

Second equation in the above equation pair clearly shows that the goal of LOS vector stabilization is achieved. On the other hand, the first equation represents an interesting fact. The second row of this equation is actually the body yaw velocity of traverse frame which is also controlled by traverse actuator.

$$\omega_{Ty} = \omega_{Tyaw} = \tan\psi\left(\omega_{Hx}\cos\theta - \omega_{Hz}\sin\theta\right) \tag{2.34}$$

Examining the right hand side of this equation reveals that when there exists a platform angular motion and elevation axis relative angle; ψ; is non-zero, traverse

frame must have a non-zero body angular velocity component in its rotation axis, which also implies a non-zero acceleration term for this axis may exist.

Continuing with angular acceleration components, one can obtain body acceleration components by taking derivatives of equation pair (2.33) paying utmost attention to chain rule. Since equations for angular acceleration components are already in hand, the other way around which is substituting equations into each other is chosen.

The first step is to get rid of the body kinematic quantity vector and axis relative angular velocity components in first equation of pair (2.32), which can be accomplished by substituting equation pairs (2.31) and (2.33) into (2.32). After simplifying the resultant equations by applying some trigonometric identities the resultant gimbal axis relative angular acceleration components become:

$$\begin{aligned}
&\ddot{\theta} = \alpha_{Hx}\cos\theta\tan\psi - \alpha_{Hy} - \alpha_{Hz}\sin\theta\tan\psi \\
&-\omega_{Hx}{}^{2}\frac{\sin 2\theta}{2}\left(1+2\tan^{2}\psi\right) + \omega_{Hz}{}^{2}\frac{\sin 2\theta}{2}\left(1+2\tan^{2}\psi\right) + \frac{\omega_{Hz}{}^{2}\sin 2\theta}{\cos^{2}\psi} \\
&+\omega_{Hx}\omega_{Hy}\sin\theta\tan\psi + \omega_{Hy}\omega_{Hz}\cos\theta\tan\psi + \omega_{Hx}\omega_{Hz}\cos 2\theta - \frac{2\omega_{Hx}\omega_{Hz}\cos 2\theta}{\cos^{2}\psi} \\
&\ddot{\psi} = -\alpha_{Hx}\sin\theta - \alpha_{Hz}\cos\theta \\
&-\omega_{Hx}{}^{2}\cos^{2}\theta\tan\psi - \omega_{Hz}{}^{2}\sin^{2}\theta\tan\psi \\
&+\omega_{Hx}\omega_{Hz}\sin 2\theta\tan\psi + \omega_{Hy}\omega_{Hx}\cos\theta - \omega_{Hy}\omega_{Hz}\sin\theta
\end{aligned} \tag{2.36}$$

The next step is to substitute this equation pair (2.36) and equation pair (2.33) into equation pair (2.21) to get an explicit representation of gimbal frame body angular acceleration components and apply a few trigonometric identities to simplify the results, which gives:

For traverse gimbal body;

$$\overset{\rightarrow(T)}{\alpha}_{T,STAB} = \begin{bmatrix} \alpha_{Tx,STAB} \\ \alpha_{Ty,STAB} \\ \alpha_{Tz,STAB} \end{bmatrix} \tag{2.37}$$

where;

$$\begin{aligned}
&\alpha_{Tx,STAB} = \alpha_{Hx}\cos\theta - \alpha_{Hz}\sin\theta \\
&-\frac{\omega_{Hx}{}^{2}\sin 2\theta\tan\psi}{2} + \frac{\omega_{Hz}{}^{2}\sin 2\theta\tan\psi}{2} \\
&+\omega_{Hx}\omega_{Hy}\sin\theta - \omega_{Hx}\omega_{Hz}\cos 2\theta\tan\psi + \omega_{Hy}\omega_{Hz}\cos\theta
\end{aligned} \tag{2.38}$$

$$\alpha_{Ty,STAB} = \alpha_{Hx}\cos\theta\tan\psi - \alpha_{Hz}\sin\theta\tan\psi$$
$$-\omega_{Hx}{}^{2}\frac{\sin 2\theta}{2}\left(1+2\tan^{2}\psi\right)+\omega_{Hz}{}^{2}\frac{\sin 2\theta}{2}\left(1+2\tan^{2}\psi\right) \quad (2.39)$$
$$+\omega_{Hx}\omega_{Hy}\sin\theta\tan\psi - \omega_{Hx}\omega_{Hz}\cos 2\theta\left(1+2\tan^{2}\psi\right)+\omega_{Hy}\omega_{Hz}\cos\theta\tan\psi$$

$$\alpha_{Tz,STAB} = \alpha_{Hz}\cos\theta + \alpha_{Hx}\sin\theta$$
$$+\omega_{Hx}{}^{2}\cos^{2}\theta\tan\psi + \omega_{Hz}{}^{2}\sin^{2}\theta\tan\psi \quad (2.40)$$
$$-\omega_{Hx}\omega_{Hy}\cos\theta - \omega_{Hx}\omega_{Hz}\sin 2\theta\tan\psi + \omega_{Hy}\omega_{Hz}\sin\theta$$

For elevation gimbal body;

$$\overset{\rightarrow(E)}{\alpha}_{E,STAB} = \begin{bmatrix}\alpha_{Ex,STAB}\\ \alpha_{Ey,STAB}\\ \alpha_{Ez,STAB}\end{bmatrix} = \overset{\rightarrow(LOS)}{\alpha}_{LOS,STAB} = \begin{bmatrix}\alpha_{LOSroll,STAB}\\ \alpha_{LOSpitch,STAB}\\ \alpha_{LOSyaw,STAB}\end{bmatrix} \quad (2.41)$$

where

$$\alpha_{Ex,STAB} = \alpha_{LOSroll,STAB} = \frac{1}{\cos\psi}\left(\alpha_{Hx}\cos\theta - \alpha_{Hz}\sin\theta\right.$$
$$-\omega_{Hx}{}^{2}\sin 2\theta\tan\psi + \omega_{Hz}{}^{2}\sin 2\theta\tan\psi \quad (2.42)$$
$$\left.+\omega_{Hx}\omega_{Hy}\sin\theta - \omega_{Hx}\omega_{Hz}2\cos 2\theta\tan\psi + \omega_{Hy}\omega_{Hz}\cos\theta\right)$$

$$\alpha_{Ey,STAB} = \alpha_{LOSpitch,STAB} = 0 \quad (2.43)$$

$$\alpha_{Ez,STAB} = \alpha_{LOSyaw,STAB} = 0 \quad (2.44)$$

Similar to equation pair (2.33), the equation (2.41) represents LOS frame body angular acceleration components and it can clearly be seen that the condition for LOS vector stabilization is satisfied as last two rows of the vector corresponding to controlled LOS angular acceleration components come out to be zero.

The first equation in this pair, representing traverse frame body angular acceleration components and it is seen that the second row depicting the controlled angular acceleration component is non-zero as expected.

$$\alpha_{Ty,STAB} = \alpha_{Tyaw} = \alpha_{Hx}\cos\theta\tan\psi - \alpha_{Hz}\sin\theta\tan\psi$$
$$-\omega_{Hx}{}^{2}\frac{\sin 2\theta}{2}\left(1+2\tan^{2}\psi\right)+\omega_{Hz}{}^{2}\frac{\sin 2\theta}{2}\left(1+2\tan^{2}\psi\right) \quad (2.45)$$
$$+\omega_{Hx}\omega_{Hy}\sin\theta\tan\psi - \omega_{Hx}\omega_{Hz}\cos 2\theta\left(1+2\tan^{2}\psi\right)+\omega_{Hy}\omega_{Hz}\cos\theta\tan\psi$$

Equations (2.34) and (2.45) depicting required angular velocity and acceleration components in controlled traverse axis for LOS vector stabilization are complicated

to clearly identify the effect of kinematic coupling on the traverse axis acceleration requirements since they include platform angular motion components in all three axes. To simplify equations, platform angular motion components only in one axis is set to be non-zero , others being zero; $\omega_{Hy} = \omega_{Hz} = 0$ and $\alpha_{Hy} = \alpha_{Hz} = 0$. Then equations (2.34) and (2.45) becomes:

$$\omega_{Tyaw}\Big|_{\omega_{Hy}=\omega_{Hz}=0} = \omega_{Hx} \cos\theta \tan\psi \tag{2.46}$$

$$\alpha_{Tyaw}\Big|_{\substack{\omega_{Hy}=\omega_{Hz}=0 \\ \alpha_{Hy}=\alpha_{Hz}=0}} = \alpha_{Hx} \cos\theta \tan\psi - \omega_{Hx}{}^{2} \frac{\sin 2\theta}{2}\left(1 + 2\tan^{2}\psi\right) \tag{2.47}$$

Examining the first equation, one can see that there exists an amplification factor in the form of $\tan\psi$ in projecting platform angular velocity into required traverse axis body angular velocity; and from the nature of tangent function this amplification even reaches infinity at $\psi = \pi/2$ when the gimbal assembly is pointing upwards to zenith. This increasing amplification factor in velocity relations can also be considered as a similar amplification factor which reaches its asymptote even with a faster rate due to $\tan^{2}\psi$ appearing in the second equation. These conclusions are also accordant with gimbal lock phenomena where a two axis gimbal of yaw-pitch configuration loses the effect of azimuth axis when gimbal is pointing towards zenith or nadir points. To clarify the findings, required body angular velocity and acceleration values at controlled traverse axis for different elevation angles are given in Figure 2-9. The values are calculated as the base undergoes a sinusoidal roll motion with 5° amplitude and 1 Hz frequency. Initial elevation angles are selected as 15°, 30°, 45°, 60° and 75°, angles 0° and 90° are omitted since they represent two limits of kinematic coupling effect where it diminishes at one limit and reaches infinity at the other limit respectively. Initial traverse angle is selected as 0° in accordance with base roll motion.

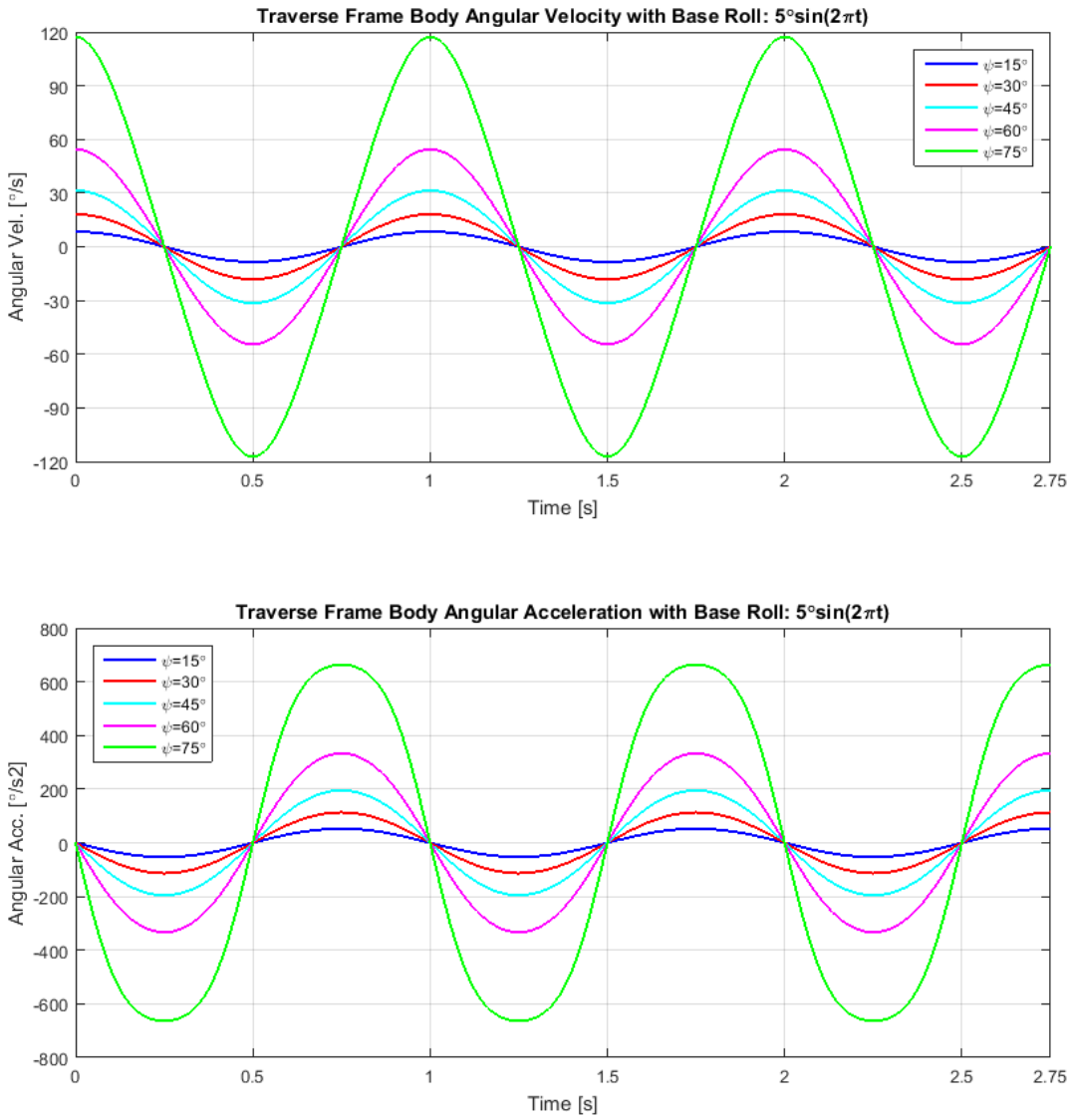

Figure 2-9: Traverse frame angular velocity and acceleration requirements in kinematic coupling.

In terms of controlling the gimbal motion, explained kinematic coupling phenomena in LOS vector stabilization manifests itself as a non-zero angular acceleration requirement for the controlled axis of traverse frame when platform is in motion and LOS vector is not orthogonal to traverse axis, i.e. gimbal is pointing upwards or downwards. This non-zero angular acceleration requirement for the controlled axis also indicates a requirement of torque applied to the gimbal frame by the controller to stabilize LOS vector. Requirement of a torque generated by controller in the event of kinematic coupling can be considered as a "pseudo" disturbance torque which

must be generated in order to stabilize LOS vector even there is not an actual torque acting on the system in inertial frame.

2.4. Target Motion

The main goal in this study is to improve performance of a target tracking gimbal, thus target motion characteristics have a very considerable importance for the success of this study. As mentioned before, target tracking sensors and target estimation algorithms implemented for these sensors generate target motion parameters to some extent as inputs to the servo controller. But unfortunately obtaining all required kinematic quantities of the target motion is not possible with target tracking sensors mounted on the specific gimbal system. Readily available outputs from these sensors are relative angular position of the target with respect to sensor frame and angular velocity estimates of target motion resolved in sensor frame. The first of these outputs is actually instantaneous angular error between current LOS vector and an ideal LOS vector connecting gimbal intersection point and actual target position, this kind of target position output is generally referred as "boresight error", a term originated from gun turret systems but also used for other target tracking systems. The second output is actually the two required orthogonal angular velocity components of LOS frame, and these angular velocity outputs mostly utilized as feed forward commands into stabilization controller in order to increase performance of target tracking under high target speed and acceleration. The exact utilization of these outputs in the control architecture is presented in the chapter devoted to control algorithm. In this section, kinematic resolution of target motion in the format dictated by tracking sensor outputs is presented since required LOS orientation is an essential component of proposed control structure. Later, a sample target scenario and its resolutions in gimbal axes are presented, and a discussion on target trajectories and kinematic coupling is presented.

2.4.1. Kinematic Resolution of Target Motion into Gimbal Requirements

As mentioned before, there exists a requirement to resolve target tracking sensor outputs into gimbal requirements for the control structure and for simulation

purposes, a given target motion is required to be converted into equivalent outputs given by the sensors.

The first step is to obtain boresight error and velocity feed forward quantities from a given target motion trajectory for simulation purposes from below given known quantities:

$\vec{r}_T^{(Earth)} = \begin{bmatrix} r_{Tx} \\ r_{Ty} \\ r_{Tz} \end{bmatrix}$: Target location in Earth frame w.r.t. a common origin

$\vec{r}_G^{(Earth)} = \begin{bmatrix} r_{Gx} \\ r_{Gy} \\ r_{Gz} \end{bmatrix}$: Gimbal location in Earth frame w.r.t. a common origin

$\vec{V}_T^{(Earth)} = \begin{bmatrix} V_{Tx} \\ V_{Ty} \\ V_{Tz} \end{bmatrix}$: Target linear velocity resolved in Earth frame

$\vec{V}_G^{(Earth)} = \begin{bmatrix} V_{Gx} \\ V_{Gy} \\ V_{Gz} \end{bmatrix}$: Gimbal linear velocity resolved in Earth frame

$\overline{R}_H$: Angular orientation of hull body in Earth frame

θ : Gimbal traverse axis relative angle w.r.t. hull frame

ψ : Gimbal elevation axis relative angle w.r.t. traverse frame

A schematics of target tracking with defined variables can be found in Figure 2-10.

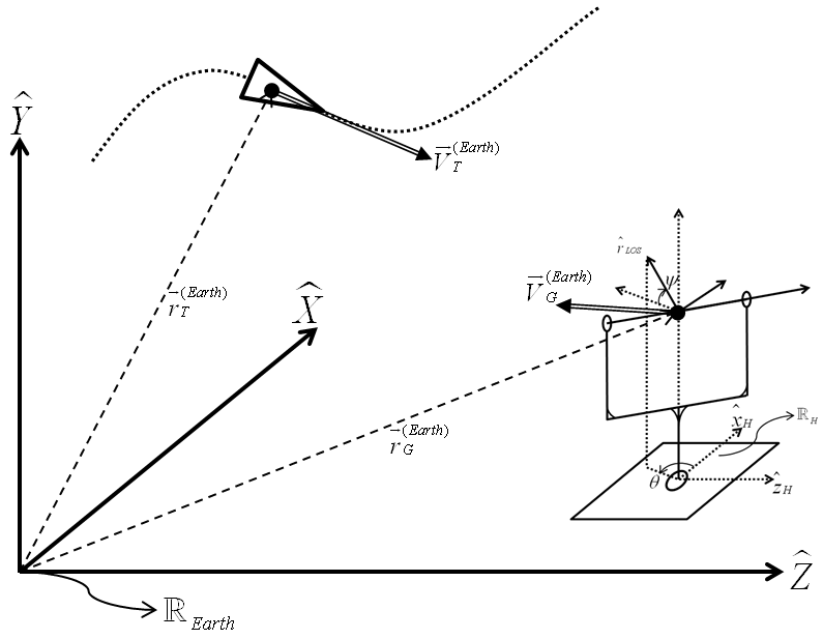

Figure 2-10: Target tracking schematics

The next step is to calculate boresight error values from gimbal position, orientation and target position, which can be accomplished as:

$$\Delta\vec{r}_T^{(Earth)} = \vec{r}_T^{(Earth)} - \vec{r}_G^{(Earth)} = \begin{bmatrix} r_{Tx} - r_{Gx} \\ r_{Ty} - r_{Gy} \\ r_{Tz} - r_{Gy} \end{bmatrix}$$; target relative position w.r.t. gimbal

$$\hat{r}_{\substack{LOS \\ ideal}}^{(Earth)} = \frac{\Delta\vec{r}_T^{(Earth)}}{\left|\Delta\vec{r}_T^{(Earth)}\right|}$$; required LOS unit vector resolved in Earth frame

Boresight error values can be depicted as amounts of body fixed rotations performed on actual LOS frame, so one can transform LOS vector in Earth frame to actual LOS frame and solve the resultant orientation in terms of boresight errors as:

$$\hat{r}_{\substack{LOS \\ ideal}}^{(LOS)} = \bar{R}_\psi \bar{R}_\theta \bar{R}_H \hat{r}_{\substack{LOS \\ ideal}}^{(Earth)}$$; projection of ideal LOS vector into actual LOS frame.

$\hat{r}_{\substack{LOS \\ ideal}}^{(LOS)} = \overline{R}_{\Delta\psi}\overline{R}_{\Delta\theta}\hat{r}_{LOS}^{(LOS)} = \overline{R}_{\Delta\psi}\overline{R}_{\Delta\theta}\begin{bmatrix}1\\0\\0\end{bmatrix}$; ideal LOS vector resolved in LOS frame represented as body fixed rotations $\Delta\theta$ and $\Delta\psi$ which are also boresight error values and can be obtained through the same procedure of obtaining equation pair (2.12) where additional matrix quantities are:

$$\overline{R}_{\Delta\theta} = \begin{bmatrix}\cos\Delta\theta & 0 & -\sin\Delta\theta\\ 0 & 1 & 0\\ \sin\Delta\theta & 0 & \cos\Delta\theta\end{bmatrix} \text{ and } \overline{R}_{\Delta\psi} = \begin{bmatrix}\cos\Delta\psi & \sin\Delta\psi & 0\\ -\sin\Delta\psi & \cos\Delta\psi & 0\\ 0 & 0 & 1\end{bmatrix} \quad (2.48)$$

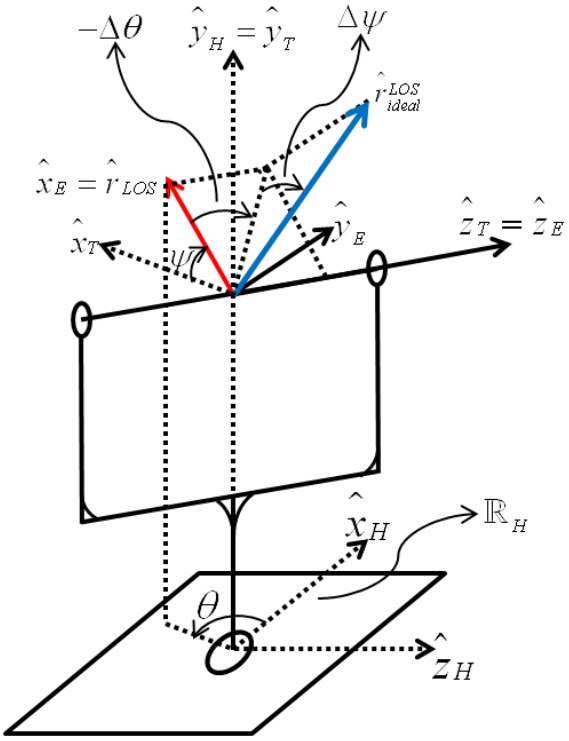

Figure 2-11: Ideal LOS orientation in actual LOS frame and boresight error angles

After obtaining required boresight errors $\Delta\theta$ and $\Delta\psi$ one can also obtain ideal LOS frame orientation easily as:

$$\overline{R}_{ideal}^{LOS} = \overline{R}_{\Delta\psi}\overline{R}_{\Delta\theta}\overline{R}_{LOS} \quad (2.49)$$

The next step is to obtain feed forward angular velocity outputs from given variables:

$$\Delta\vec{V}_T^{(Earth)} = \vec{V}_T^{(Earth)} - \vec{V}_G^{(Earth)} = \begin{bmatrix} V_{Tx} - V_{Gx} \\ V_{Ty} - V_{Gy} \\ V_{Tz} - V_{Gy} \end{bmatrix}$$; target relative linear velocity w.r.t. gimbal

Feed forward angular velocity outputs are the angular projections of this relative linear velocity transformed into ideal LOS frame, so one can simply calculate them as:

$\Delta\vec{V}_T^{\left(\substack{LOS \\ idea}\right)} = \begin{bmatrix} \Delta V_x \\ \Delta V_y \\ \Delta V_z \end{bmatrix} = \bar{R}_{ideal}^{LOS}\Delta\vec{V}_T^{(Earth)}$; Target relative linear velocity transformed into ideal LOS frame.

$\omega_{LOSyaw} = \dfrac{-\Delta V_z}{\left|\Delta\vec{r}_T^{(Earth)}\right|}$ $\omega_{LOSpitch} = \dfrac{\Delta V_y}{\left|\Delta\vec{r}_T^{(Earth)}\right|}$ Feed forward angular velocity outputs obtained as angular projections of relative linear velocity components divided by target distance in space.

Now with boresight error; $\Delta\theta$ and $\Delta\psi$; and angular velocity feed forward; ω_{LOSyaw} and $\omega_{LOSpitch}$; variables in hand one can utilize them in simulations for a given target motion. The presented method of obtaining target tracking variables is constructed as MATLAB Simulink blocks for simulation purposes given in Figure 2-12 and Figure 2-13.

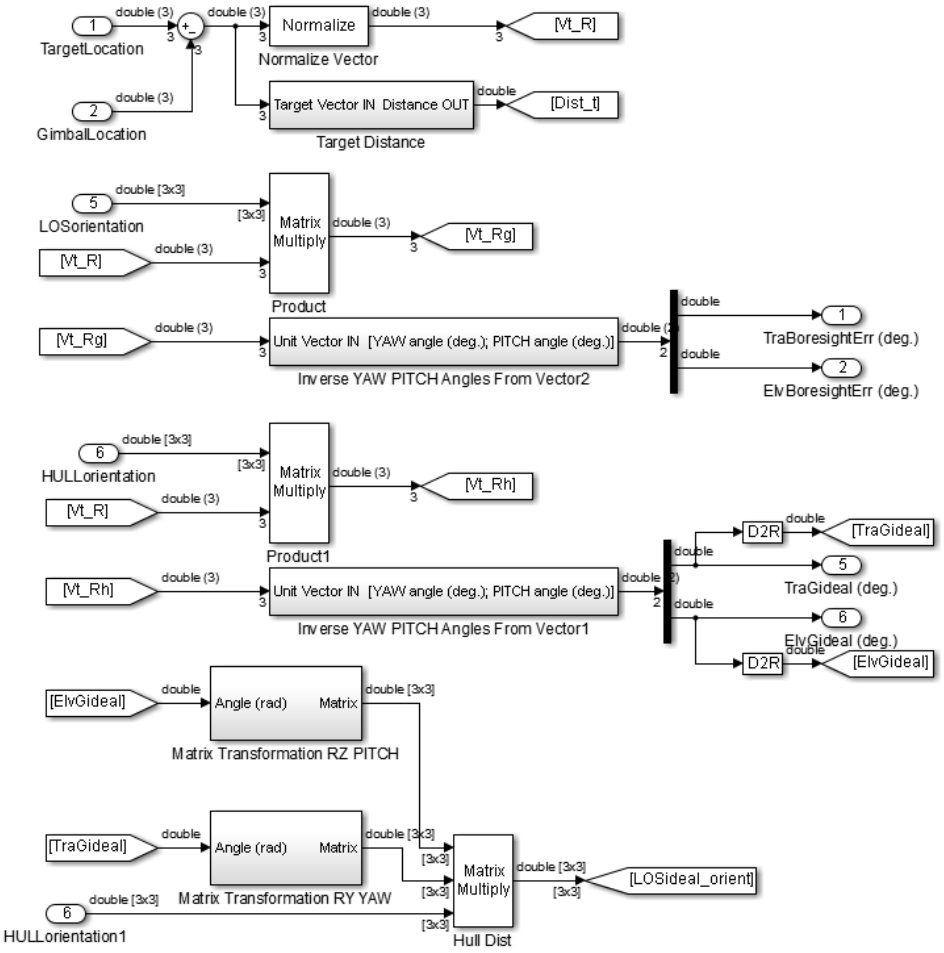

Figure 2-12: Boresight error variables and ideal gimbal axis calculations in MATLAB Simulink

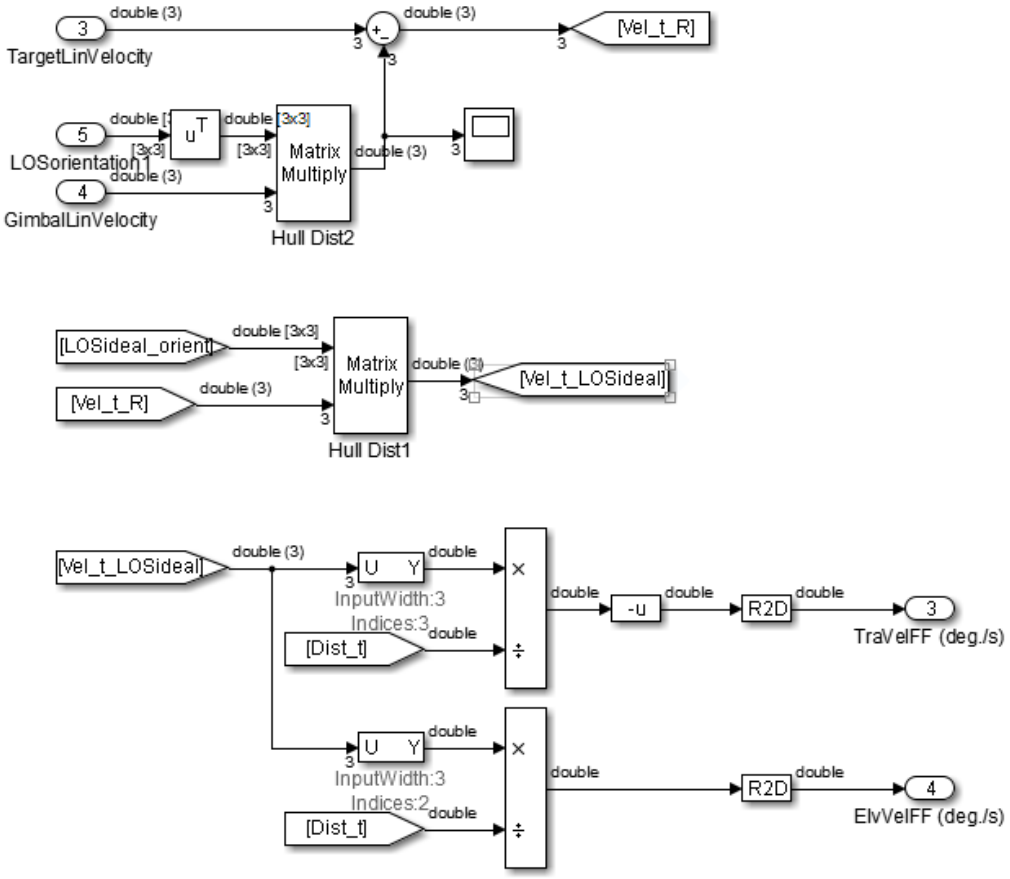

Figure 2-13: Feed forward angular velocity calculations in MATLAB Simulink

For actual implementation in real system, boresight error and feed forward angular velocity signals are readily available in hand as outputs of target tracking sensors, so one only needs to calculate the ideal LOS vector orientation in Earth frame which can be obtained through applying above mentioned calculations in an inverse manner as represented below:

$$\hat{r}_{\substack{LOS \\ ideal}}^{\left(\substack{LOS \\ idea}\right)} = \begin{bmatrix} 1 \\ 0 \\ 0 \end{bmatrix} = \overline{R}_{ideal}^{LOS} = \overline{R}_{\Delta\psi}\,\overline{R}_{\Delta\theta}\,\overline{R}_{LOS} = \overline{R}_{\Delta\psi}\,\overline{R}_{\Delta\theta}\,\overline{R}_{\psi}\,\overline{R}_{\theta}\,\overline{R}_{H}\,\hat{r}_{\substack{LOS \\ ideal}}^{(Earth)} \tag{2.50}$$

Using orthonormality of transformation matrices:

$$\hat{r}_{\substack{LOS \\ ideal}}^{(Earth)} = \overline{R}_{H}^{\,T}\,\overline{R}_{\theta}^{\,T}\,\overline{R}_{\psi}^{\,T}\,\overline{R}_{\Delta\theta}^{\,T}\,\overline{R}_{\Delta\psi}^{\,T} \begin{bmatrix} 1 \\ 0 \\ 0 \end{bmatrix} \tag{2.51}$$

2.4.2. Gimbal Motion Requirements in Target Tracking

In this section a sample target motion and its corresponding gimbal motion requirements calculated through methods given in the previous section is presented. Later discussions about target tracking and kinematic coupling are presented.

The selected target scenario is a low altitude straight flyby of a target cruising at 400 m/s which is slightly above Mach 1. The schematics of the target scenario is given in Figure 2-14.

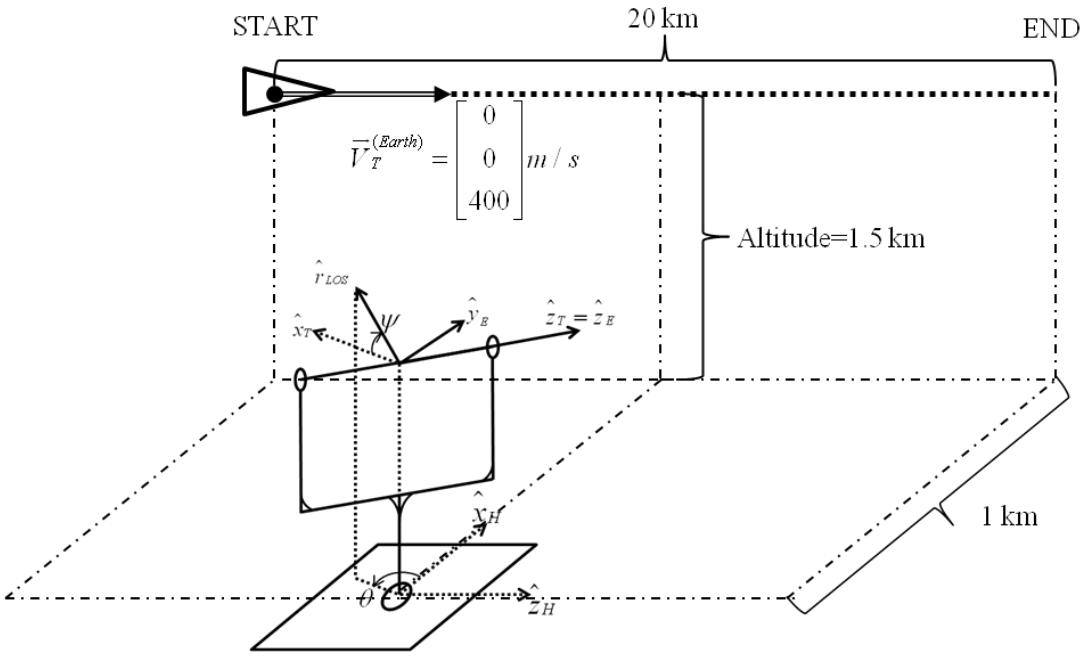

Figure 2-14: Sample target scenario schematics

In this scenario, tracked vehicle hull is taken as stationary to clearly represent target motion requirements. The gimbal axis relative angles and feed forward angular velocity components calculated through previously described method is given in Figure 2-15.

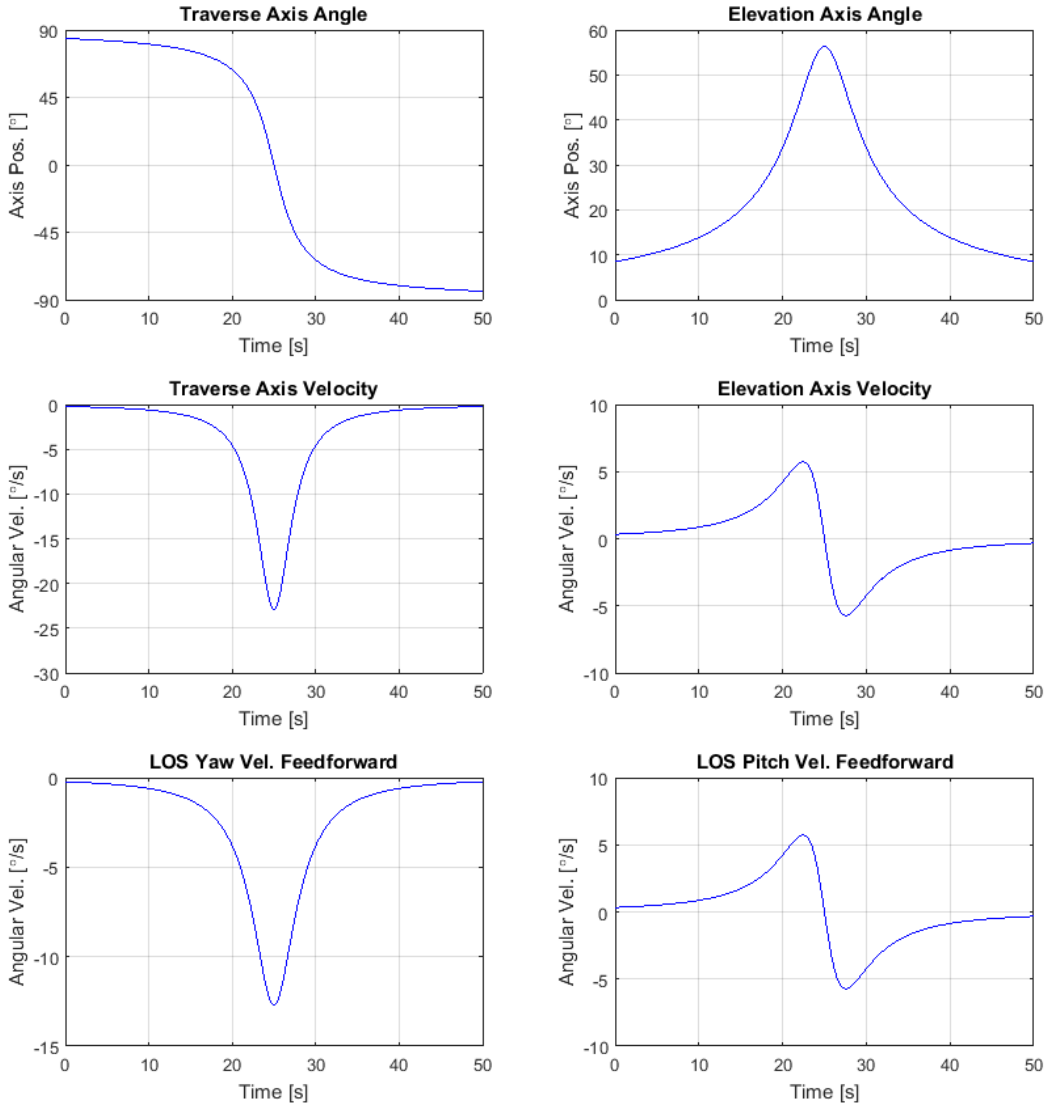

Figure 2-15: Gimbal motion requirements for sample target scenario

Remark that in the given figure, there is a considerable amplitude difference between traverse axis velocity and LOS yaw velocity feed forward which is due to the fact that feed forward velocity signals are supplied in LOS coordinate frame. In addition, is seen that in the middle of the scenario, elevation angle increases close to 60° at which point the gimbal would severely suffer from kinematic coupling, also this instant in time the target is at its closest point to the system making the vicinity of this point a good candidate for eliminating the target, so a reduction in target tracking performance is intolerable which justifies developing a countermeasure method to overcome kinematic coupling.

A proper justification for a necessity to overcome kinematic coupling effect also requires examining many different target scenarios, so 30 different target scenarios are examined in the same manner and a distribution of elevation axis angles is obtained.

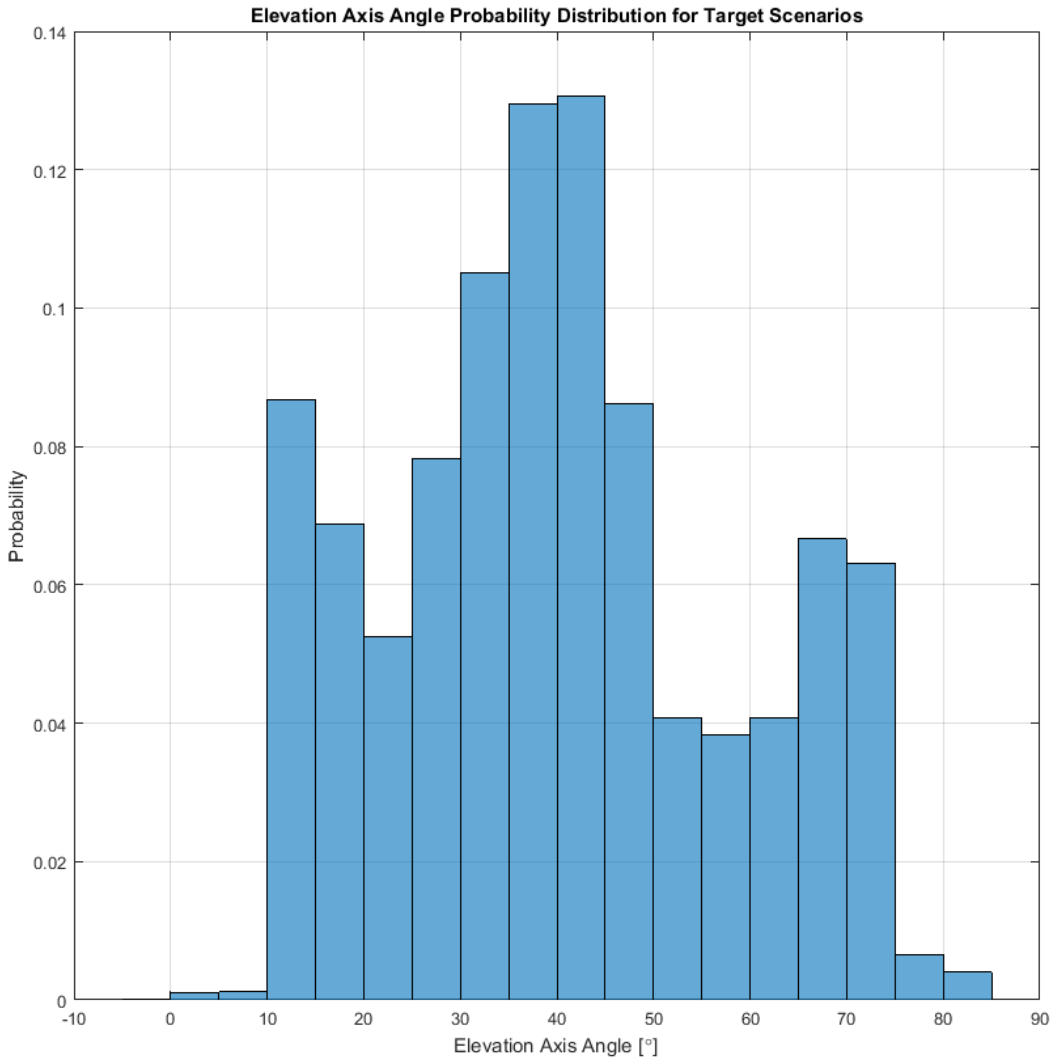

Figure 2-16: Elevation axis angle probability distribution for target scenarios

Unfortunately target trajectories and velocity profiles of target scenarios studied to construct probability distribution of elevation axis angle values cannot be presented since such knowledge would disclose all the intended targets in armaments of different countries which is a highly classified information.

From Figure 2-16 it is clearly seen that the operation point of elevation axis focuses around 45° and even goes up to as high as 80° where kinematic coupling would play an important role justifying development of a countermeasure method to overcome this phenomena.

2.5. Platform Motion

In previous sections, the methods of obtaining different kinematic quantities are presented except how kinematic quantities related to platform motion. In this section how to measure and/or calculate kinematic quantities is presented, later tests performed on the actual system and outcomes of these tests are discussed.

2.5.1. Measurement and Calculation of Kinematic Quantities of Base Motion

The main function of inertial navigation system is to supply position of the vehicle in a geographic coordinate system so that via incoming command control transmissions, initial crude engagement to an approaching target can be performed. For this purposes, the navigation system is focused on having extremely low angular random walk, bias instability and temperature bias; not having very dynamic outputs. Despite the fact that inertial navigation system is high quality, the system fails to meet output sampling rate and time delay requirements for high performance motion control applications. So, additional means of measuring base motion arises. The required kinematic quantities of platform are angular velocity and acceleration components for the decoupling controller in this study. But to run simulations of target tracking, angular orientation is also of significant importance since it is the only quantity that binds target trajectories and gimbal motion.

The easiest of all the measurements is angular velocity, which can be obtained by a triad of rate gyroscopes mounted orthogonally in the directions dictated by vehicle coordinate frame. For this purpose, DSP-3000 high performance single axis fiber optic gyroscope as shown in Figure 2-17 can be utilized. This gyroscope also has very desirable characteristics in terms of bias instability, angular random walk and temperature bias.

Figure 2-17: Fiber optic rate gyroscope, KVH DSP-3000 (Photo courtesy of KVH Industries Inc.)

The next step is to obtain angular acceleration components of vehicle motion. One straightforward method is to take discrete derivative of rate gyroscope outputs, yet this method would create a signal with very low signal to noise ratio [22] rendering this method inappropriate for this aim. Instead, a direct method of obtaining angular accelerations should be chosen. But direct measurement of angular acceleration is also a problematic issue since angular accelerometers are not widely available and existing ones have the problem of limited rotation range [22]. However, simple technique to obtain angular acceleration through a number of linear acceleration measurements is widely used [23], [24]. This technique can also be extended into obtaining angular velocity components but number of required linear accelerometers increase considerably and their orientation becomes complex. This technique may not be considered a direct method but involving operations are just algebraic manipulations rather than a derivative or integral operation.

This technique is based on using the simple relation between linear accelerations of two points located on a rigid body undergoing a rotational motion:

$$\vec{a}_B = \vec{a}_A + \vec{\alpha} \times \vec{r}_{B/A} + \vec{\omega} \times \left(\vec{\omega} \times \vec{r}_{B/A} \right) \tag{2.52}$$

If looked closely, rotational acceleration and velocity of the rigid body appears in the equation as an operand of a cross product. To obtain angular acceleration components, four 3-axis linear accelerometers are enough. For this manner, these 4 accelerometers should be placed equidistantly as to construct a triad; i.e. four vertices of a cube with combinations of each three being in the same plane as shown in Figure 2-18.

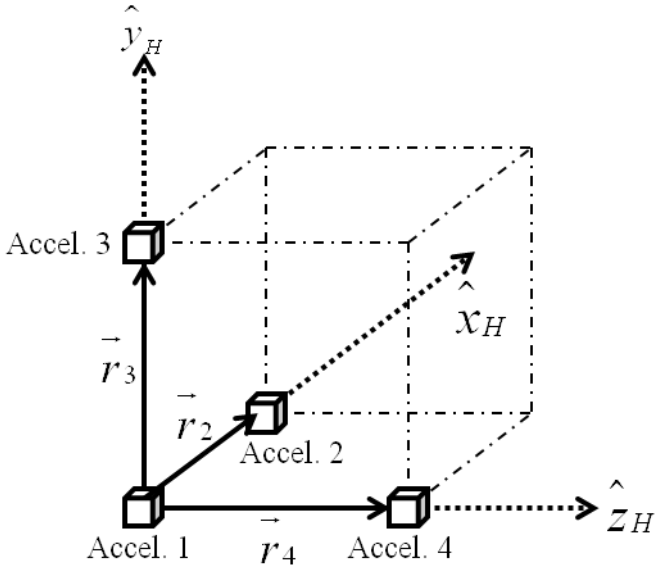

Figure 2-18: Placement of four linear 3-axis accelerometers to obtain angular acceleration

Taking relative position vectors between accelerometers as:

$$\vec{r}_2^{(H)} = \begin{bmatrix} L \\ 0 \\ 0 \end{bmatrix}, \vec{r}_3^{(H)} = \begin{bmatrix} 0 \\ L \\ 0 \end{bmatrix}, \vec{r}_4^{(H)} = \begin{bmatrix} 0 \\ 0 \\ L \end{bmatrix} \tag{2.52}$$

One can write the mentioned relation for each accelerometer as:

$$\vec{a}_2^{(H)} = \begin{bmatrix} a_{2x} \\ a_{2y} \\ a_{2z} \end{bmatrix} = \vec{a}_1^{(H)} + \vec{\alpha}_H^{(H)} \times \vec{r}_2^{(H)} + \vec{\omega}_H^{(H)} \times \left(\vec{\omega}_H^{(H)} \times \vec{r}_2^{(H)} \right)$$
$$= \begin{bmatrix} a_{1x} - L\omega_{Hz}{}^2 - L\omega_{Hy}{}^2 \\ a_{1y} + L\alpha_{Hz} + L\omega_{Hx}\omega_{Hy} \\ a_{1z} - L\alpha_{Hy} + L\omega_{Hx}\omega_{Hz} \end{bmatrix} \tag{2.53}$$

$$\vec{a}_3^{(H)} = \begin{bmatrix} a_{3x} \\ a_{3y} \\ a_{3z} \end{bmatrix} = \vec{a}_1^{(H)} + \vec{\alpha}_H^{(H)} \times \vec{r}_3^{(H)} + \vec{\omega}_H^{(H)} \times \left(\vec{\omega}_H^{(H)} \times \vec{r}_3^{(H)} \right)$$
$$= \begin{bmatrix} a_{1x} - L\alpha_{Hz} + L\omega_{Hx}\omega_{Hy} \\ a_{1y} - L\omega_{Hz}{}^2 - L\omega_{Hx}{}^2 \\ a_{1z} + L\alpha_{Hx} + L\omega_{Hy}\omega_{Hz} \end{bmatrix} \tag{2.54}$$

$$\vec{a}_4^{(H)} = \begin{bmatrix} a_{4x} \\ a_{4y} \\ a_{4z} \end{bmatrix} = \vec{a}_1^{(H)} + \vec{\alpha}_H^{(H)} \times \vec{r}_4^{(H)} + \vec{\omega}_H^{(H)} \times \left(\vec{\omega}_H^{(H)} \times \vec{r}_4^{(H)} \right)$$
$$= \begin{bmatrix} a_{1x} + L\alpha_{Hy} + L\omega_{Hx}\omega_{Hz} \\ a_{1y} - L\alpha_{Hx} + L\omega_{Hy}\omega_{Hz} \\ a_{1z} - L\omega_{Hy}{}^2 - L\omega_{Hx}{}^2 \end{bmatrix} \tag{2.55}$$

Resultant equations can be solved for angular acceleration components as:

$$\alpha_{Hx} = \frac{\left(a_{3z} - a_{1z}\right) - \left(a_{4y} - a_{1y}\right)}{2L}$$
$$\alpha_{Hy} = \frac{\left(a_{4x} - a_{1x}\right) - \left(a_{2z} - a_{1z}\right)}{2L} \tag{2.56}$$
$$\alpha_{Hz} = \frac{\left(a_{2y} - a_{1y}\right) - \left(a_{3x} - a_{1x}\right)}{2L}$$

Here it is shown that angular acceleration components of the vehicle can be obtained through simple addition and subtraction operations from four 3-axis linear accelerometers placed in a certain way.

A good candidate for a 3-axis linear accelerometer for the described purpose is capacitive MEMS type ASC 5411LN from Advanced Sensor Calibration GmbH as shown in Figure 2-19. This sensor is able to measure static acceleration values, have very low output noise, and is very compact in size.

Figure 2-19: Capacitive MEMS 3-axis linear accelerometer, ASC 5411LN (Photo courtesy of Advanced Sensor Calibration GmbH)

Although angular orientation of the vehicle is not required for the developed platform motion disturbance decoupling controller as explained in Chapter 4,

obtaining angular orientation of the vehicle is a crucial component for simulations performed with test data lacking this quantity. The reason behind this argument is that without angular orientation of the vehicle it would not be possible to simulate target tracking as target trajectories are defined in Earth coordinate frame and vehicle angular orientation is the only kinematic quantity that connects gimbal kinematics to Earth frame. So the last step in this section is to obtain angular orientation of the vehicle. One can use an additional sensor like a high performance attitude heading reference system to measure angular orientation of the vehicle but usage of such an additional sensor would justify itself if absolute angular orientation with respect to a certain stationary coordinate frame or direction is of significant importance. But for the application in this study, a change in rotational orientation of vehicle in time, invariant of a specific initial orientation is required rather than an absolute angular orientation. This fact is explained at the end of this section after governing equations are presented. So without using an additional sensor, one can obtain rotational orientation through rotational velocity measurements through the relation between angular orientation and angular velocity vector [25] as:

$\frac{d\overline{R}_H^{\,T}}{dt} = \overline{R}_H^{\,T}\overline{W}_H$ where $\overline{W}_H = \begin{bmatrix} 0 & -\omega_{Hz} & \omega_{Hy} \\ \omega_{Hz} & 0 & -\omega_{Hx} \\ -\omega_{Hy} & \omega_{Hx} & 0 \end{bmatrix}$ is the skew-symmetric form of angular velocity $\vec{\omega}_H^{(H)} = \begin{bmatrix} \omega_{Hx} \\ \omega_{Hy} \\ \omega_{Hz} \end{bmatrix}$, known as angular velocity tensor.

One can take integral of the above equation to obtain angular orientation after a finite time as [25]:

$$\overline{R}_H^{\,T}(t+\tau) = \overline{R}_H^{\,T}(t)\, e^{\int_t^{t+\tau} \overline{W}_H\, dt} \tag{2.57}$$

This equation can also be converted into discrete time form using trapezoidal integration as:

$$\overline{R}_H^{\,T}[k+1] = \overline{R}_H^{\,T}[k] e^{\frac{T_s}{2}\left(\overline{W}_H[k]+\overline{W}_H[k+1]\right)} \tag{2.58}$$

This method of obtaining angular orientation through measured angular velocity can be said to suffer from drift of the used gyroscopes and even orthonormality property of the transformation matrix can be defected severely which would require periodic orthogonalization of the findings. But this is only important for applications where obtaining rotational orientation for a long period of time is required. For this study, as target scenarios take at most one minute, limiting maximum required time of the simulations as well. Also a very low drift fiber optic rate gyroscope is utilized to obtain test data for vehicle motion, rendering this argument to have minimal effect. So the given method utilized as it is to obtain angular orientation of the vehicle from test data. This equation pair (2.58) is also constructed as MATLAB Simulink blocks for further use in simulations given in Figure 2-20.

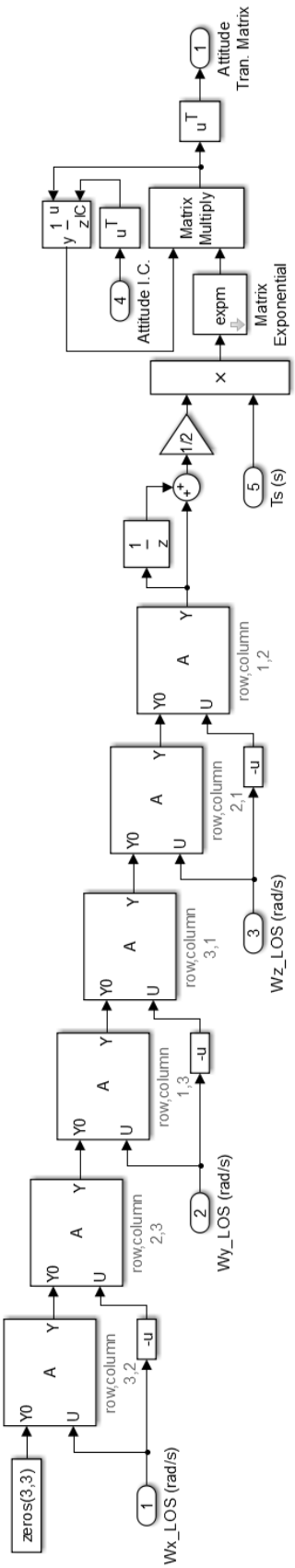

Figure 2-20: Obtaining platform angular orientation in MATLAB Simulink

2.5.2. Vehicle Motion Tests

A set of tests were performed with the tracked vehicle in order to gather vehicle kinematic data to be used in simulations. Superstructure of the system was not available at the time of these tests, so weight mock-ups are used instead as showed in Figure 2-21.

Figure 2-21: Tracked vehicle prepared for tests with weight mock-ups

In these tests, motion data was obtained through a set of inertial sensors; which are identical to previously mentioned; using a portable data acquisition system. These sensors mounted on the vehicle can be seen in Figure 2-22.

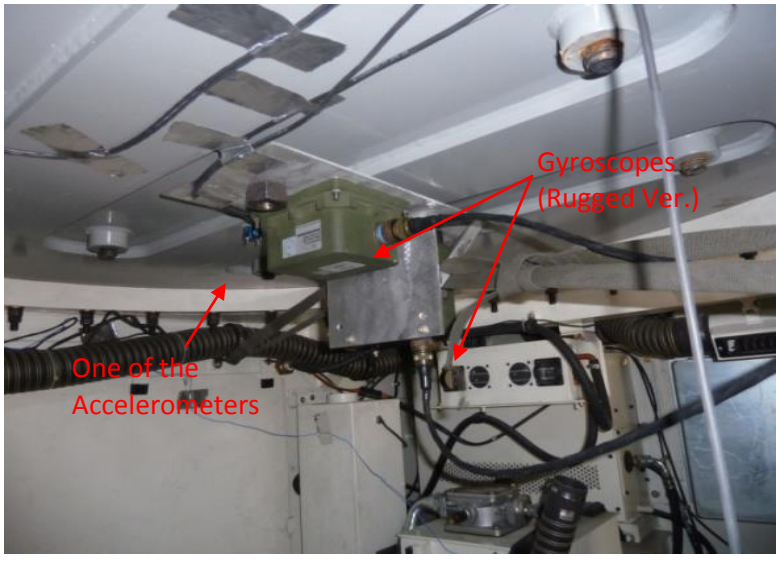

Figure 2-22: Inertial sensors mounted on the vehicle

To simulate vehicle's motion on a rough terrain, vehicle was driven over a special test track at speeds 10, 20, 30 and 40 km/h. A sample photo of vehicle cruising over the test track can be seen in Figure 2-23.

Figure 2-23: Vehicle testing track

Unfortunately it was later understood that there was a mishap with accelerometer setup; rendering acceleration data unusable; and no opportunity was found to conduct the tests again. So instead of real measurements, discrete derivatives of angular velocity data were used which were filtered offline to match sensor noise levels accordingly.

Angular motion data obtained through these tests can be seen at Figure 2-24 for 10 km/h, Figure 2-25 for 20 km/h, Figure 2-26 for 30 km/h and Figure 2-27 for 40 km/h. In the figures, platform rotational orientation is presented in yaw, pitch, roll angles as resolved in YZX Euler sequence. Also values at y-axes of these figures are presented in normalized form in order not to disclose classified information about the platform dynamic characteristics.

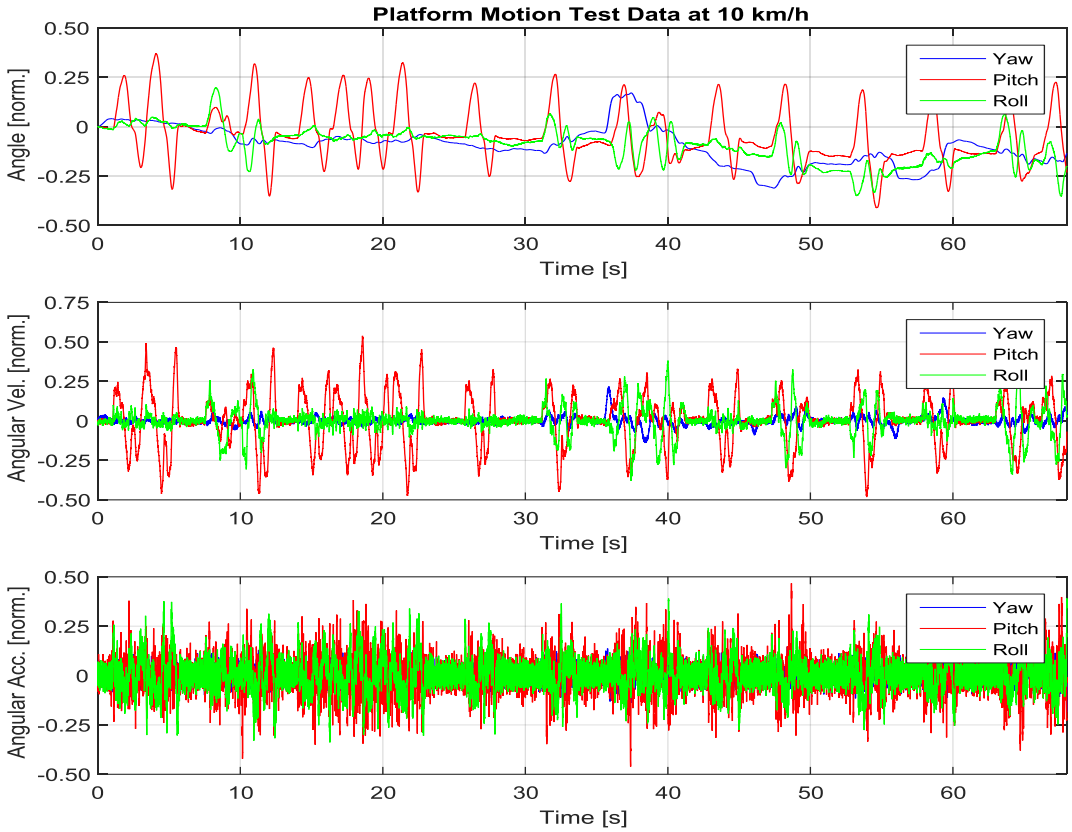

Figure 2-24: Platform motion data for 10 km/h

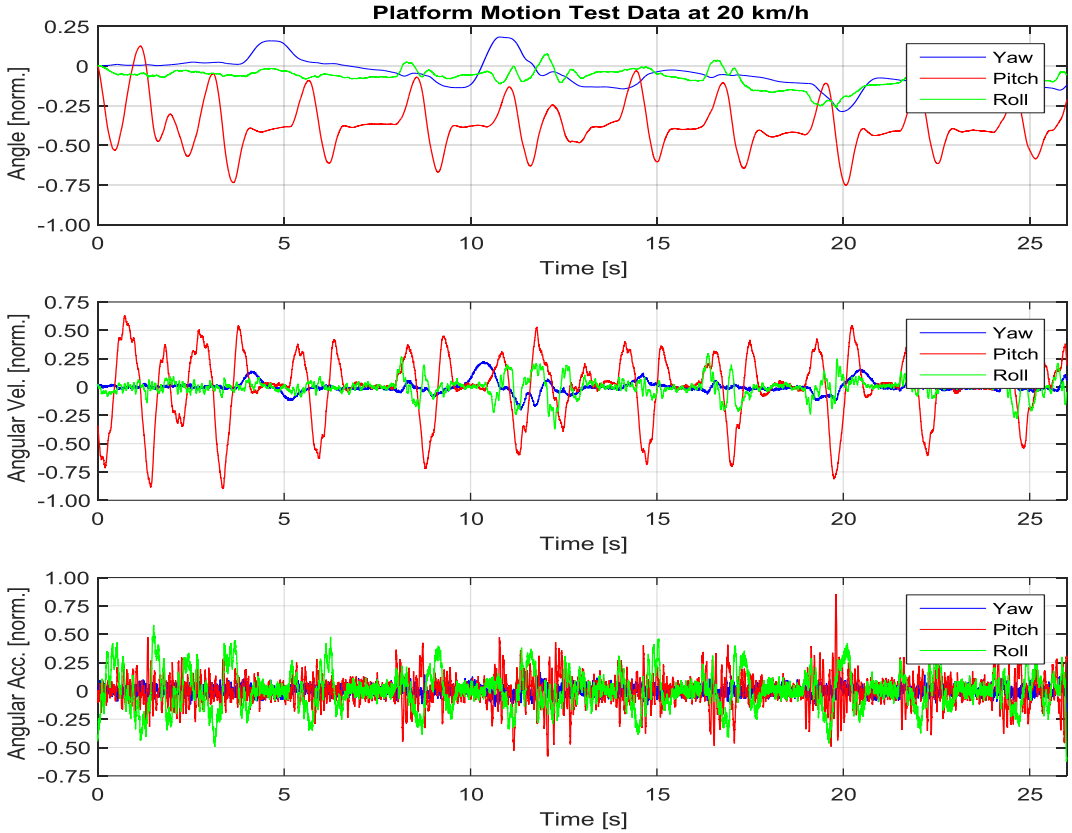

Figure 2-25: Platform motion data for 20 km/h

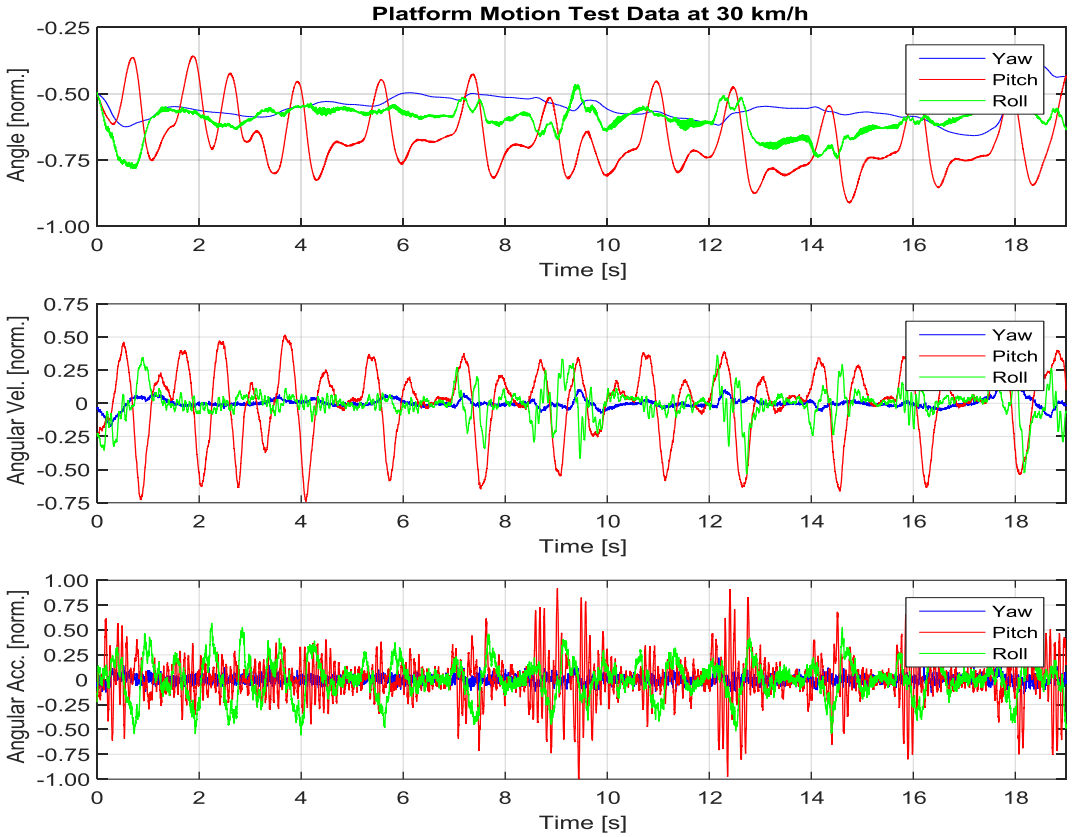

Figure 2-26: Platform motion data for 30 km/h

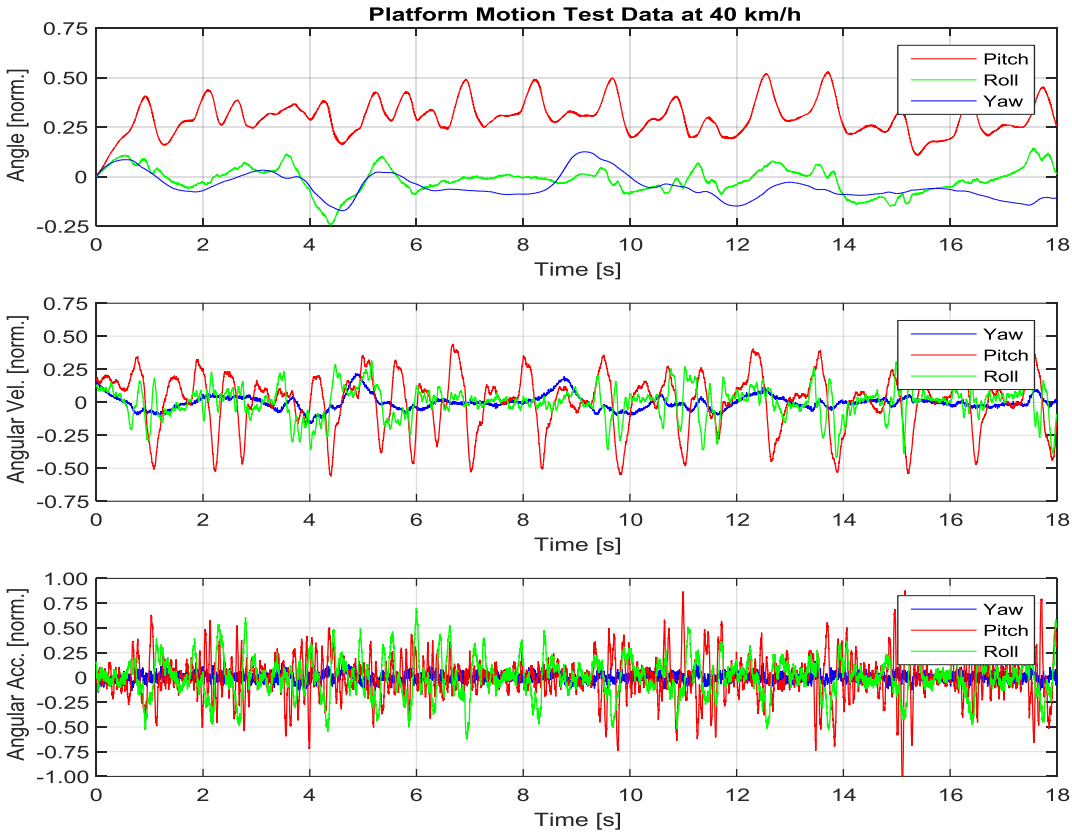

Figure 2-27: Platform motion data for 40 km/h

2.6. Kinematics Verification Models

All the kinematic relations obtained up to this point were verified using two constructed models utilizing MATLAB SimMechanics; one for LOS rate stabilization and one for target tracking. The models are constructed as to impose LOS rate stabilization and target tracking requirements in the form of virtual kinematic joints connecting inner gimbal body to Earth frame and a target body moving three dimensionally in space. The gimbal model is also placed on top of a freely movable body to represent platform motion. Since constructing such a model is considered to be trivial except defining concepts of LOS stabilization and target tracking in the forms of virtual kinematic joints. So only these concepts are explained which are considered to give superior visual insights about the topic.

In Figure 2-28, the schematics of realizing LOS stabilization by virtual kinematic pairs is presented. Since LOS stabilization is to keep angular orientation of LOS vector in three dimensional space regardless of the base motion, this can be accomplished by connecting LOS vector to Earth frame by means of three orthogonally placed prismatic joints which constrains the angular orientation but frees any linear movement in space. Also it is presented in previous sections that roll motion of the LOS vector cannot be controlled by means of a two axis gimbal, this statement holds for the required virtual joints as well. So an additional rotational joint collinear with LOS vector is placed as well.

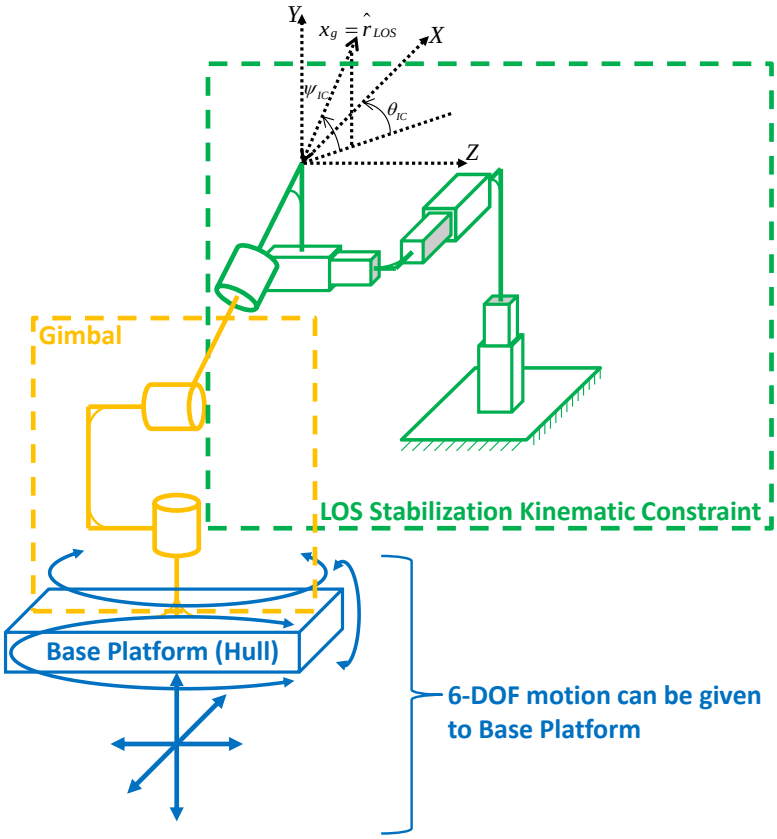

Figure 2-28: Realization of LOS stabilization kinematics by virtual joints

In Figure 2-29, the schematics of realizing target tracking by virtual kinematic pairs is presented. Since target tracking is to keep LOS vector pointing to the target regardless of the base motion, this can be accomplished by connecting the LOS vector to target body using a virtual cylindrical joint which keeps the LOS vector pointing to target also freeing LOS roll motion. One additional joint is also required since target's angular orientation has no effect on gimbal motion, so the target and LOS connection is ended with a spherical joint at the center of the target to free target angular orientation.

With the described additional joints, gimbal structure in the form of a kinematic tree is transformed into a kinematic closure which can be solved numerically with the addition of base motion, LOS vector orientation for stabilization and target trajectory for target tracking.

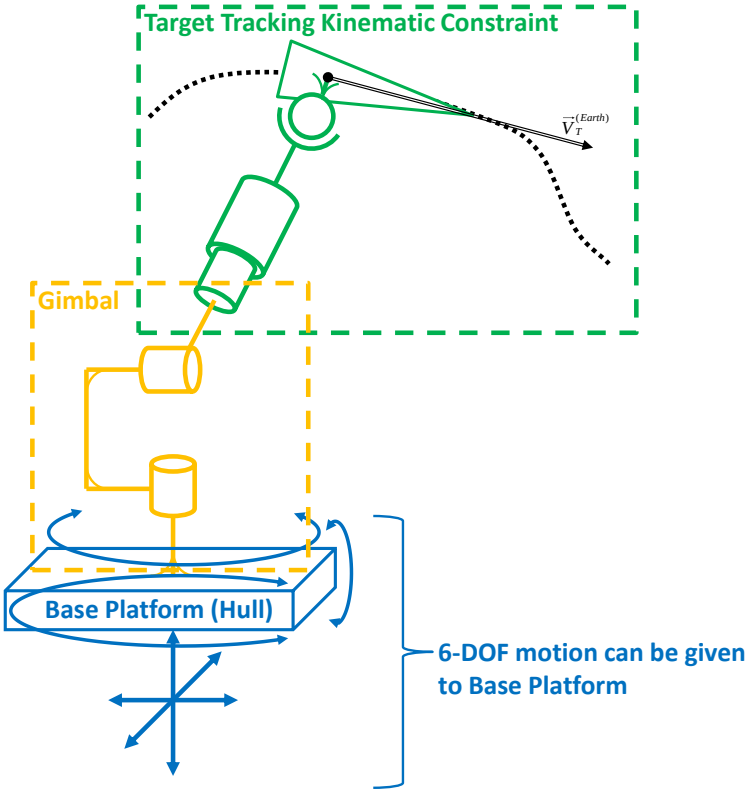

Figure 2-29: Realization of target tracking kinematics by virtual joints

CHAPTER 3

DYNAMICS OF 2-AXIS GIMBAL AND SYSTEM MODELING

3.1. Introduction

The kinematic relationships of gimbal motion presented in Chapter 2 are essential yet insufficient. Thus, it is essential to study the gimbal dynamics in order to develop a decoupling algorithm. In this section, rigid body dynamics for a two axis gimbal is discussed, later a method of approximating torque path transfer function through an identification process is given, and finally the overall modeled dynamics of the gimbal system is presented.

3.2. Dynamic Equations

Governing dynamics of bodies undergoing motion in three dimensional space can be represented as Newton-Euler equations [26] in body fixed coordinate frame located at center of mass as:

$$\begin{bmatrix} \Sigma\vec{F} \\ \Sigma\vec{T} \end{bmatrix} = \begin{bmatrix} m\bar{I} & 0 \\ 0 & \bar{J} \end{bmatrix} \begin{bmatrix} \overrightarrow{a_{CM}} \\ \vec{\alpha} \end{bmatrix} + \begin{bmatrix} 0 \\ \vec{\omega} \times \bar{J}\vec{\omega} \end{bmatrix} \tag{3.1}$$

Euler equations for elevation and traverse axes are selected to be written for body frames about gimbal axes intersection points as depicted in Figure 2-1. This configuration raises the requirement of using Newton-Euler equations in a more generic format where the center of the body fixed frame is not concentric with center of mass.

$$\begin{bmatrix} \Sigma\vec{F} \\ \Sigma\vec{T} \end{bmatrix} = \begin{bmatrix} m\bar{I} & -m\tilde{c} \\ m\tilde{c} & \bar{J} - m\tilde{c}\tilde{c} \end{bmatrix} \begin{bmatrix} \vec{a}_c \\ \vec{\alpha} \end{bmatrix} + \begin{bmatrix} m\vec{\omega} \times \left(\vec{\omega} \times \vec{c}\right) \\ \vec{\omega} \times \left(\bar{J} - m\tilde{c}\tilde{c}\right)\vec{\omega} \end{bmatrix} \tag{3.2}$$

Since the purpose is to obtain torque relations for a gimbal system, main focus is on the second row of the given equation.

$$\Sigma\vec{T} = m\tilde{c}\vec{a}_c + \left(\bar{J} - m\tilde{c}\tilde{c}\right)\vec{\alpha} + \vec{\omega}\times\left(\bar{J} - m\tilde{c}\tilde{c}\right)\vec{\omega} \tag{3.3}$$

In equation (3.3), the term $\bar{J} - m\tilde{c}\tilde{c}$ is actually parallel axis theorem implemented in three dimensional space, so one can use an equivalent inertia tensor instead.

The other additional term $m\tilde{c}\vec{a}_c$ is the effect of linear acceleration in rotational motion. For gimbal systems this term is generally named as static unbalance. This static unbalance term is a well understood effect in gimbal dynamics, [27] and [28]. In high performance stabilization and target tracking applications, eliminating the effect of static unbalance is highly sought. This goal can be achieved by arranging weight distribution of gimbal frames accordingly to decrease resultant torque values, which is the case for the studied gimbal too. The mass center of elevation frame was designed to be on the elevation axis and resultant mass center of both elevation and traverse axes was designed to be on traverse axis to ensure that forces due to linear accelerations have no effect in torque relations. The locations for individual and combined mass centers can be seen in Figure 3-1, Figure 3-2 and Figure 3-3.

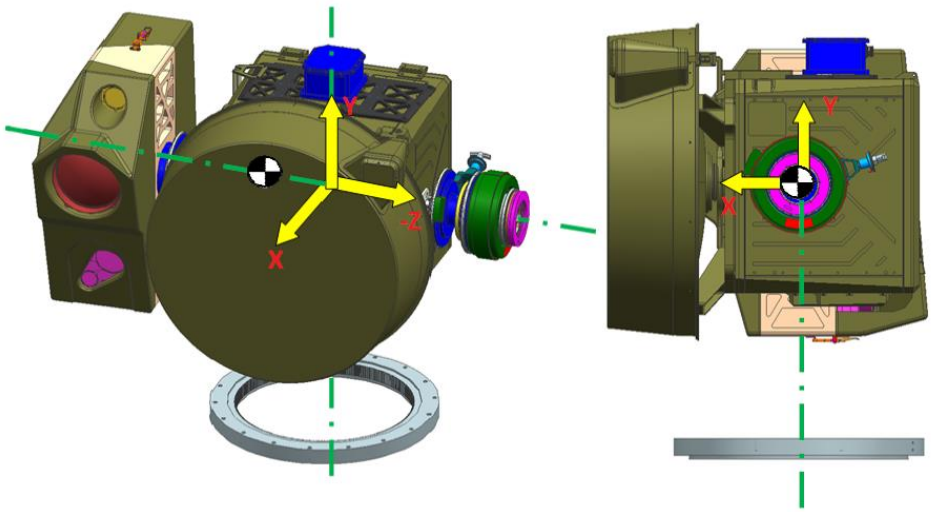

Figure 3-1: Position of elevation frame center of mass on elevation axis (Photo courtesy of ASELSAN Inc.)

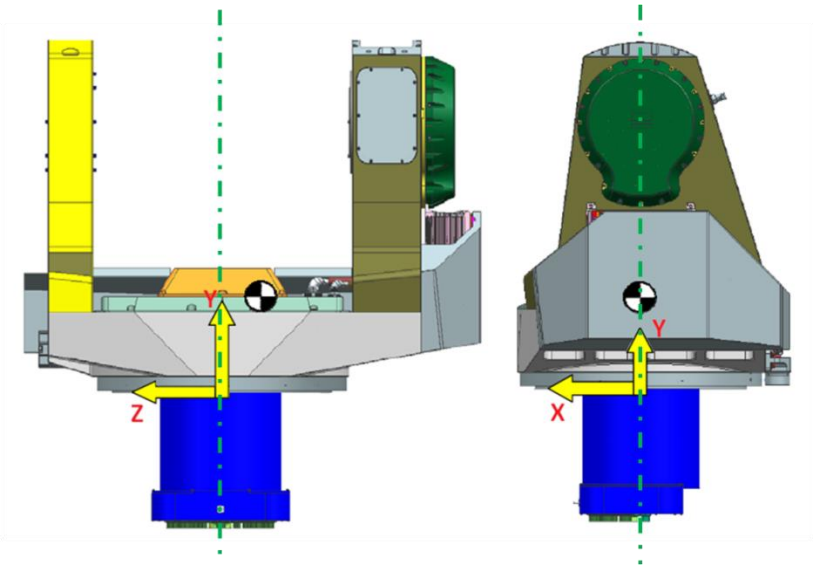

Figure 3-2: Position of traverse frame center of mass with respect to traverse axis (Photo courtesy of ASELSAN Inc.)

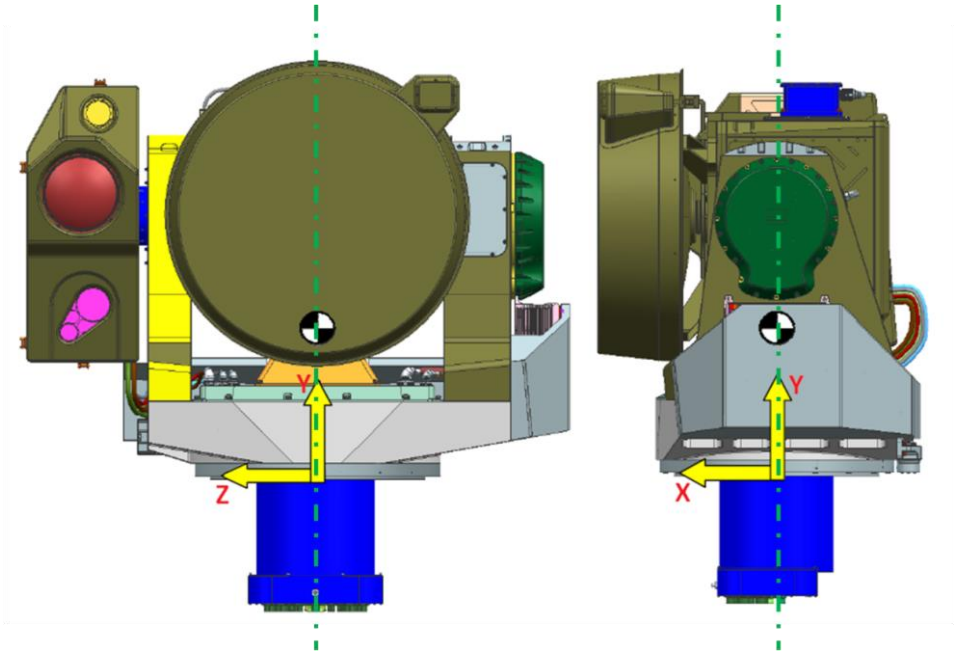

Figure 3-3: Position of elevation and traverse frames resultant center of mass on traverse axis (Photo courtesy of ASELSAN Inc.)

After these clarifications, the Euler equations to be used for two gimbal frames can be represented in a simpler manner:

$$\Sigma\vec{T} = \bar{J}\vec{\alpha} + \vec{\omega} \times \bar{J}\vec{\omega} \tag{3.4}$$

3.2.1. Dynamic Equations of Elevation Axis

Elevation frame Euler equation in elevation body frame about gimbal axes intersection point can be written as:

$$\begin{aligned}
&\vec{T}_E^{(E)} = \bar{J}_E \vec{\alpha}_E^{(E)} + \vec{\omega}_E^{(E)} \times \bar{J}_E \vec{\omega}_E^{(E)} \\
&= \begin{bmatrix} T_{Ex} \\ T_{Ey} \\ T_{Ez} \end{bmatrix} = \begin{bmatrix} J_{Exx}\alpha_{Ex} + J_{Exy}\alpha_{Ey} + J_{Exz}\alpha_{Ez} \\ J_{Exy}\alpha_{Ex} + J_{Eyy}\alpha_{Ey} + J_{Eyz}\alpha_{Ez} \\ J_{Exz}\alpha_{Ex} + J_{Eyz}\alpha_{Ey} + J_{Ezz}\alpha_{Ez} \end{bmatrix} \\
&+\omega_{Ey}\left(J_{Exz}\omega_{Ex} + J_{Eyz}\omega_{Ey} + J_{Ezz}\omega_{Ez}\right) - \omega_{Ez}\left(J_{Exy}\omega_{Ex} + J_{Eyy}\omega_{Ey} + J_{Eyz}\omega_{Ez}\right) \\
&-\omega_{Ex}\left(J_{Exz}\omega_{Ex} + J_{Exy}\omega_{Ey} + J_{Exz}\omega_{Ez}\right) + \omega_{Ez}\left(J_{Exx}\omega_{Ex} + J_{Exy}\omega_{Ey} + J_{Exz}\omega_{Ez}\right) \\
&+\omega_{Ex}\left(J_{Exy}\omega_{Ex} + J_{Eyy}\omega_{Ey} + J_{Exz}\omega_{Ez}\right) - \omega_{Ey}\left(J_{Exx}\omega_{Ex} + J_{Exy}\omega_{Ey} + J_{Exz}\omega_{Ez}\right)
\end{aligned} \tag{3.5}$$

Given equation's third row is of significant importance for elevation frame since it is the controlled axis which actuates the gimbal. One can also include motor torque as an external input at this point as:

$$\begin{aligned}
&J_{Ezz}\alpha_{Ez} = T_{Emotor} - J_{Exz}\alpha_{Ex} - J_{Eyz}\alpha_{Ey} \\
&-\omega_{Ex}\left(J_{Exy}\omega_{Ex} + J_{Eyy}\omega_{Ey} + J_{Exz}\omega_{Ez}\right) + \omega_{Ey}\left(J_{Exx}\omega_{Ex} + J_{Exy}\omega_{Ey} + J_{Exz}\omega_{Ez}\right)
\end{aligned} \tag{3.6}$$

The term on the left hand side of this equation is the output desired to be controlled and motor torque is the control input, so rest of the torque terms appearing in this equation are torque disturbances acting on the body.

$$J_{Ezz}\alpha_{Ez} = T_{Emotor} - T_{Edist} \tag{3.7}$$

where;

$$\begin{aligned}
&T_{Edist} = J_{Exz}\alpha_{Ex} + J_{Eyz}\alpha_{Ey} + \omega_{Ex}\left(J_{Exy}\omega_{Ex} + J_{Eyy}\omega_{Ey} + J_{Exz}\omega_{Ez}\right) \\
&-\omega_{Ey}\left(J_{Exx}\omega_{Ex} + J_{Exy}\omega_{Ey} + J_{Exz}\omega_{Ez}\right)
\end{aligned} \tag{3.8}$$

Disturbance torque acting on the elevation frame; which is essentially summation of moments induced due to asymmetry and gyroscopic moments acting on the

controlled axis; is called as geometric coupling torque. This is due to the fact that this value is heavily related to geometric shape and mass distribution of the body which defines the distribution of inertia tensor. This resulting disturbance torque manifests itself as governing kinematic quantities become nonzero when elevation frame undergoes a rotational movement.

3.2.2. Dynamic Equations of Traverse Axis

Traverse frame Euler equation in traverse body frame about gimbal axes intersection point can be written as:

$$\begin{aligned}
&\vec{T}_T^{(T)} = \bar{J}_T \vec{\alpha}_T^{(T)} + \vec{\omega}_T^{(T)} \times \bar{J}_T \vec{\omega}_T^{(T)} \\
&= \begin{bmatrix} T_{Tx} \\ T_{Ty} \\ T_{Tz} \end{bmatrix} = \begin{bmatrix} J_{Txx}\alpha_{Tx} + J_{Txy}\alpha_{Ty} + J_{Txz}\alpha_{Tz} \\ J_{Txy}\alpha_{Tx} + J_{Tyy}\alpha_{Ty} + J_{Tyz}\alpha_{Tz} \\ J_{Txz}\alpha_{Tx} + J_{Tyz}\alpha_{Ty} + J_{Tzz}\alpha_{Tz} \end{bmatrix} \\
&\begin{bmatrix} +\omega_{Ty}\left(J_{Txz}\omega_{Tx} + J_{Tyz}\omega_{Ty} + J_{Tzz}\omega_{Tz}\right) - \omega_{Tz}\left(J_{Txy}\omega_{Tx} + J_{Tyy}\omega_{Ty} + J_{Tyz}\omega_{Tz}\right) \\ -\omega_{Tx}\left(J_{Txz}\omega_{Tx} + J_{Txy}\omega_{Ty} + J_{Txz}\omega_{Tz}\right) + \omega_{Tz}\left(J_{Txx}\omega_{Tx} + J_{Txy}\omega_{Ty} + J_{Txz}\omega_{Tz}\right) \\ +\omega_{Tx}\left(J_{Txy}\omega_{Tx} + J_{Tyy}\omega_{Ty} + J_{Txz}\omega_{Tz}\right) - \omega_{Ty}\left(J_{Txx}\omega_{Tx} + J_{Txy}\omega_{Ty} + J_{Txz}\omega_{Tz}\right) \end{bmatrix}
\end{aligned} \tag{3.9}$$

Likewise to elevation axis, given equation's second row is of significant importance for traverse frame since it is the controlled axis to actuate the gimbal. Again, one can also include motor torque as an external input at this point as:

$$\begin{aligned}
&J_{Tyy}\alpha_{Ty} = T_{Tmotor} - J_{Txz}\alpha_{Tx} - J_{Tyz}\alpha_{Tz} \\
&+\omega_{Tx}\left(J_{Txz}\omega_{Tx} + J_{Txy}\omega_{Ty} + J_{Txz}\omega_{Tz}\right) - \omega_{Tz}\left(J_{Txx}\omega_{Tx} + J_{Txy}\omega_{Ty} + J_{Txz}\omega_{Tz}\right)
\end{aligned} \tag{3.10}$$

The term on the left hand side of this equation is the output desired to be controlled and motor torque is the control input, so rest of the torque terms appearing is the geometric coupling disturbance torque acting on the traverse body.

$$J_{Tyy}\alpha_{Ty} = T_{Tmotor} - T_{Tdist} \tag{3.11}$$

where;

$$T_{Tdist} = J_{Txz}\alpha_{Tx} + J_{Tyz}\alpha_{Tz} - \omega_{Tx}\left(J_{Txz}\omega_{Tx} + J_{Txy}\omega_{Ty} + J_{Txz}\omega_{Tz}\right) + \omega_{Tz}\left(J_{Txx}\omega_{Tx} + J_{Txy}\omega_{Ty} + J_{Txz}\omega_{Tz}\right) \quad (3.12)$$

3.2.3. Dynamic Interaction Between Two Axes and Overall Dynamics of 2-axis Gimbal System

In the discussion of dynamic equations up to this point, interaction between two gimbal frames is not mentioned. In Figure 3-4, it can be observed that resultant torques in x and y axes of elevation body also have components on traverse axis, also suggesting an opposite torque component acting on traverse body through Newton's third law. This argument is logical in a sense that actuation of elevation body in the direction of traverse axis is performed as rotating the traverse body by traverse motor.

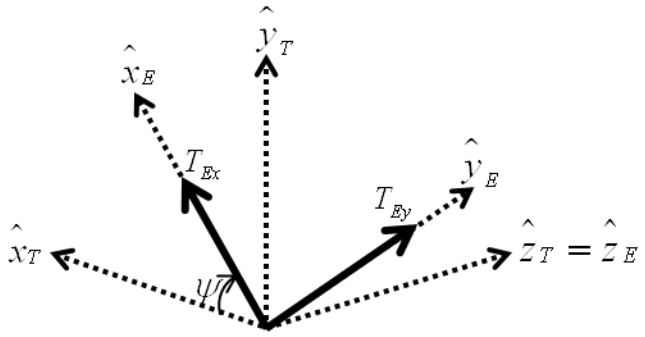

Figure 3-4: Elevation body x and y axis torque components

The explained additional disturbance torque acting on the traverse body can be expressed using equation (3.5) and elevation axis relative angle as:

$$
\begin{aligned}
&T_{TdistE} = T_{Ex}\sin\psi + T_{Ey}\cos\psi \\
&= \sin\psi\Big[J_{Exx}\alpha_{Ex} + J_{Exy}\alpha_{Ey} + J_{Exz}\alpha_{Ez} \\
&+\omega_{Ey}\left(J_{Exz}\omega_{Ex} + J_{Eyz}\omega_{Ey} + J_{Ezz}\omega_{Ez} \right) \\
&-\omega_{Ez}\left(J_{Exy}\omega_{Ex} + J_{Eyy}\omega_{Ey} + J_{Eyz}\omega_{Ez} \right)\Big] \\
&+\cos\psi\Big[J_{Exy}\alpha_{Ex} + J_{Eyy}\alpha_{Ey} + J_{Eyz}\alpha_{Ez} \\
&-\omega_{Ex}\left(J_{Exz}\omega_{Ex} + J_{Exy}\omega_{Ey} + J_{Exz}\omega_{Ez} \right) \\
&+\omega_{Ez}\left(J_{Exx}\omega_{Ex} + J_{Exy}\omega_{Ey} + J_{Exz}\omega_{Ez} \right)\Big]
\end{aligned}
\tag{3.13}
$$

The equation for traverse axis torque relations given in the previous section needs to be updated with the explained additional disturbance torque as:

$$
J_{Tyy}\alpha_{Ty} = T_{Tmotor} - T_{Tdist} - T_{TdistE} \tag{3.14}
$$

3.3. System Identification

After the system model is constructed for simulations (presented in the next section in its final form), it was observed that there was a slight difference between gyro speed closed loop step responses of the model and the real system with same closed loop controller parameters (detail about closed loop feedback controllers can be found in Chapter 4) as can be seen in Figure 3-5. Even though, a considerable resemblance existed between system and model, the difference in step response waveforms suggested that there was a missing dynamic effect which results in two different closed loop system responses. This unmatched closed loop dynamics also suggests unmatched disturbance rejection characteristics which cannot be tolerated in this study since the utmost objective is to construct a method to increase platform motion disturbance rejection.

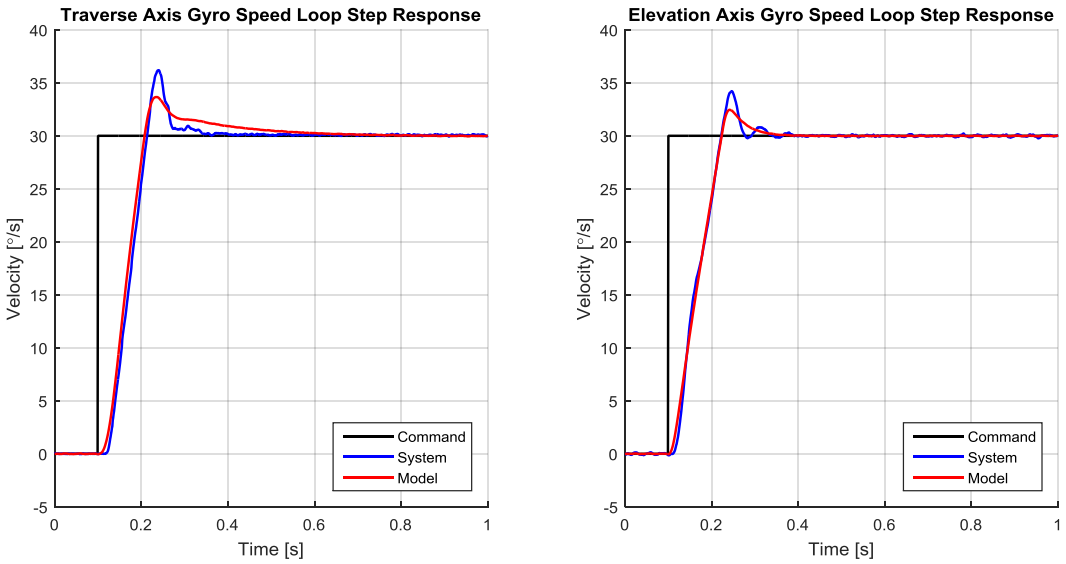

Figure 3-5: Real system vs. model closed loop step responses

In the model, torque path from motor torque to body angular velocity was first modeled as only an inertia term and an integrator, whereas results of torque frequency sweep tests tells a completely different story as can be seen in Figure 3-6. To resolve this discrepancy between torque path transfer functions of the system and the model, a frequency domain based identification algorithm was performed. Although different techniques can be found in literature; applications of well known methods on a stabilized gimbal system can be found in [29]. To stay in the scope of this study, a simpler and more straightforward method of approximating the frequency response functions in the form of known transfer functions via non linear least squares optimization was selected.

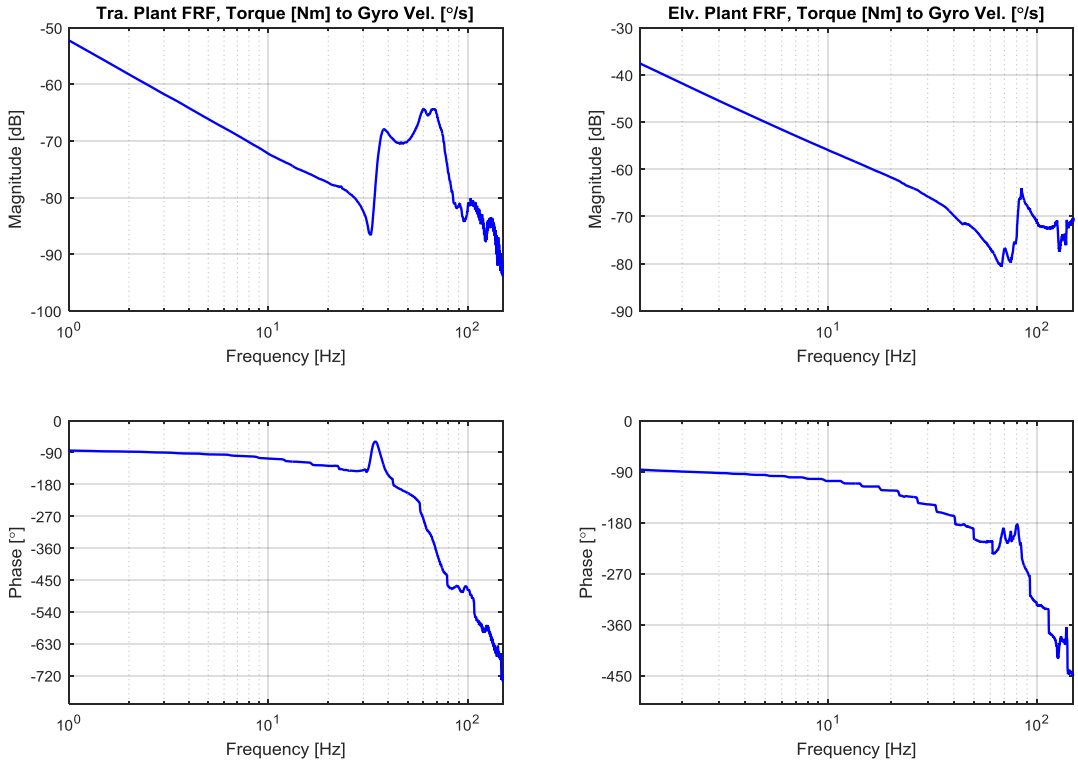

Figure 3-6: Plant frequency response functions

Shapes of the frequency response functions suggests that plant transfer functions can be considered as composed of an inertia term, a transfer function for high frequency resonance/anti-resonance behavior (mostly due to flexibility of mechanical structure) and time delay, all of which can separately be identified. The form of approximate plant transfer function in Laplace domain as multiplication of described terms is given below:

$$G_{Plant}(s) \cong \frac{1}{Js} G_{Flex}(s) e^{st_{delay}} \tag{3.15}$$

The easiest term to identify is the inertia component which can be calculated from response at lowest frequency data in hand. The experimentally found inertia terms were found to be very close to inertia tensor about gimbal axes intersection point obtained from CAD software which are:

$$\bar{J}_T^{CAD} = \begin{bmatrix} 58.3 & -2.1 & -0.4 \\ -2.1 & 36.9 & -7.2 \\ -0.4 & -7.2 & 38.0 \end{bmatrix} kgm^2 \text{ and } \bar{J}_E^{CAD} = \begin{bmatrix} 29.9 & 0.1 & -0.1 \\ 0.1 & 29.1 & -0.9 \\ -0.1 & -0.9 & 9.3 \end{bmatrix} kgm^2$$

$$J_{TraAxis}^{CAD} = J_{Tyy}^{CAD} + J_{Eyy}^{CAD} = 66 kgm^2 \text{ and } J_{TraAxis}^{Exp.} = 65.1596 kgm^2$$

$$J_{ElvAxis}^{CAD} = J_{Ezz}^{CAD} = 9.3 kgm^2 \text{ and } J_{TraAxis}^{Exp.} = 9.5975 kgm^2$$

Although experimental values for inertia terms at gimbal axes were obtained, the distribution of traverse axis equivalent inertia amongst individual gimbal frames could not be identified from FRFs. In addition, as this study centered on gimbal dynamics in three dimensional space, all the terms in inertia tensors have significant importance. To obtain whole inertia tensor experimentally, a much more sophisticated experimental process requiring additional sensors placed on the gimbal system which is beyond the scope of this study [28]. CAD program results of inertia tensors are utilized in simulations since results for axis equivalent inertia values are found to be within 1.3% and 3.1% of experimental values for traverse and elevation respectively. This gives a clue about the accuracy of the CAD outputs, similar results could be achieved for other inertia terms if measured experimentally.

The next step is to obtain approximations for high frequency behavior of the system. Considering time delay component in plant transfer function is omitted at this step, one can assume that system exhibits a minimum phase behavior and use only magnitude responses for filter approximations. To identify transfer functions related to flexible modes, nonlinear linear least squares approximation was chosen and it was realized by using MATLAB Optimization toolbox. To aid and restrict the numerical process on finding stable and minimum phase transfer function results, it was chosen to approximate resonance and anti-resonance peaks in the form of multiple cascaded bi-quad filters(which are composed of two zeros and two poles with different damping ratios for resonance and anti-resonance) rather than a high order transfer function in canonical form. In detail, results are assured to be stable and minimum phase by restricting damping ratio and natural frequency parameters to only positive real number. This constraint makes all the poles and zeros found for

each bi-quad filter to be in the left hand plane as a result of well-known Routh criterion. In addition, search parameters were also confined at the upper bound in order not to obtain high frequency dynamics out of the range of available system data. The format of the bi-quad filters can be found below.

$$G_{Bi-quad}(s) = \frac{\omega_{nD}{}^2 \left(s^2 + 2\xi_N \omega_{nN} s + \omega_{nN}{}^2 \right)}{\omega_{nN}{}^2 \left(s^2 + 2\xi_D \omega_{nD} s + \omega_{nD}{}^2 \right)} \tag{3.16}$$

So by using nonlinear least squares approximation, for each axis four cascaded bi-quad filters were fitted to system response in the form;

$$G_{Flex}(s) = G_{Bi-quad\,\#1}(s) G_{Bi-quad\,\#2}(s) G_{Bi-quad\,\#3}(s) G_{Bi-quad\,\#4}(s) \tag{3.17}$$

using the initial guesses for parameters given in Table 3-1. The parameters obtained for bi-quad filters can be found Table 3-2. The resultant, frequency response functions of the obtained bi-quad filters and plant without inertia components can be found in Figure 3-8.

Table 3–1: Initial Guesses for bi-quad filter approximations

Tra.	Denominator		Numerator	
	f_n (Hz)	ξ	f_n (Hz)	ξ
Bi-quad #1	23	0.5	32	0.5
Bi-quad #2	38	0.5	43	0.5
Bi-quad #3	66	0.5	89	0.5
Bi-quad #4	109	0.5	140	0.5
Elv.	Denominator		Numerator	
	f_n (Hz)	ξ	f_n (Hz)	ξ
Bi-quad #1	70	0.5	67	0.5
Bi-quad #2	75	0.5	84	0.5
Bi-quad #3	124	0.5	127	0.5
Bi-quad #4	138	0.5	140	0.5

Table 3–2: Obtained bi-quad filter parameters for modeling structural flexibility

Tra.	Denominator		Numerator	
	f_n (Hz)	ξ	f_n (Hz)	ξ
Bi-quad #1	36.7159	0.0521	32.8767	0.0411
Bi-quad #2	65.2224	0.1476	84.6304	0.0941
Bi-quad #3	74.6536	0.1225	149.9905	1.7392
Bi-quad #4	120.8152	0.2176	150.0000	0.9117
Elv.	Denominator		Numerator	
	f_n (Hz)	ξ	f_n (Hz)	ξ
Bi-quad #1	83.2987	0.0342	78.5533	0.0456
Bi-quad #2	73.8979	0.2042	66.2427	0.1178
Bi-quad #3	125.9250	0.0138	127.1698	0.0135
Bi-quad #4	150.0000	0.1242	134.2688	0.1751

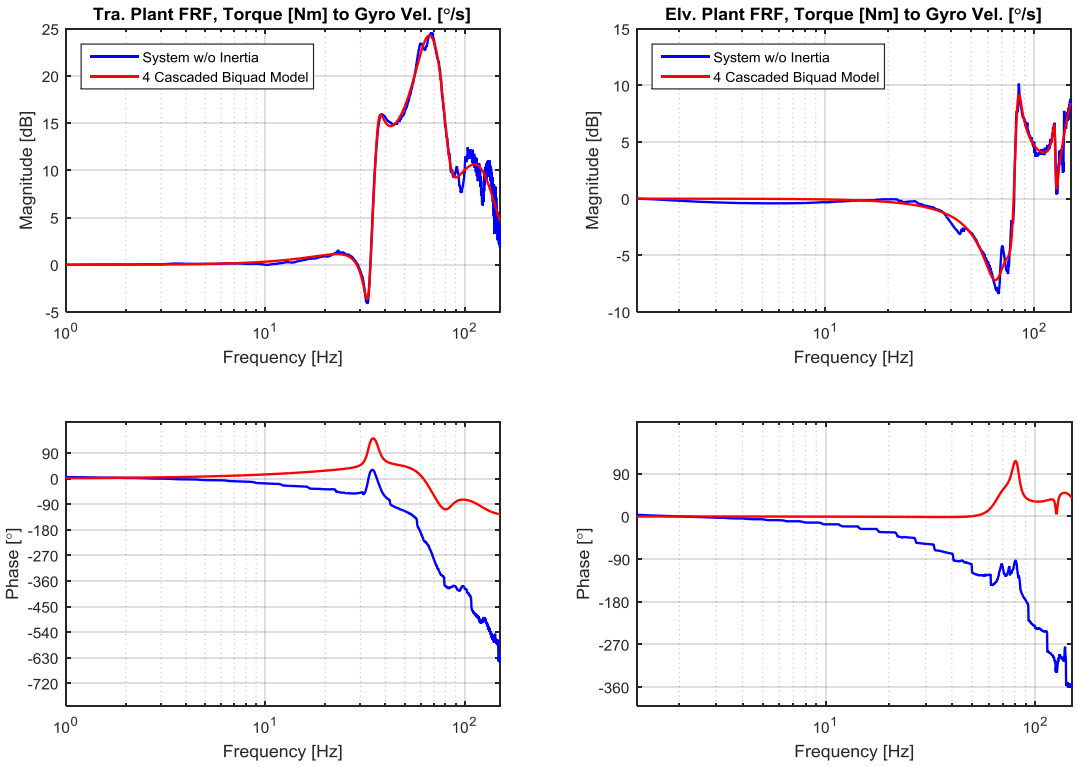

Figure 3-7: FRFs of plant without inertia versus bi-quad filter approximations.

The phase difference differences observable in Figure 3-7 are due to time delay in real system, the next step is to determine these time delay values for different axes. For this purpose, nonlinear least squares approximation was used again on phase

responses as the bi-quad filter parameters kept constant. Initial guesses for time delay values were set as 3 milliseconds for both axes, and later found as 8.988 milliseconds for traverse axis, and 6.9164 milliseconds for elevation axis. The result of approximated time delay can be seen in Figure 3-8. In the same figure, one can also observe that the minimum phase assumption for contribution of flexible modes is justified as only magnitude responses were utilized for their approximation which resulted in consistent phase responses.

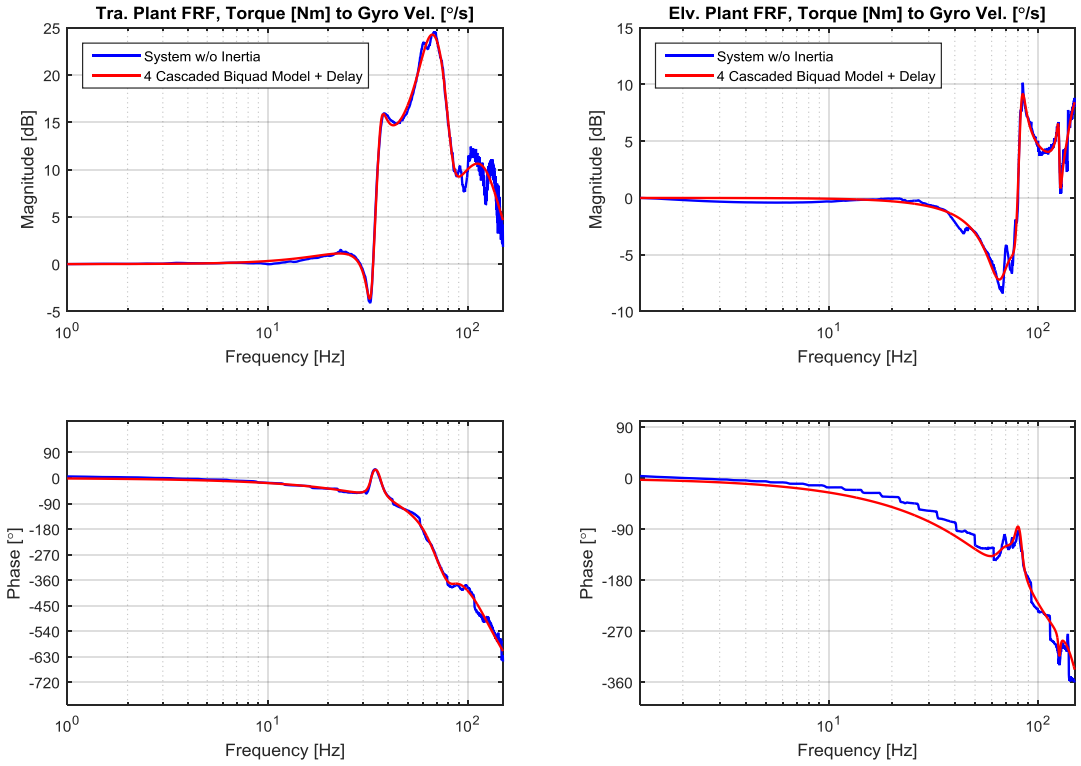

Figure 3-8: FRF of plant without inertia versus time delay and bi-quad filter approximations.

Combining bi-quad filters and time delay, overall approximations to plant frequency response functions are given in Figure 3-9.

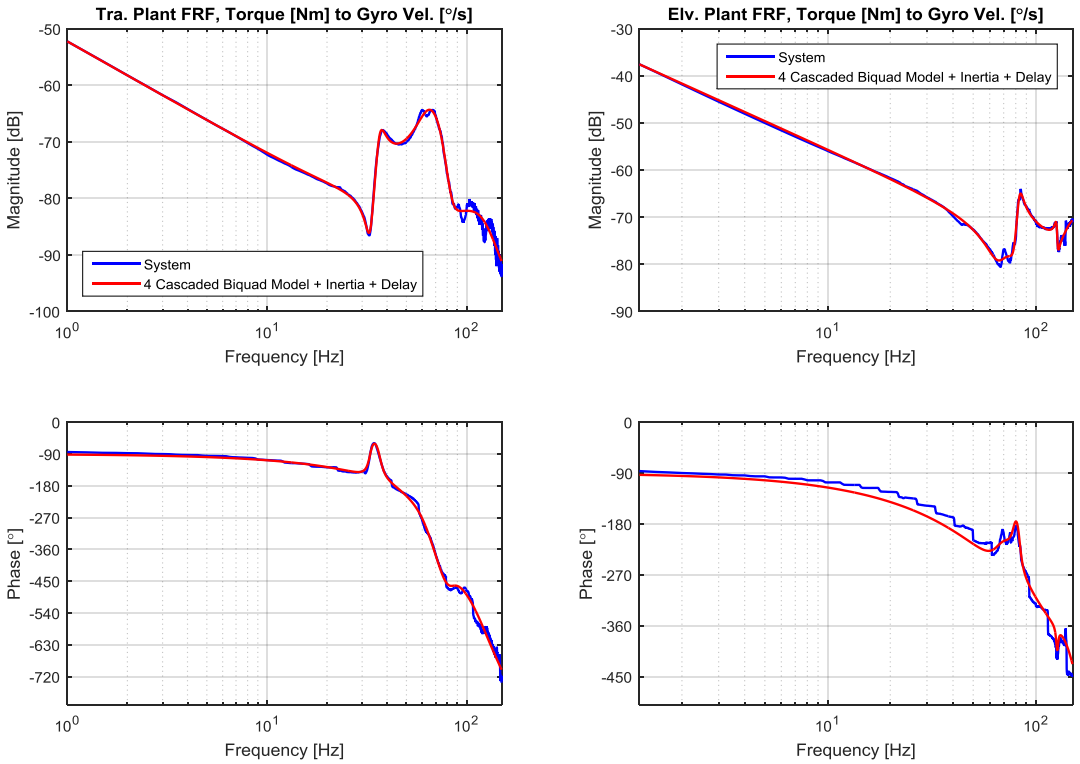

Figure 3-9: FRFs of plant and identified transfer function

Bi-quad filter and time delay parameters were incorporated into system model in the form of continuous time transfer functions placed at motor torque paths(can be seen in Figure 3-12) for each axis in the form of blocks shown in Figure 3-10.

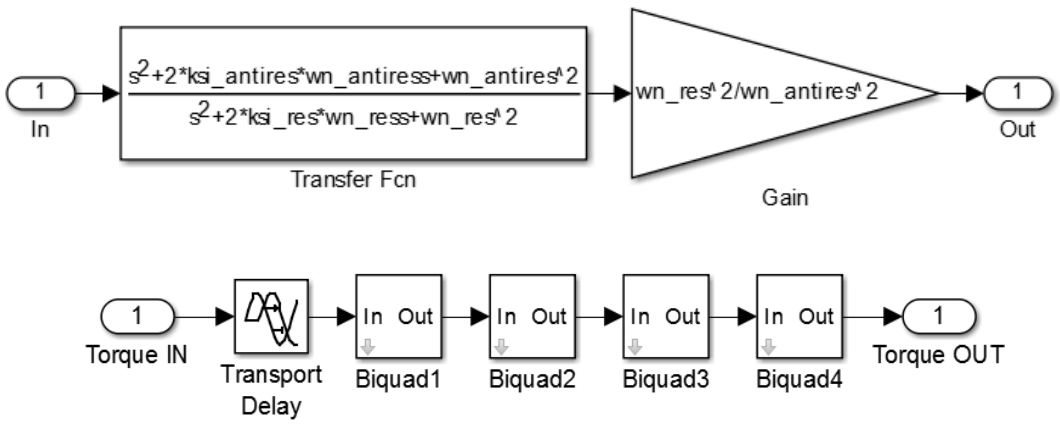

Figure 3-10: Bi-quad filter and combined transfer function models constructed in MATLAB Simulink

After addition of flexible modes and time delay, a considerable increase in the similarity between system and model step responses was achieved as shown in Figure 3-11.

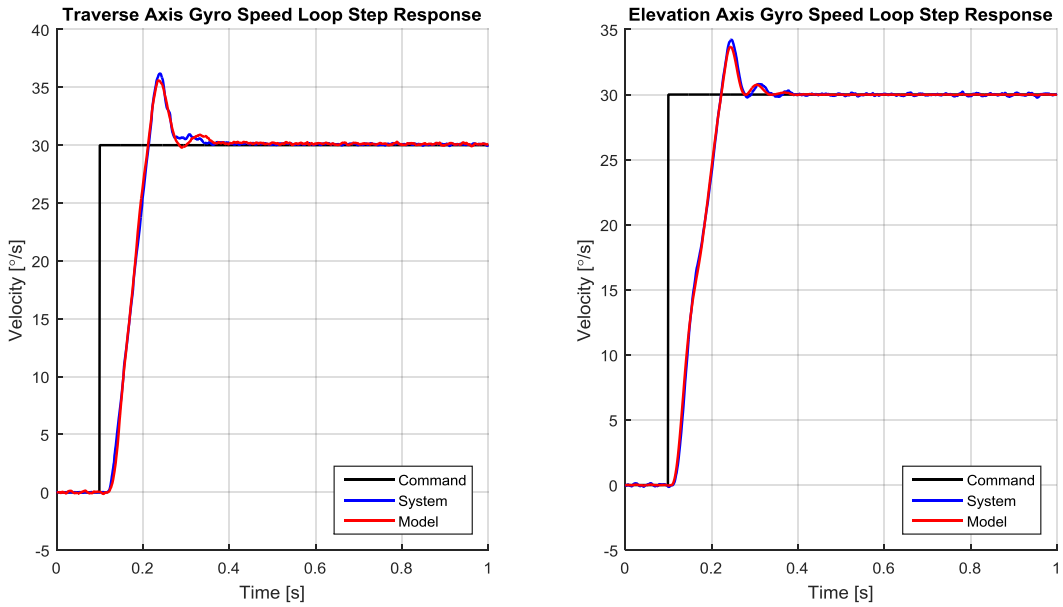

Figure 3-11: Real system vs. model closed loop step responses after identification process

3.4. System Dynamic Model

All the outcomes obtained up to this point; namely dynamic torque equations (3.7), (3.8), (3.12), (3.14); were combined into one diagram; given in Figure 3-12; to represent internal dynamics of the two axis gimbal system. The diagram is constructed to show certain variables in vector form (shown as bold lines) in order not complicate the representation beyond intelligibility. For the same purpose, geometric coupling torques are represented similar to Euler equations in vector form with exclusion of inertia terms at controlled axes which are later incorporated in the calculation of body angular accelerations.

In the given diagram, torque disturbances acting on individual axes can clearly be identified as subtraction operations performed on motor torque paths until they reach inertia terms. Remark that kinematic coupling torque explained in Chapter 2 cannot be found in this diagram since it is not an actual disturbance torque input to the

traverse axis, rather it is a non-zero torque requirement that the controller must generate in order to keep LOS stabilized when LOS vector is not orthogonal to traverse axis and platform undergoes an angular motion. Thus it can be thought as a "pseudo" disturbance torque on the controller also described in Chapter 2.

In addition, LOS rate gyro outputs can be found in the diagram. These two outputs are utilized as sensor feedbacks for LOS stabilization controller and their noise characteristics are included in the model in the form of added time series signals which were collected from original system in a motionless state. The model constructed in MATLAB Simulink for simulations can be seen in Figure 3-13.

One important aspect about gimbal dynamics represented so far is that dynamic interactions between platform and the gimbal are not considered since platforms tend to be very large and heavy compared to target tracking gimbals mounted on them (for the specific system studied, gimbal assembly to tracked platform weight ratio is approximately 1/100). So dynamic effects of gimbal motion on platform are considerably low, and platform motion is taken as pure kinematic constraints imposed on gimbal base for this study. But as the weight ratio approaches unity; i.e. large caliber gun turrets on tracked vehicles; given assumption would not hold and one should consider gimbal system and platform dynamic interactions as well.

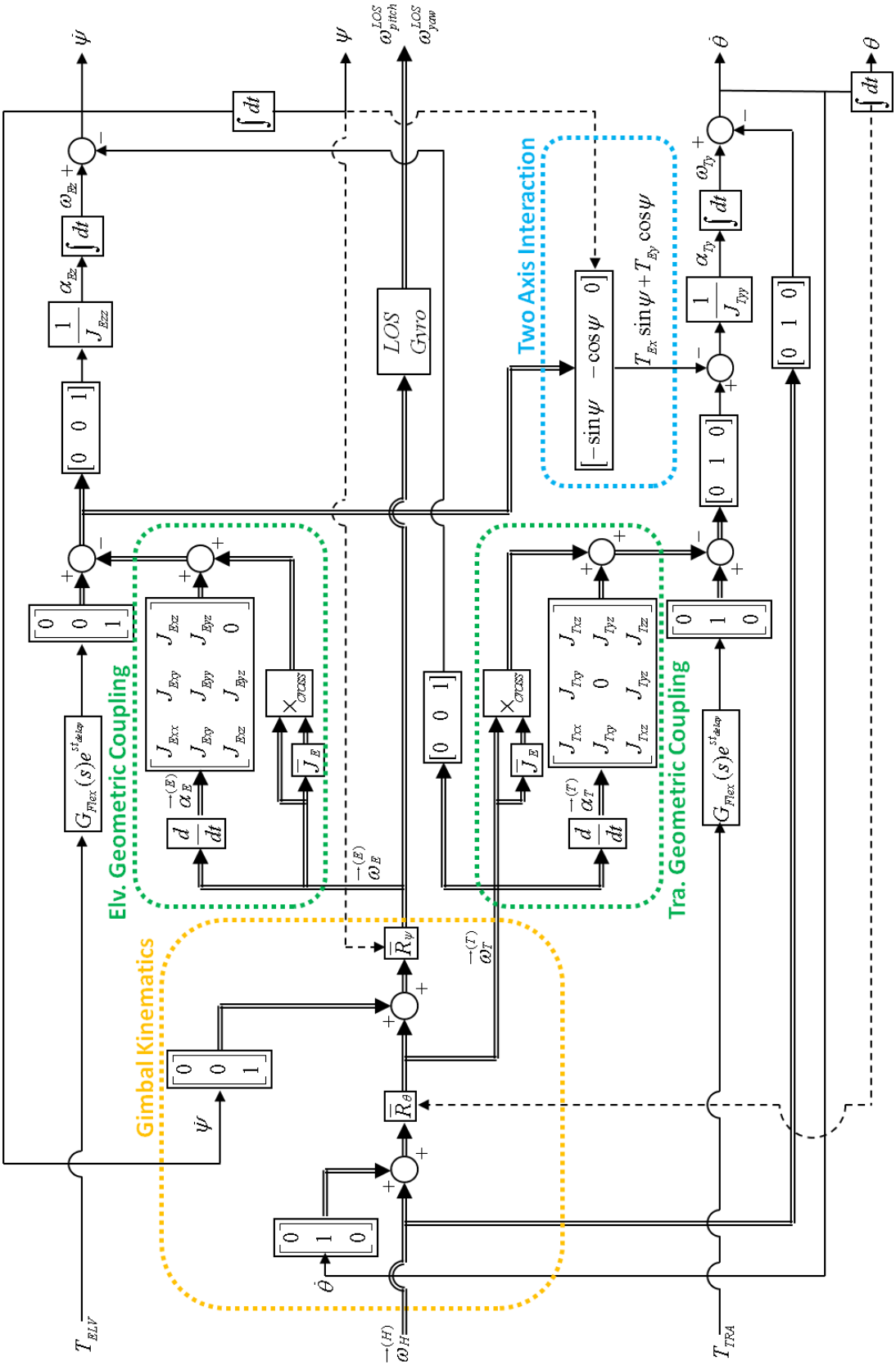

Figure 3-12: Dynamics of gimbal system with internal kinematics

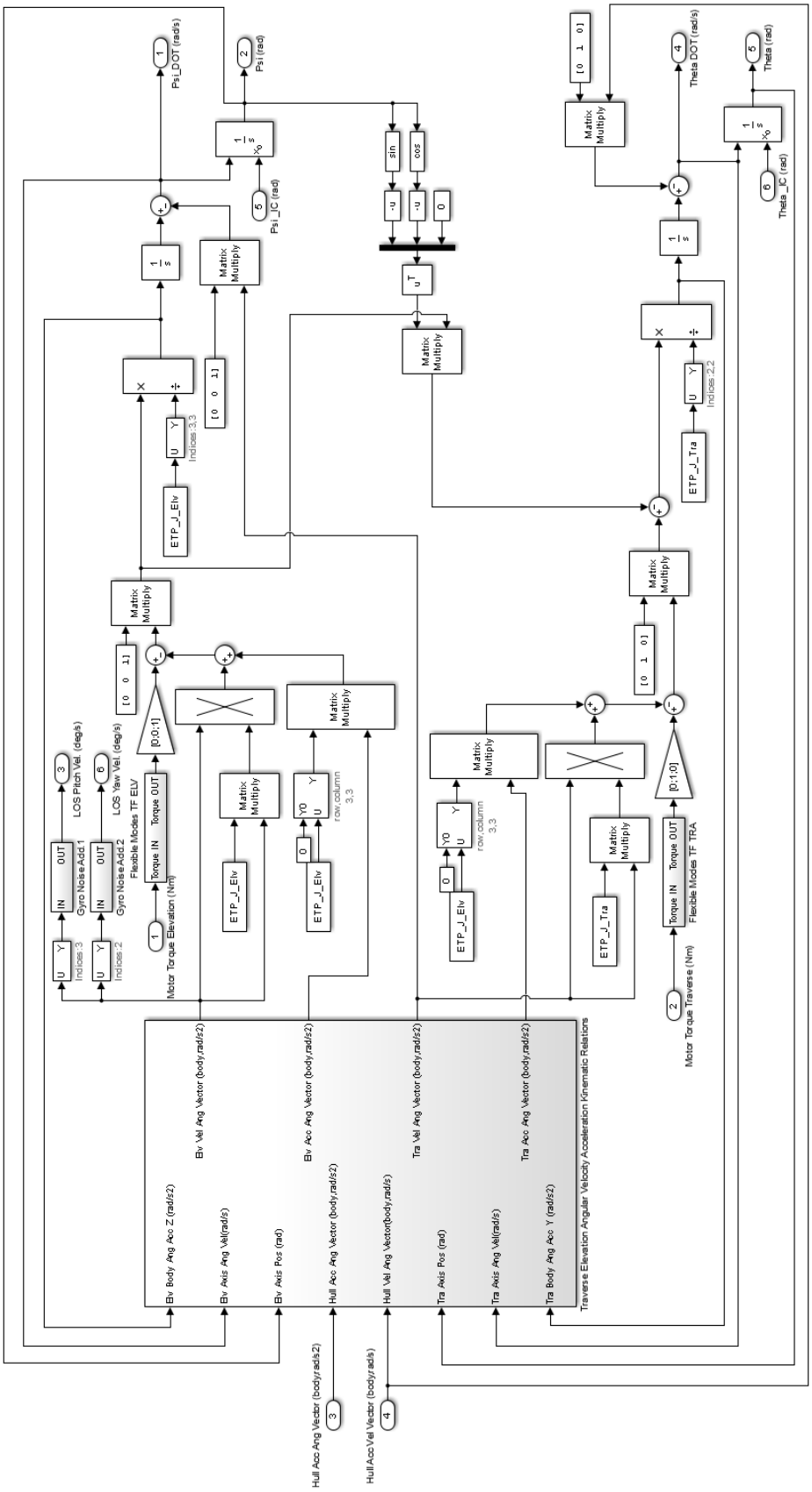

Figure 3-13: System model constructed in MATLAB Simulink

CHAPTER 4

PLATFORM MOTION DISTURBANCE DECOUPLING CONTROLLER

4.1. Introduction

In this chapter, the feedback control methods for LOS stabilization and target tracking are introduced. Then the devised method to decouple platform motion disturbances from the system is explained in detail.

4.2. Feedback Control Methods for LOS Stabilization and Target Tracking

The requirements for LOS stabilization and target tracking are to eliminate angular velocity components orthogonal to LOS vector and rotate LOS vector in order to keep its direction pointing to target respectively. These two requirements are linked to each other in a sense that there is an integral relation between controlled variables. In such circumstances a cascaded feedback control strategy with different forms is very desirable and used in a wide variety of high performance motion control applications. A sample block diagram of a cascaded PID control can be seen in Figure 4-1.

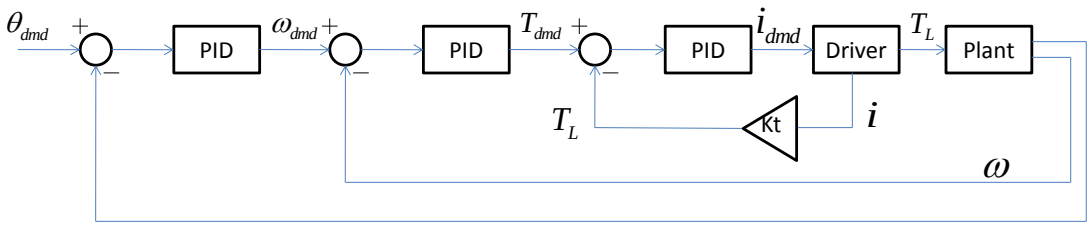

Figure 4-1: A sample cascaded PID control structure

Different studies utilizing cascaded feedback control on different subjects about LOS stabilization and target tracking can also be found in the literature [30].

For the specific gimbal system studied, feedback control is performed by an inner loop for LOS velocity control and an outer loop for target tracking which are to be discussed in the following sections.

4.2.1. LOS Velocity Feedback Control Structure

Gimbal LOS velocity control is performed by two separate PI feedback controllers for each axis. The schematics of the controllers for two axes can be seen in Figure 4-2.

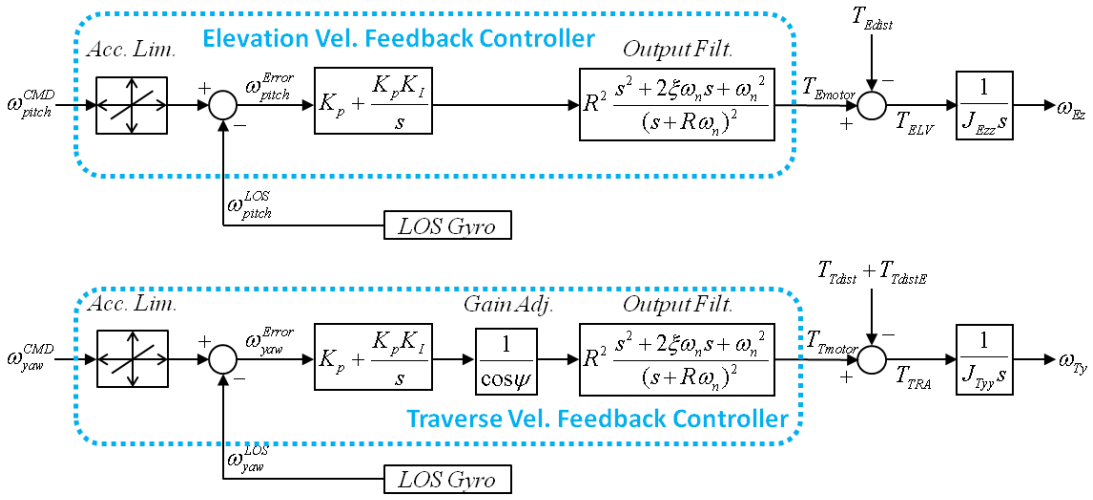

Figure 4-2: Gimbal LOS velocity feedback controllers

At first glance, three distinct features different than a conventional PI structure stand out. These are acceleration limiters at the command input, a gain adjustment component for the traverse axis, and output filters at the torque output.

Acceleration limiters are utilized to restrict the equivalent acceleration of the velocity commands into design requirements before torque output saturation occurs. They play a significant role in the final response of the system to given commands which require higher acceleration than system can handle.

The other component; gain adjustment for traverse axis; is utilized to keep total loop gain of the traverse axis constant with changing elevation axis angles. This adjustment is required since the control input is applied torque to the traverse axis and the desired output is the yaw rate of the LOS vector whose projection to traverse

axis changes with elevation angle. In addition, this adjustment can also be performed on the feedback path to project LOS yaw rate into traverse axis, but this configuration would create a contradiction with target tracking since outputs from target tracker are supplied in LOS frame.

The final extra component is the output filter which is used to suppress high frequency components of the torque command in order not to excite flexible modes of the system. Different forms of torque output filters can be found in [31]. For the specific system in this study, a modified bi-quad filter acting as a notch filter with adjustable damping ratio and high frequency magnitude response level is selected. The transfer function of the output filter is given below:

$$G_{\substack{Torque \\ Filter}}(s) = R^2 \frac{s^2 + 2\xi\omega_n s + \omega_n{}^2}{(s + R\omega_n)^2} \tag{4.1}$$

The parameters ω_n and ξ are used to control notch frequency and damping ratio of the filter and parameter R is used to control the high frequency region(higher than notch frequency) magnitude response. The notch part of this filter is utilized to attenuate frequency components of the torque output close to system flexible modes and high frequency magnitude response is shaped as to attenuate further noise (working like a low-pass filter). Another important aspect about using the given and other type of notch filters is that exact pole-zero cancellations and suppressing only one resonance peak at a specific frequency should be avoided [31] since that would severely damage robustness of the overall system. So in the design process, one can implement these filters to attenuate structural resonances in a wide frequency band using high damping ratio which unfortunately creates a challenge in obtaining satisfactory stability margins. The characteristics of described output filter are given in Figure 4-3.

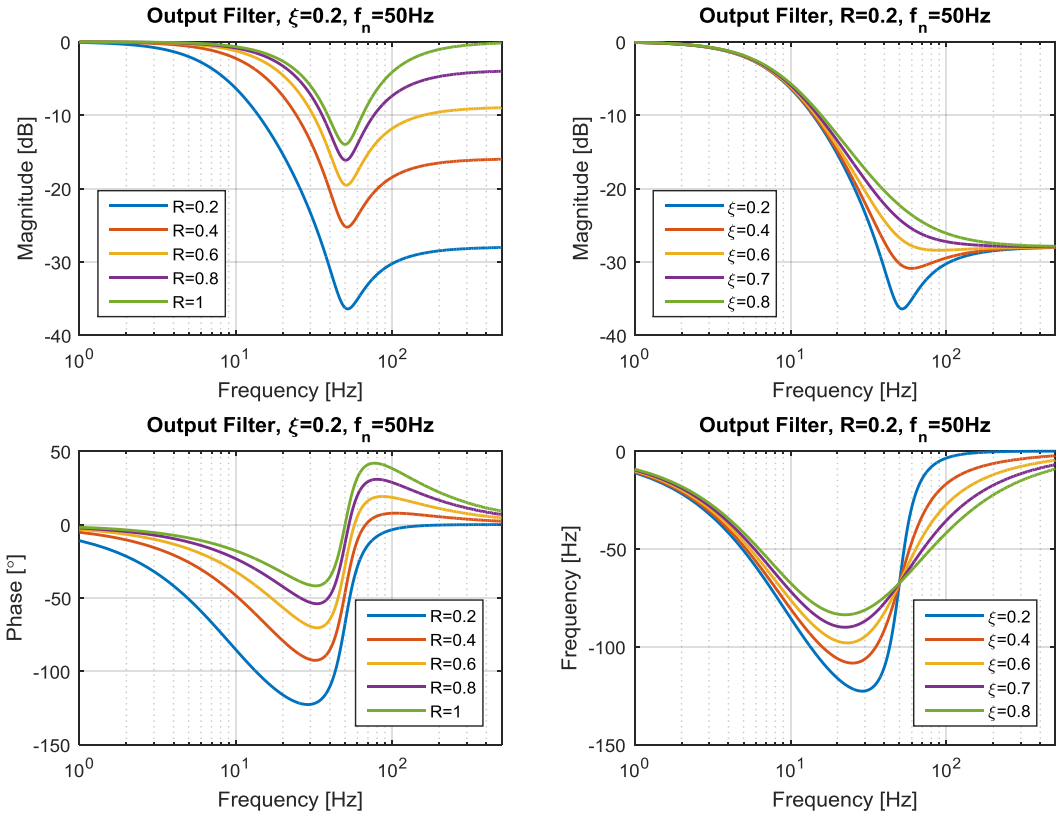

Figure 4-3: Torque output characteristics with changing parameters

Tuning for the velocity feedback control parameters were performed in frequency domain using plant frequency response functions which are obtained from torque frequency sweep tests on both axes. The design criteria for this tuning process were set as; gain margin higher than 6 dB, phase margin higher than 30°, and closed loop -3dB crossover bandwidth higher than 10 Hz without any amplification beyond. Later, the obtained parameters were tested on the system and minor adjustments were performed as fine tuning. Controller parameters obtained after tuning process are presented in Table 4-1. In addition, calculated open loop, closed loop and torque disturbance rejection characteristics with given parameters can be found in Figure 4-4 and Figure 4-5.

Table 4–1: LOS velocity controller parameters

Parameter	Axis	
	Traverse	Elevation
K_p	65.65	14.40
K_i	5.00	20.00
f_{notch} (Hz)	100.00	180.00
R_{notch}	0.80	0.50
ξ_{notch}	0.20	0.50

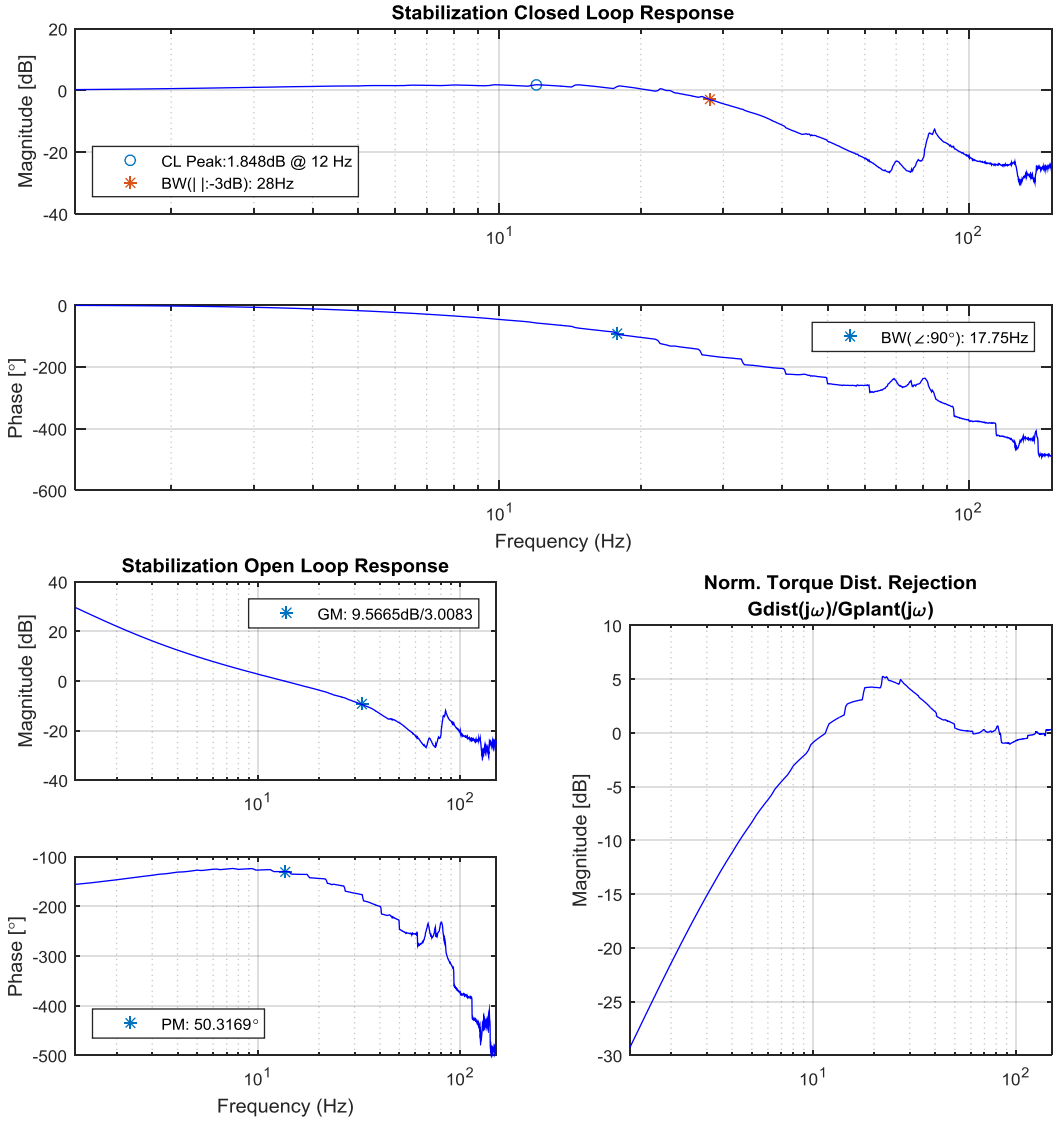

Figure 4-4: Elevation axis LOS velocity feedback closed loop, open loop and torque disturbance rejection characteristics

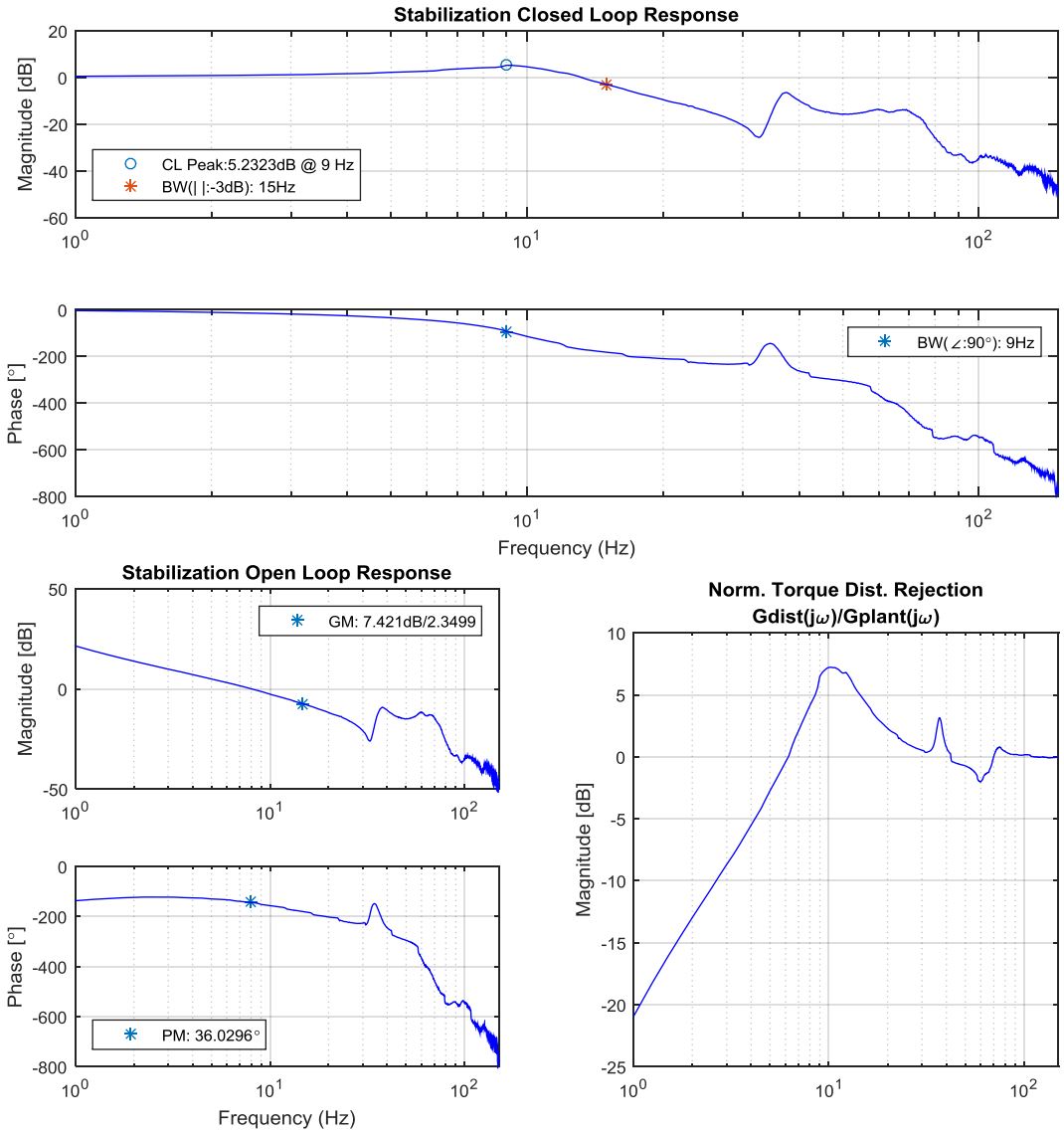

Figure 4-5: Traverse axis LOS velocity feedback closed loop, open loop and torque disturbance rejection characteristics

4.2.2. Target Tracking Control Structure

The target tracking operation is performed by a feedback loop with P control closed over the LOS velocity control loop with addition of velocity feed forward to increase performance for tracking dynamic targets. One important aspect is that this control loop differs from traditional feedback controllers in a way that error generation is not performed by the motion controller, but by the target tracker itself. So instead of feedbacks from plant, motion controller is directly fed with error and velocity feed forward signals. Hence target tracker can be thought as a combination of a feedback

sensor and a command generator. The schematics of described target tracking controllers can be found in Figure 4-6.

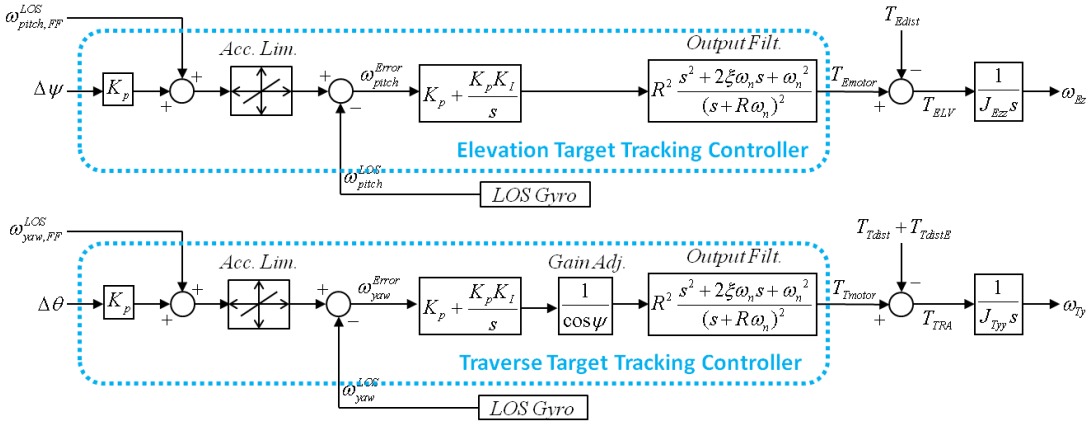

Figure 4-6: Target tracking feedback control structure with velocity feed forward

Due to complex target tracker dynamics; (i.e. changing resolution and time delay with target distance and size) the tuning of corresponding proportional gains for the original system was performed experimentally and proportionate gains for each axis are found as 4.13 for traverse axis and 5.30 for elevation axis as given in Table 4–2.

Table 4–2: Target tracking controller gains

Parameter	Axis	
	Traverse	Elevation
K_p	4.13	5.30

Tuning LOS stabilization and target tracking controllers only based on system model and simulations was also a possible option. However, such a method would alter disturbance rejection characteristics. Since this study is focused on a method to overcome described torque disturbances without imposing a burden on feedback controllers, parameters were used in simulations as they were tuned in the original system to establish a viable benchmark.

4.3. Platform Motion Disturbance Decoupling Control Structure

Given the controller structures for LOS stabilization and target tracking (Figure 4-2 and Figure 4-6), it can be seen that for the controller to produce motor torque, there should be a non-zero velocity error. This suggests that in the event of any torque disturbance, there should be an amount of error build-up in order the controller to take corrective action. The capability of the system to overcome such disturbances solely depends on the disturbance rejection characteristics of feedback controllers, unless additional methods are implemented. Devised method to overcome described platform motion disturbance comes into action at this point where the main goal is to eliminate torque disturbances before any error builds up in system outputs.

The platform motion decoupling controller is designed to calculate kinematic coupling torque requirement for traverse axis and geometric coupling torques for both axes using gimbal angles and platform angular motion sensors as if gimbal is stabilizing the LOS vector. Then the calculated torque values are added with outputs of feedback controllers. The reason behind this construction is to let feedback controllers work as if the platform is stationary and let decoupling controller undertake the task of overcoming kinematic and geometric coupling effects without a necessity of error. One important aspect to emphasize is that with this construction, workload for command tracking is still on the shoulders of feedback controllers. In addition, decoupling controller does not have any negative effect on closed loop performance of the system unless described disturbances are present.

Decoupling controller utilizes kinematic and dynamic relations presented in Chapter 2 and Chapter 3 to calculate disturbance torques with added condition of LOS stabilization ($\omega_{LOSy} = \omega_{LOSpitch} = 0$ and $\alpha_{LOSyaw} = \alpha_{LOSpitch} = 0$).

For decoupling controller, required body angular velocity and acceleration values can be calculated from measured platform angular motion quantities and gimbal angles using previously given equations (2.33), (2.37) and (2.41).

Disturbance torque values for the decoupling controller can be calculated using equations (3.8) and (3.14) with condition of LOS stabilization ($\omega_{LOSy} = \omega_{LOSpitch} = 0$

and $\alpha_{LOSyaw} = \alpha_{LOSpitch} = 0$) imposed on them for elevation axis and traverse axis respectively;

$$T_{Edist}^{STAB} = J_{Exz}\alpha_{Ex} + \omega_{Ex}J_{Exy}\omega_{Ex} \tag{4.2}$$

$$\begin{aligned} T_{Tdist}^{STAB} &= J_{Txz}\alpha_{Tx} + J_{Tyz}\alpha_{Tz} - \omega_{Tx}\left(J_{Txz}\omega_{Tx} + J_{Txy}\omega_{Ty} + J_{Txz}\omega_{Tz}\right) \\ &+\omega_{Tz}\left(J_{Txx}\omega_{Tx} + J_{Txy}\omega_{Ty} + J_{Txz}\omega_{Tz}\right) \end{aligned} \tag{4.3}$$

$$\begin{aligned} T_{TdistE}^{STAB} &= T_{Ex}^{STAB}\sin\psi + T_{Ey}^{STAB}\cos\psi \\ &= J_{Exx}\alpha_{Ex}\sin\psi + \left(J_{Exy}\alpha_{Ex} - \omega_{Ex}J_{Exz}\omega_{Ex}\right)\cos\psi \end{aligned} \tag{4.4}$$

In addition, decoupling controller should also calculate torque required to overcome kinematic decoupling to render feedback controllers work as if the platform is stationary;

$$T_{\substack{Kinematic \\ Coupling}}^{STAB} = J_{Tyy}\alpha_{Ty} \tag{4.5}$$

Now with all the torque terms are explicitly defined, the required torque values decoupling controller should apply on the system can be summarized as:

$$\begin{aligned} T_{Elv}^{DC} &= T_{Edist}^{STAB} \\ T_{Tra}^{DC} &= T_{Tdist}^{STAB} + T_{TdistE}^{STAB} + T_{\substack{Kinematic \\ Coupling}}^{STAB} \end{aligned} \tag{4.6}$$

A critical point about implementation of the decoupling controller is that the torques generated by it should be fed to the system through the torque output filters in order not to excite high frequency resonances of the system and introduce further noise. Feeding decoupling controller through a filter certainly reduces added disturbance rejection capability to some content, but doing otherwise may result in catastrophic consequences if frequency of excitations from the platform matches the gimbal structural resonance frequencies.

After required equations for decoupling controller are stated and implementation method is explained, the next step is to represent its ability to decouple platform

motion from the gimbal system and let feedback controllers to deal with command tracking only. For this purpose, a square LOS yaw velocity command is given to the system while pitch velocity kept at zero in three different conditions; platform stationary, platform undergoing 1°/2Hz sinusoidal roll motion with decoupling control inactive and the same platform motion with decoupling control active. For all these tests, initial angles of 0° for traverse axis and 45° for elevation are given to induce coupling where platform motion is present.

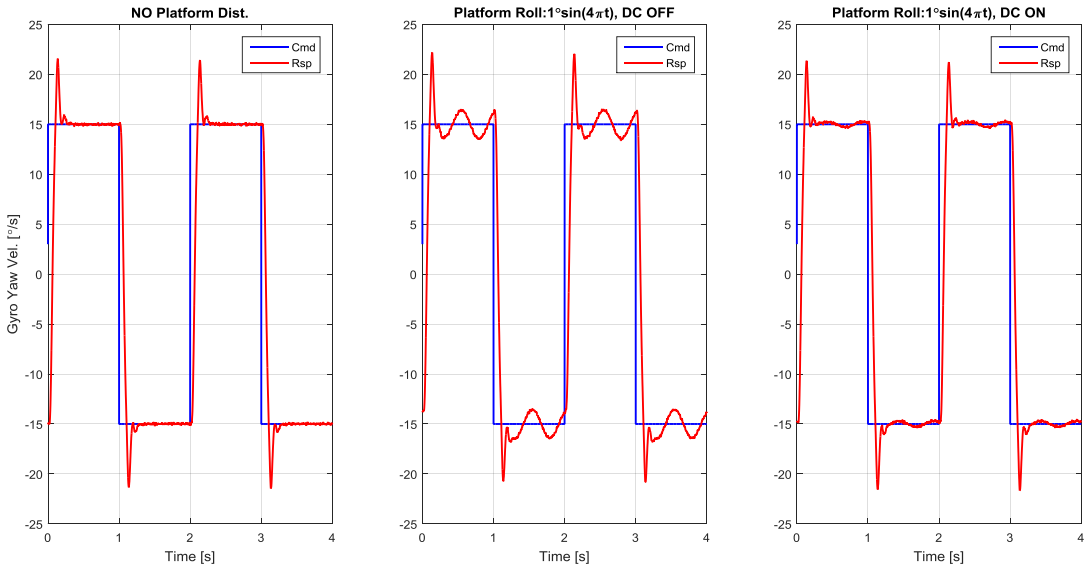

Figure 4-7: Response of system to a square yaw velocity command in three different scenarios

Closed loop responses of the system in three different scenarios are presented in Figure 4-7. The graph on the left hand side is for stationary platform with decoupling control active, and it is clearly visible that response characteristics closely resembles step response given for the system in Chapter 3. The center graph represents the response of the system under platform roll motion and it can be seen that the system considerably fails at producing the same command following characteristics adjusted with tuning of feedback controllers. The graph on the right hand side shows system response under platform roll motion but with addition of decoupling controller. The effect of decoupling controller is evident in this graph since system response is remarkably improved in a way that system is made to behave very similar to the case where platform is stationary. However, not an exact match is obtained which is due to feeding outputs of decoupling controller through

the output filter. Torque signals produced for these three scenarios give additional insight, so they are represented in Figure 4-8.

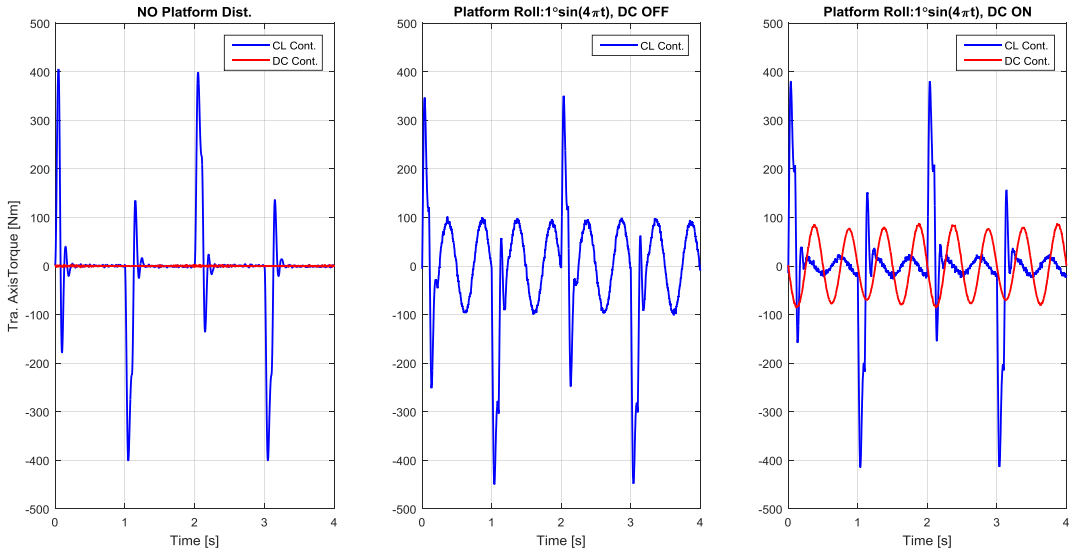

Figure 4-8: Traverse axis torque signals generated by controllers for a square yaw velocity command in three different scenarios

In the first graph given in Figure 4-8, it is seen that decoupling controller is working as intended and it does not produce any torque when platform is stationary. In the second graph, one can observe that under platform disturbance feedback controller produces additional corrective torque but at the expense of increased error as it can be seen in the previous figure. The last graph, shows torques produced by feedback and decoupling controllers. It is evident from this graph that decoupling controller produces only a corrective torque. In addition, feedback controller still seen to be producing a corrective torque in response to error which occurs due to partially decreased disturbance rejection capability of decoupling controller as described previously.

Similar scenarios are also tested in elevation axis; i.e. keeping LOS yaw velocity zero and applying a square command to pitch velocity; with the same angular position initial conditions. But due to absence of kinematic coupling and very low cross axis inertia terms for elevation frame, the resulting disturbance torques acting on this axis are moderately low and have considerably low effect on the axis. So the amplitude of the roll motion for the platform is intensified up to 10 times to obtain a

visible difference in responses. The obtained responses in three different scenarios for elevation axis can be found in Figure 4-9, where benefits of disturbance decoupling controller is again evident but not that much intense as traverse axis.

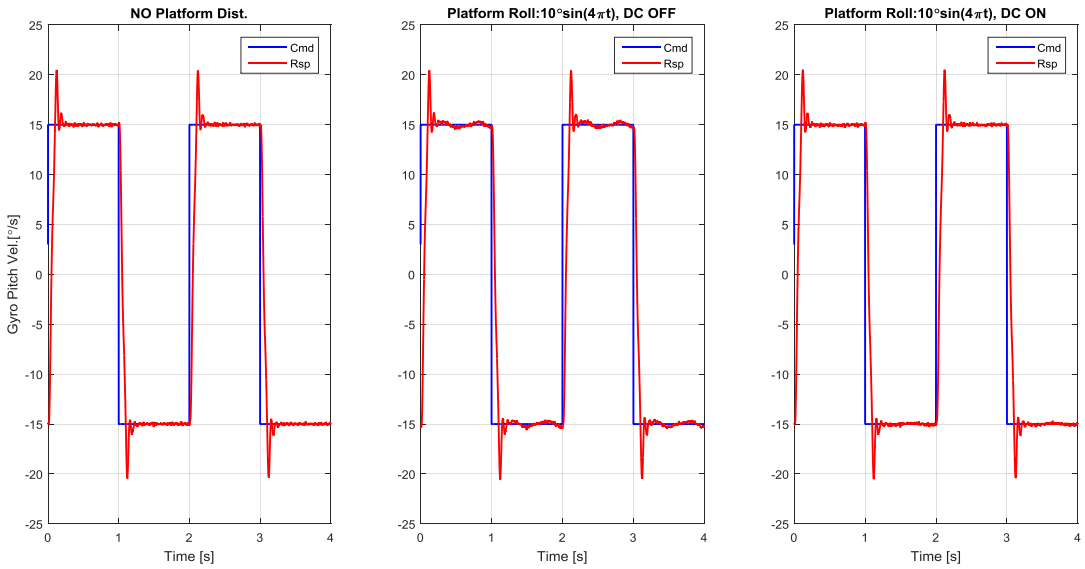

Figure 4-9: Response of system to a square pitch velocity command in three different scenarios

In the light of presented results, it is clear that the task of isolating kinematic and geometric coupling effects of platform motion from feedback controllers is successfully accomplished with devised disturbance decoupling method.

The overall system diagram with feedback controllers and decoupling controller can be found in Figure 4-10. Controllers constructed in MATLAB Simulink are also given in Figure 4-11.

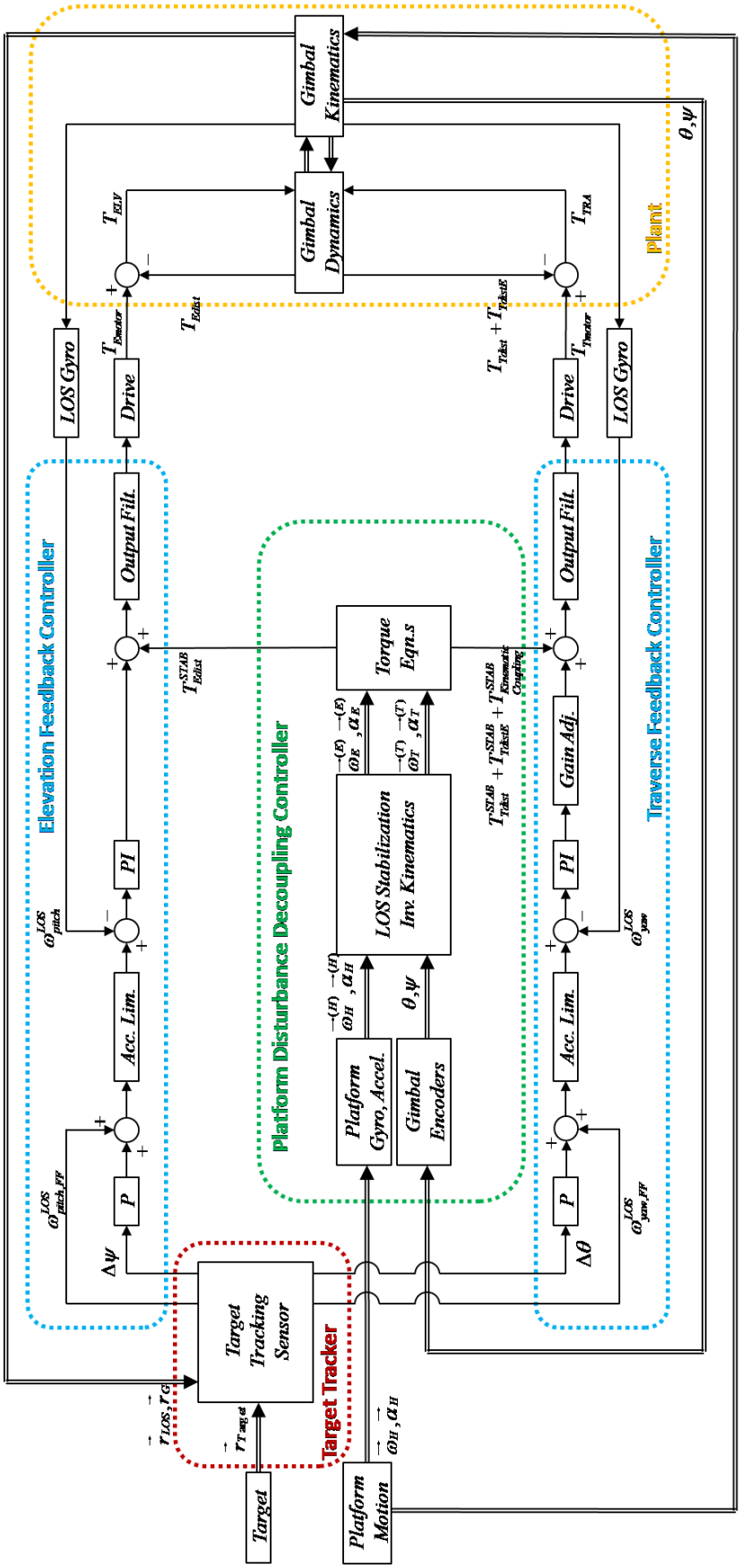

Figure 4-10: Feedback and platform motion decoupling controller in overall system

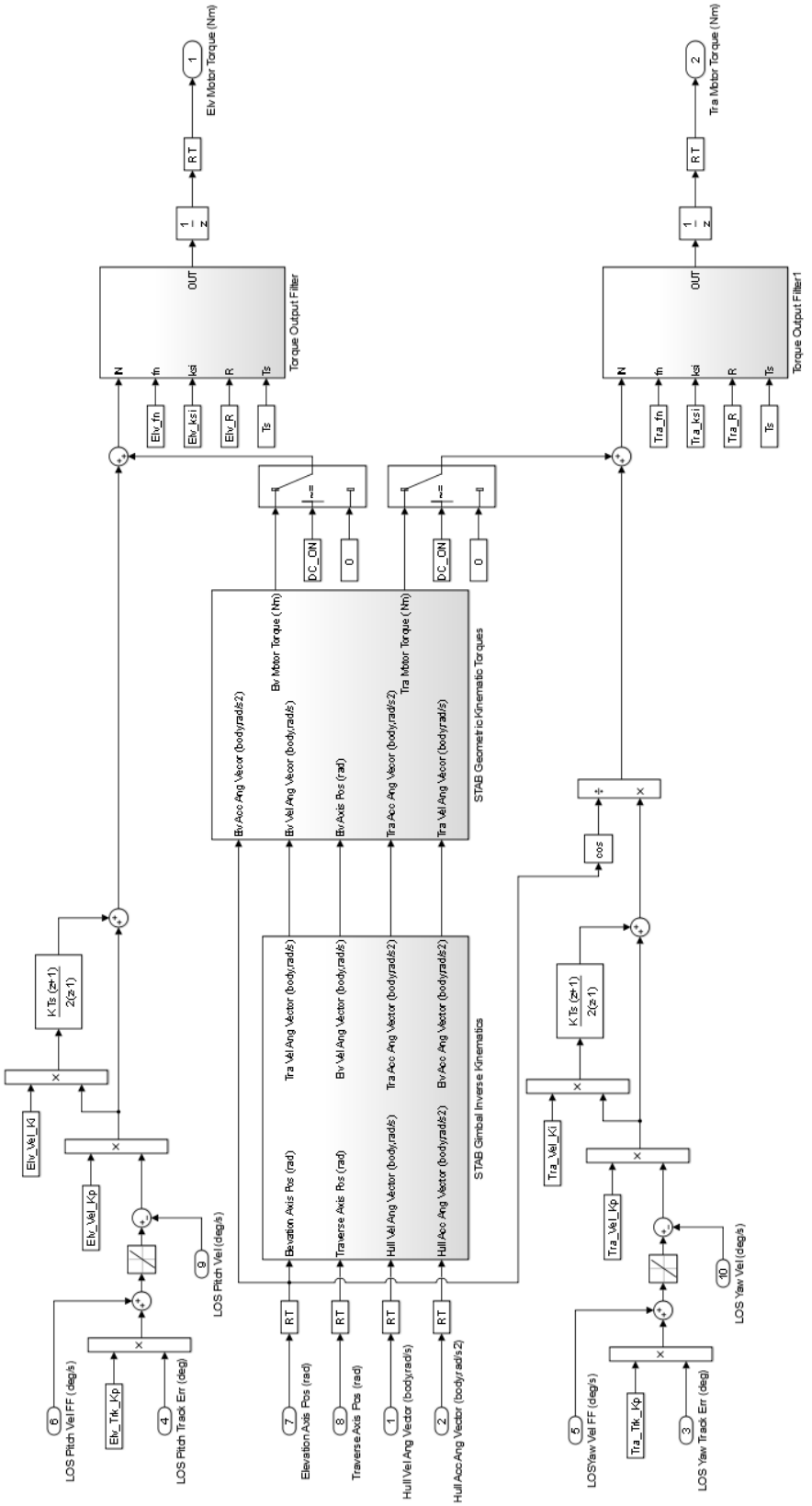

Figure 4-11: Feedback and decoupling controllers constructed in MATLAB Simulink

CHAPTER 5

SYSTEM SIMULATIONS AND RESULTS

5.1. Introduction

In this chapter, system simulations of LOS stabilization and target tracking are presented in order to demonstrate contribution of decoupling controller on system performance. In these simulations, platform angular motion data at different speed levels and sample target trajectory presented in Chapter 2 are applied as simulation inputs. For LOS stabilization simulations, performance criterion is chosen as standard deviation of LOS gyroscope velocity integrals, since this value represents a statistical measure of how much LOS vector deviated from intended orientation. For target tracking tests, standard deviation of tracking error is set as performance criterion similar to stabilization tests.

Before simulations with test data were conducted, two preliminary simulations with sinusoidal platform motion were performed in order to verify the operation of decoupling controller.

The first preliminary simulation was performed with pure sinusoidal roll motion (5°, 1Hz) of the platform while controllers were stabilizing the LOS vector with initial conditions 0° for traverse and 45° for elevation axes. The obtained results with and without decoupling controller can be seen in Figure 5-1.

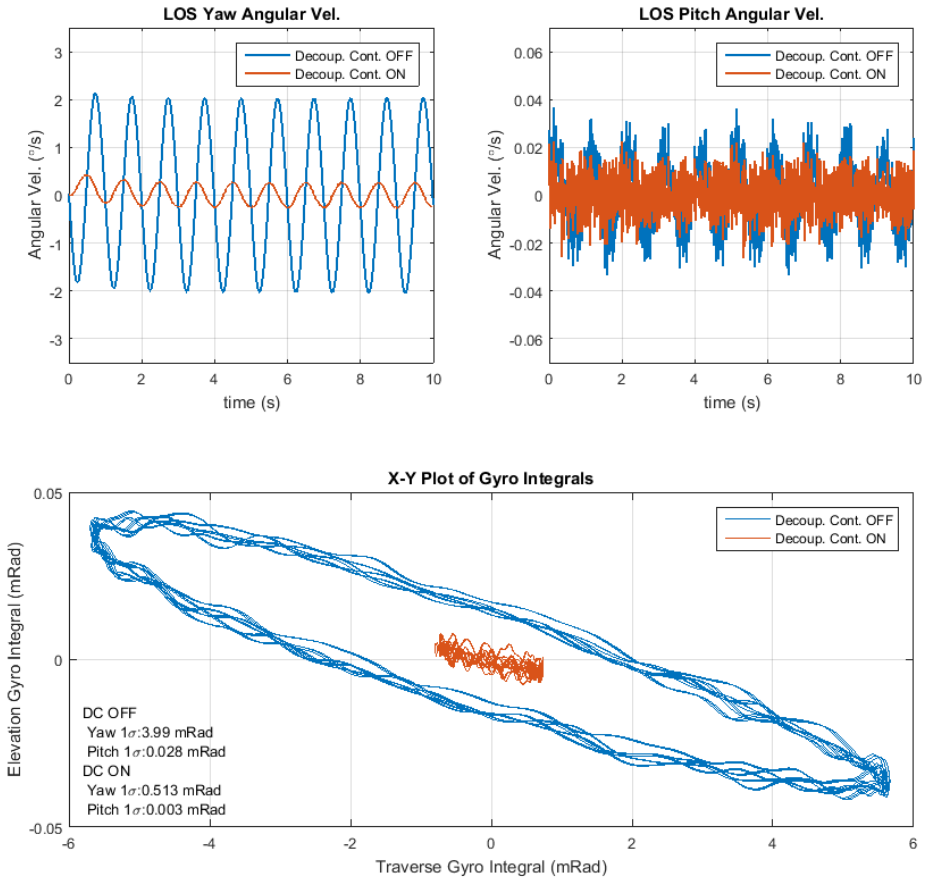

Figure 5-1: Preliminary simulation #1 results, 5°/1Hz sinusoidal platform roll, Tra. I.C.=0°, Elv. I.C.=45°

In the given figure, the effect of decoupling controller can be seen as a decrease in LOS gyro velocity signals. Also, gyro velocity integrals for both axes obtained through time are plotted with respect to each other to represent the deviation of LOS vector. The effect of decoupling controller is more comprehensible in this plot that with the application of decoupling controller LOS vector is managed to stay closer to the center for both axes. One important note about this graph is that aspect ratio is not taken unity. This is due to platform motion having substantially higher effect on traverse axis resulting in worse stabilization performance compared to elevation axis. So the aspect ratio is set accordingly to represent effects in both axes clearly. Another essential point to mention is, due to completely periodic platform motion, gyro integrals are actually banked up to upper left side of the center, but they are shifted to center origin to better represent difference between them.

The second preliminary simulation was performed with a platform motion composed of sinusoidal rotations in all three axes applied in pitch-yaw-roll Euler sequence with values 3°/1Hz for pitch, 1°/0.5Hz for yaw and 2°/1Hz for roll with a 90° phase shift. This time, initial conditions are taken as 90° for traverse and 45° in elevation axes. The result of this simulation can be found in Figure 5-2, where effect of decoupling controller is again very evident and it managed to collect LOS vector error around a center point successfully.

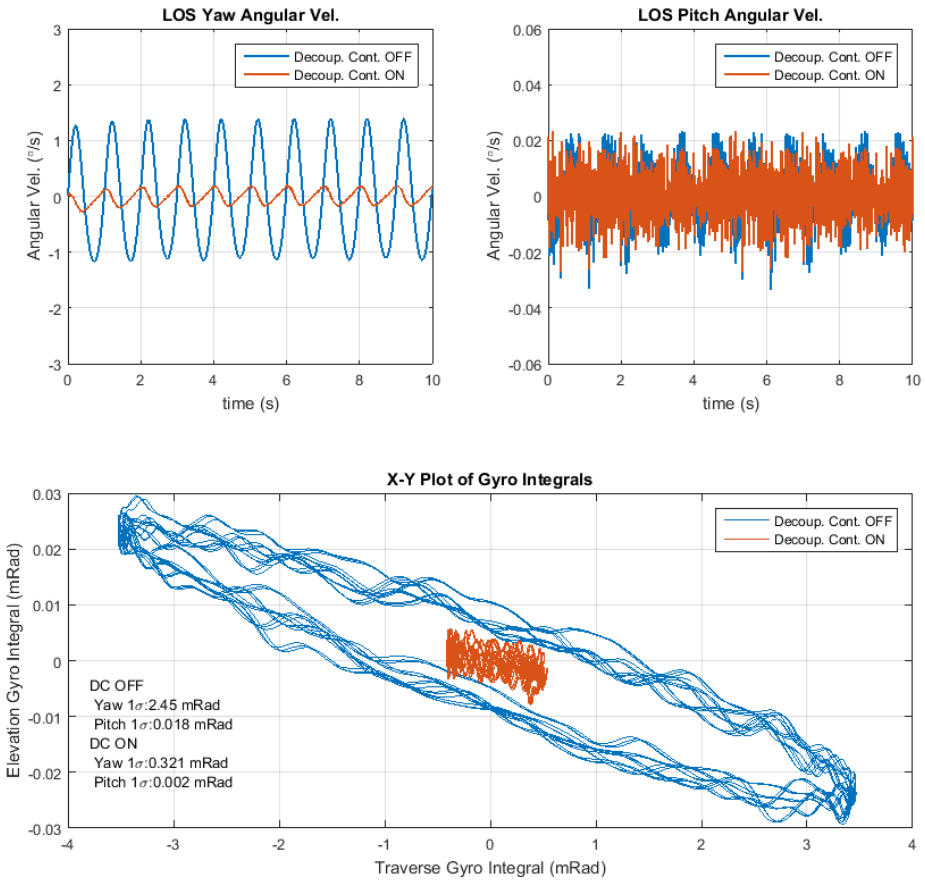

Figure 5-2: Preliminary simulation #2 results, compound sinusoidal platform roll, Tra. I.C.=90°, Elv. I.C.=45°

As the successful operation of decoupling controller was tested with two preliminary simulations, testing the effectiveness of decoupling controller was further continued with real platform data.

5.2. LOS Stabilization Simulation Results

In this section, LOS stabilization simulations performed with platform test data are presented. A considerable number of simulations were performed with different initial conditions given to LOS orientation for all four test data representing different speeds of the vehicle. The initial LOS orientations were selected as 0°, 45°, 90°, 135° and 180° for traverse axis and 15°, 30°, 45°, 60° for elevation axis at every given traverse axis orientation. Including these initial conditions and vehicle data for four different speeds, in total 160 different simulations were run with and without decoupling controller. So, instead of presenting every single result individually, the results were collected into three dimensional bar graphs for the sake of integrity. Later, individual results for the worst cases for traverse axis at different speeds are presented.

In Figure 5-3; simulation results obtained for traverse axis can be seen. Four different three dimensional bar graphs represent different vehicle speed. In the graphs, horizontal axes are for LOS orientation initial conditions and vertical axis is for obtained stabilization error with and without decoupling controller.

In each of the graphs, the effect of coupling torques acting on traverse axis as the elevation axis is raised is clearly visible, stabilization error increases monotonically with the elevation angle. Also, the benefits of the decoupling controller can be seen to boost with increasing coupling effects which verifies the design of the controller. Examining all four graphs revealed that coupling effects also increase with increasing vehicle speed, escalating the demand for decoupling controller. This is the direct consequence of the higher acceleration values observed as the vehicle speed increases (Fig 2-24, 25, 26, 27). Higher accelerations create higher inertial torques in the gimbal system, which makes decoupling controller even more essential. One additional finding is the worsening of coupling effects when gimbal is looking sideways with respect to platform which is due to characteristics of the vehicle motion.

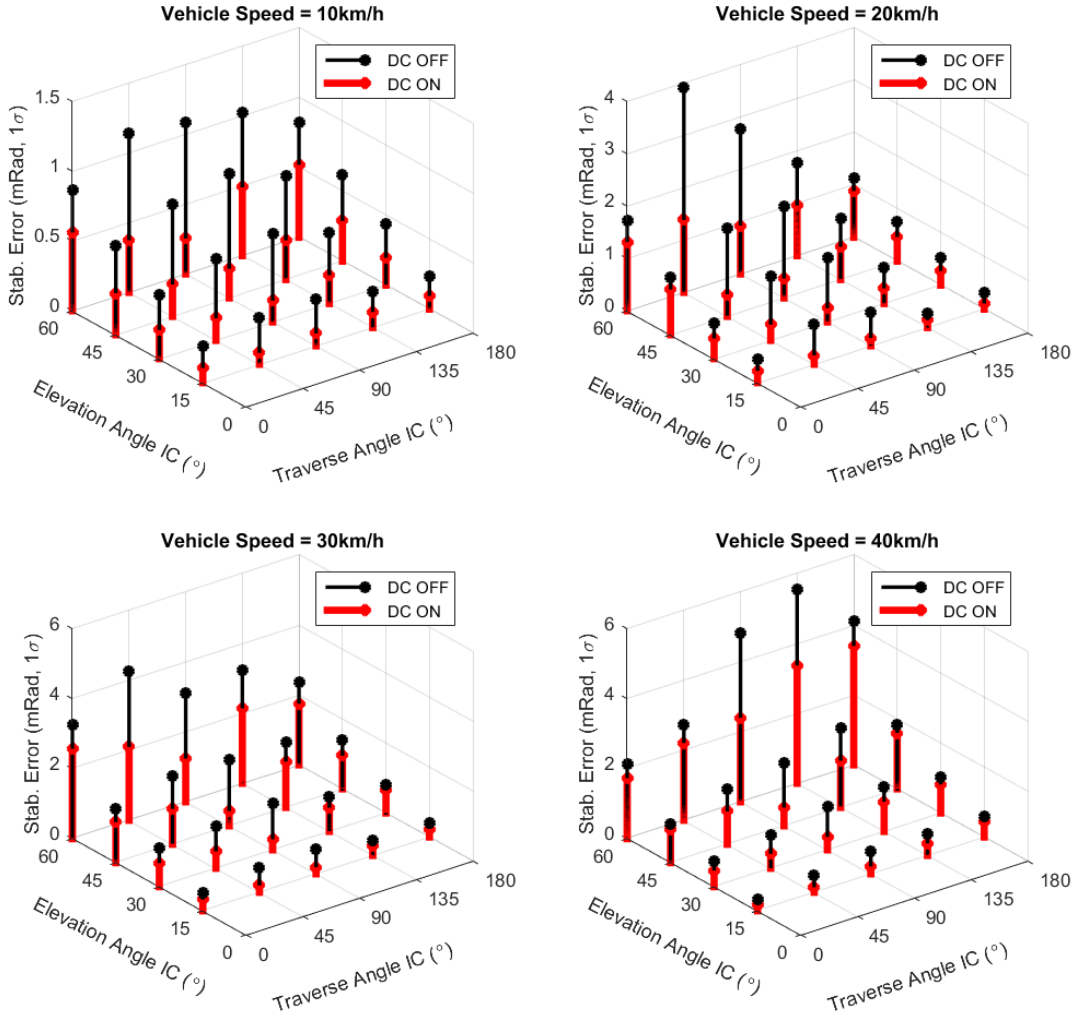

Figure 5-3: LOS stabilization simulation results for traverse axis.

A similar representation of results for elevation axis can be found in Figure 5-4; where it can be seen that decoupling controller has negligible effect as expected. Minute increases of error in elevation axis are due to the fact that with the addition of decoupling controller, traverse axis better performs at keeping up with required motion profiles which in turn increases coupling effect on elevation axis for the same disturbance profile.

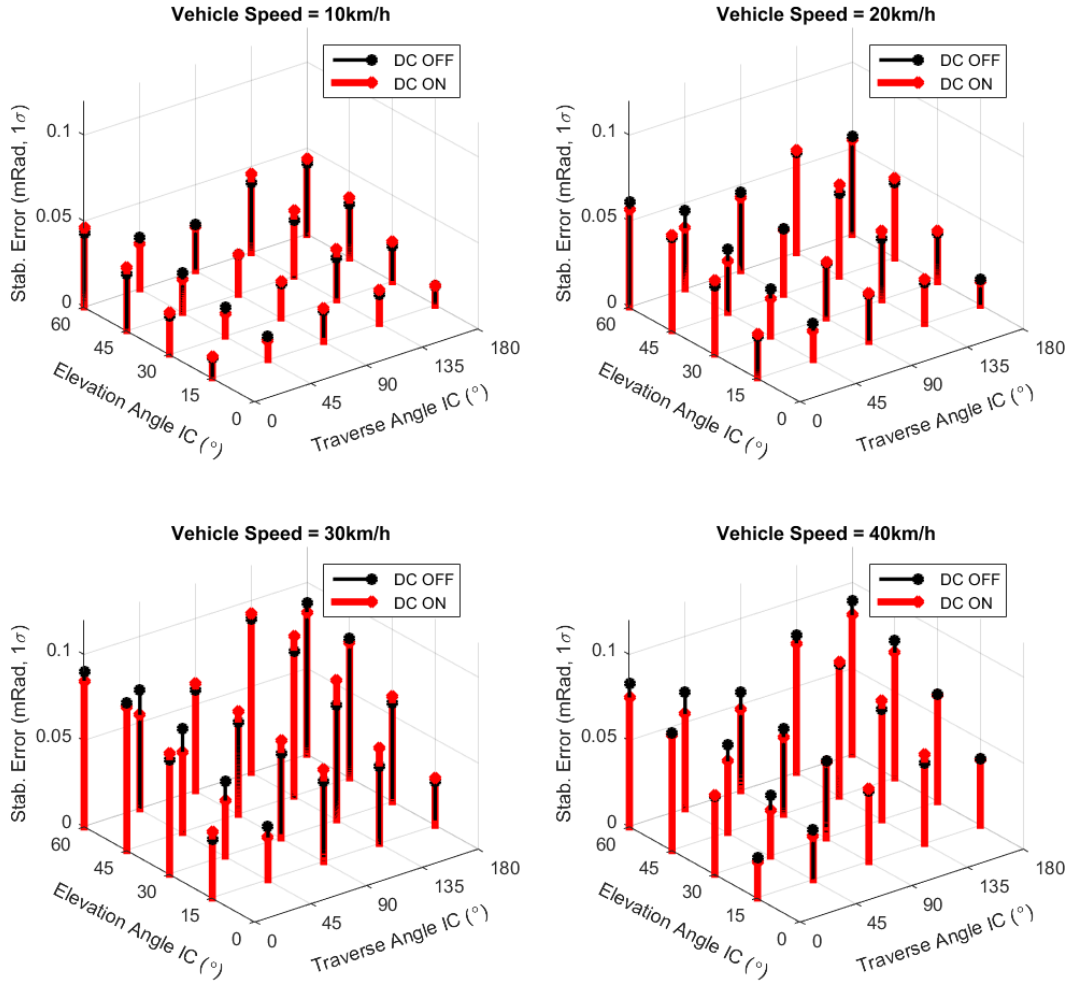

Figure 5-4: LOS stabilization simulation results for elevation axis

The numerical results presented as graphs in Figure 5-3 and Figure 5-4 can also be found in Table 10-1 and Table 10-2.

Table 5–1: Traverse stabilization error (mRad, 1σ) table

VEHICLE SPEED 10 KM/H						Decoupling Control	VEHICLE SPEED 20 KM/H					
Tra IC / Ele IC	0°	45°	90°	135°	180°		0°	45°	90°	135°	180°	Tra IC / Ele IC
15°	0.105	0.081	0.090	0.112	0.095	ON	0.225	0.171	0.150	0.141	0.107	15°
	0.259	0.336	0.333	0.258	0.237	OFF	0.448	0.776	0.636	0.261	0.320	
30°	0.206	0.159	0.153	0.203	0.196	ON	0.387	0.302	0.265	0.291	0.270	30°
	0.456	0.585	0.629	0.512	0.436	OFF	0.677	1.232	1.234	0.691	0.526	
45°	0.298	0.229	0.209	0.282	0.288	ON	0.864	0.422	0.370	0.625	0.464	45°
	0.636	0.801	0.888	0.743	0.623	OFF	1.098	1.692	1.750	1.164	0.754	
60°	0.562	0.374	0.254	0.490	0.519	ON	1.316	1.386	0.926	0.959	0.880	60°
	0.869	1.138	1.089	1.024	0.826	OFF	1.726	3.920	2.775	1.783	1.137	
VEHICLE SPEED 30 KM/H						Decoupling Control	VEHICLE SPEED 40 KM/H					
Tra IC / Ele IC	0°	45°	90°	135°	180°		0°	45°	90°	135°	180°	Tra IC / Ele IC
15°	0.315	0.197	0.187	0.267	0.230	ON	0.170	0.148	0.211	0.344	0.438	15°
	0.508	0.712	0.702	0.438	0.411	OFF	0.338	0.479	0.636	0.626	0.578	
30°	0.678	0.484	0.302	0.675	0.657	ON	0.464	0.411	0.368	0.846	0.814	30°
	1.120	1.197	1.328	0.981	0.802	OFF	0.736	0.941	1.233	1.267	1.035	
45°	1.161	1.010	0.421	1.311	0.949	ON	0.961	0.938	0.519	1.332	1.597	45°
	1.554	1.939	1.892	1.852	1.395	OFF	1.115	1.573	1.807	2.259	1.826	
60°	2.571	2.095	1.237	2.148	1.751	ON	1.728	2.209	2.401	3.374	3.401	60°
	3.262	4.267	3.102	3.239	2.356	OFF	2.139	2.726	4.827	5.559	4.107	

Table 5–2: Elevation stabilization error (mRad, 1σ) table

VEHICLE SPEED 10 KM/H						Decoupling Control	VEHICLE SPEED 20 KM/H					
Tra IC / Ele IC	0°	45°	90°	135°	180°		0°	45°	90°	135°	180°	Tra IC / Ele IC
15°	0.012	0.011	0.019	0.020	0.011	ON	0.025	0.017	0.028	0.026	0.014	15°
	0.012	0.013	0.018	0.017	0.011	OFF	0.024	0.021	0.027	0.024	0.015	
30°	0.024	0.013	0.021	0.029	0.023	ON	0.043	0.022	0.032	0.040	0.029	30°
	0.022	0.017	0.020	0.025	0.021	OFF	0.040	0.028	0.032	0.036	0.028	
45°	0.036	0.019	0.023	0.039	0.035	ON	0.055	0.030	0.038	0.053	0.046	45°
	0.033	0.023	0.023	0.033	0.032	OFF	0.054	0.037	0.038	0.048	0.044	
60°	0.046	0.026	0.026	0.046	0.044	ON	0.057	0.035	0.043	0.060	0.055	60°
	0.043	0.030	0.027	0.041	0.041	OFF	0.061	0.045	0.045	0.058	0.057	
VEHICLE SPEED 30 KM/H						Decoupling Control	VEHICLE SPEED 40 KM/H					
Tra IC / Ele IC	0°	45°	90°	135°	180°		0°	45°	90°	135°	180°	Tra IC / Ele IC
15°	0.038	0.025	0.054	0.055	0.027	ON	0.021	0.026	0.043	0.051	0.038	15°
	0.034	0.031	0.047	0.045	0.025	OFF	0.023	0.029	0.041	0.047	0.039	
30°	0.070	0.032	0.057	0.081	0.061	ON	0.046	0.027	0.044	0.069	0.061	30°
	0.066	0.043	0.049	0.066	0.057	OFF	0.045	0.036	0.045	0.064	0.062	
45°	0.083	0.047	0.060	0.093	0.079	ON	0.067	0.041	0.045	0.078	0.073	45°
	0.086	0.060	0.053	0.084	0.081	OFF	0.068	0.051	0.050	0.077	0.080	
60°	0.085	0.054	0.062	0.092	0.082	ON	0.075	0.055	0.047	0.075	0.081	60°
	0.090	0.069	0.059	0.089	0.088	OFF	0.083	0.068	0.057	0.080	0.089	

In Figure 5-3; worst conditions for traverse axis can be seen to occur at:

- Traverse I.C.=45°, Elevation I.C.=60° for 10 km/h vehicle speed
- Traverse I.C.=45°, Elevation I.C.=60° for 20 km/h vehicle speed
- Traverse I.C.=45°, Elevation I.C.=60° for 30 km/h vehicle speed
- Traverse I.C.=135°, Elevation I.C.=60° for 40 km/h vehicle speed

The individual results for these conditions are presented in Figure 5-4, Figure 5-5, Figure 5-6 and Figure 5-7 where effect of decoupling controller can further be seen on keeping the LOS orientation.

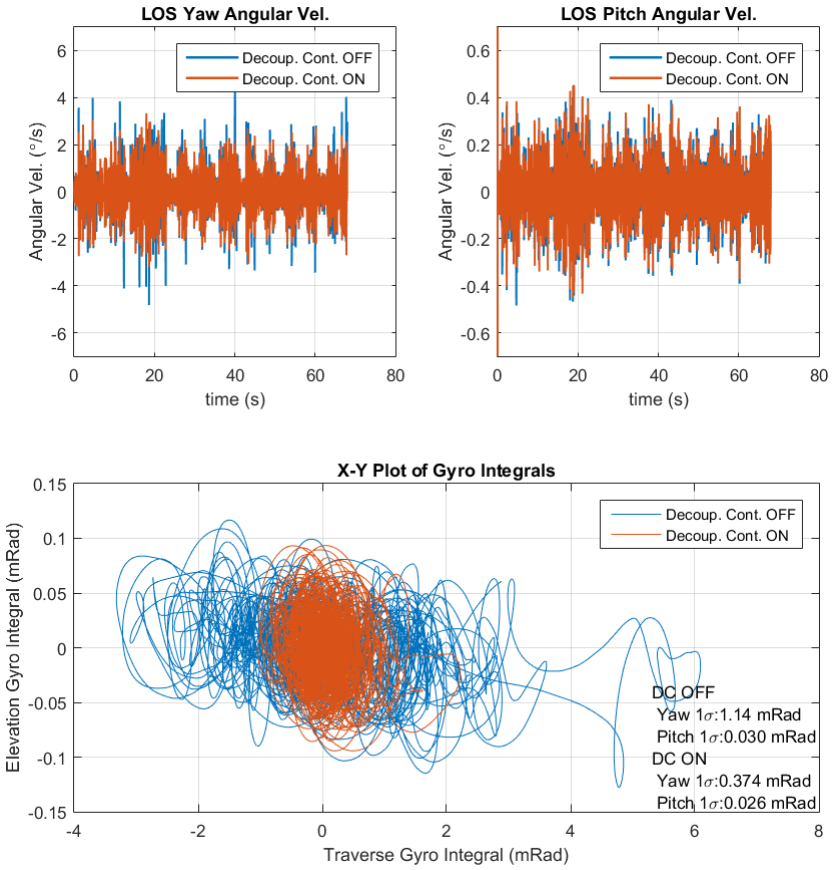

Figure 5-5: LOS stabilization simulation result, worst case in 10 km/h vehicle speed

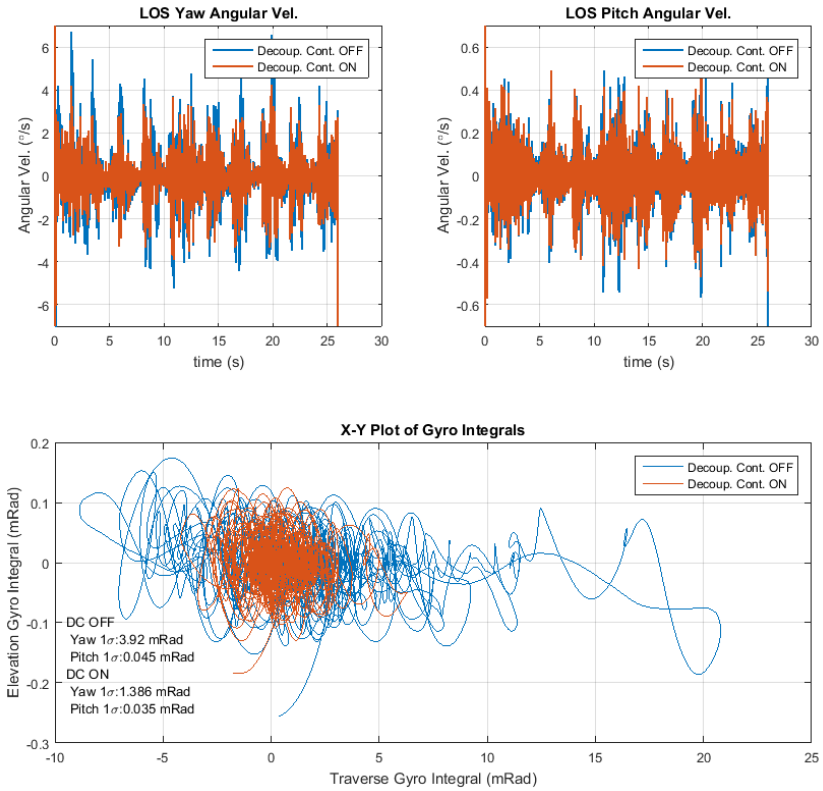

Figure 5-6: LOS stabilization simulation result, worst case in 20 km/h vehicle speed

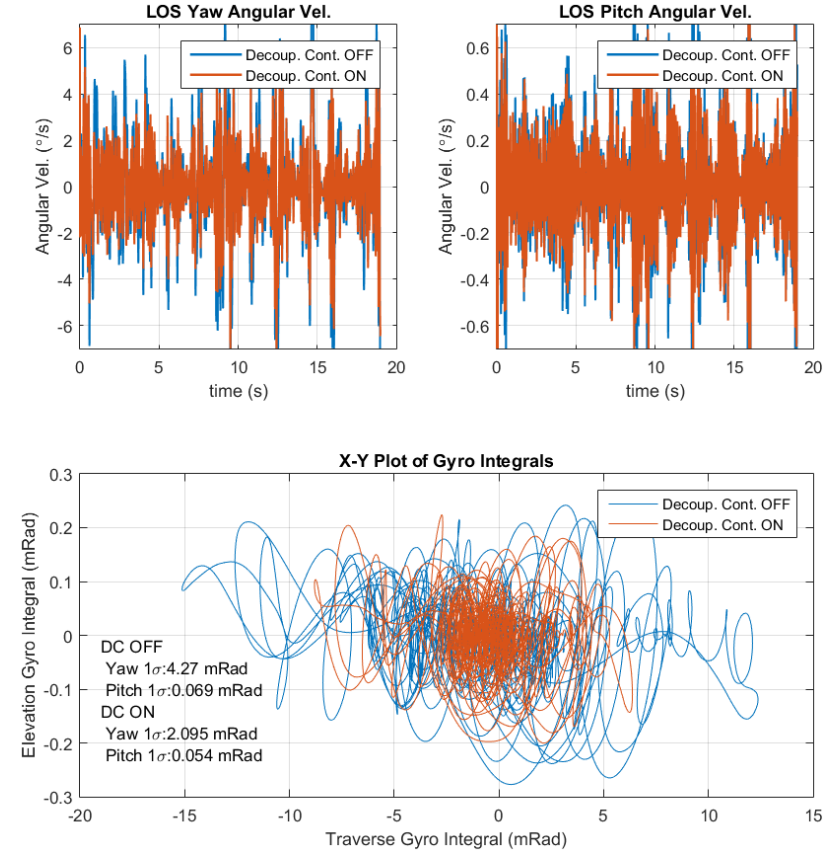

Figure 5-7: LOS stabilization simulation result, worst case in 30 km/h vehicle speed

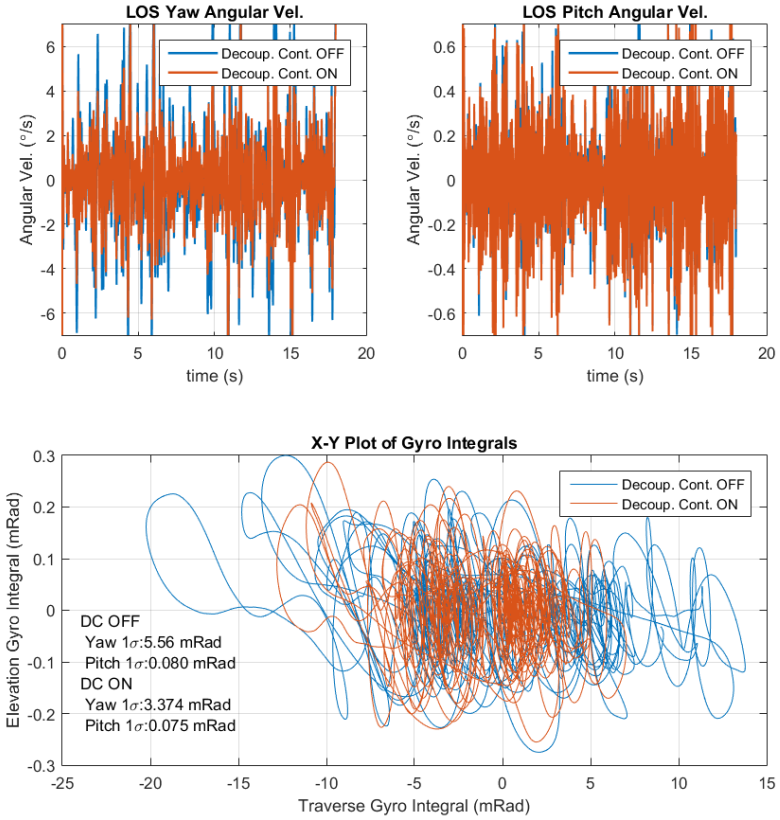

Figure 5-8: LOS stabilization simulation result, worst case in 40 km/h vehicle speed

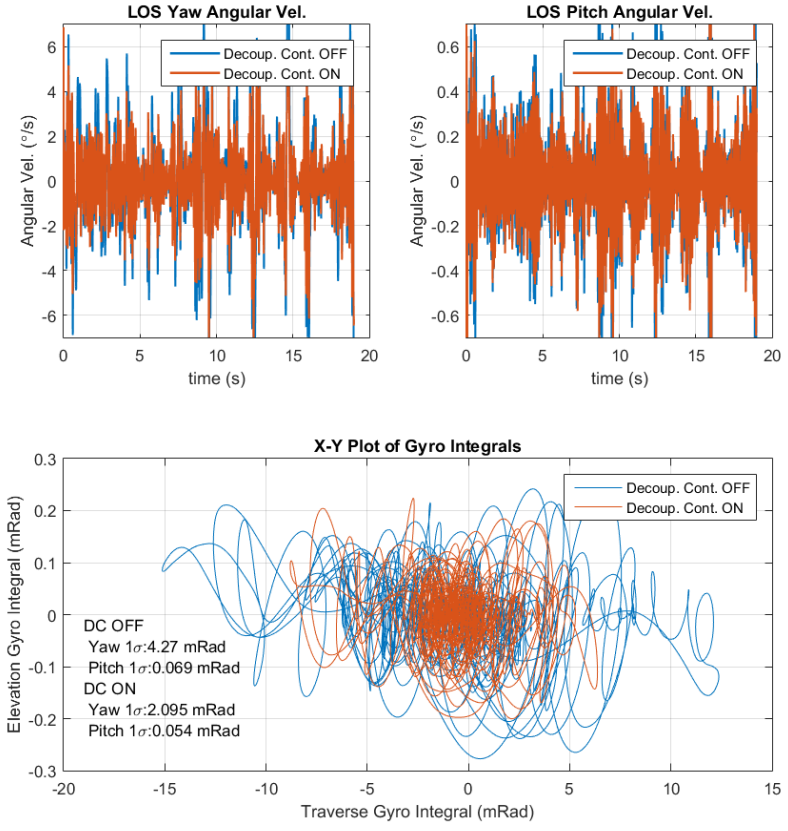

Figure 5-9: LOS stabilization simulation result, worst case in 30 km/h vehicle speed

5.3. Target Tracking Simulation Results

In this section, target tracking simulations performed with platform test data are presented. In the previous section it was found that stabilization performance worsens as gimbal is looking sideways with respect to vehicle, thus the sample target trajectory is modified as if the target is flying sideways to the vehicle while keeping same vertical distances and target speed. This is done to better elaborate effect of decoupling controller on target tracking. The result of target tracking simulations with different vehicle speeds can be found in Table 5-3.

Table 5–3: Target tracking error (mRad, 1σ) table

AXIS	VEHICLE SPEED				Decoupling Control
	10 KM/H	20 KM/H	30 KM/H	40 KM/H	
Traverse	0.208	0.439	0.597	0.699	ON
	0.350	0.965	1.245	1.313	OFF
Elevation	0.025	0.051	0.085	0.081	ON
	0.024	0.052	0.077	0.077	OFF

As can be seen in the given table, the performance increase with decoupling controller is obvious in traverse axis, but decoupling action caused negligible increases in three different situations and again a negligible decrease in one situation. This result is expected for elevation axis in the light of LOS stabilization simulations. Individual graphs representing performance of decoupling controller on target tracking at different vehicle speeds are given in Figure 5-10, Figure 5-11, Figure 5-12 and Figure 5-13. In these figures, one can see how decoupling controller managed to compress tracking errors into smaller profiles.

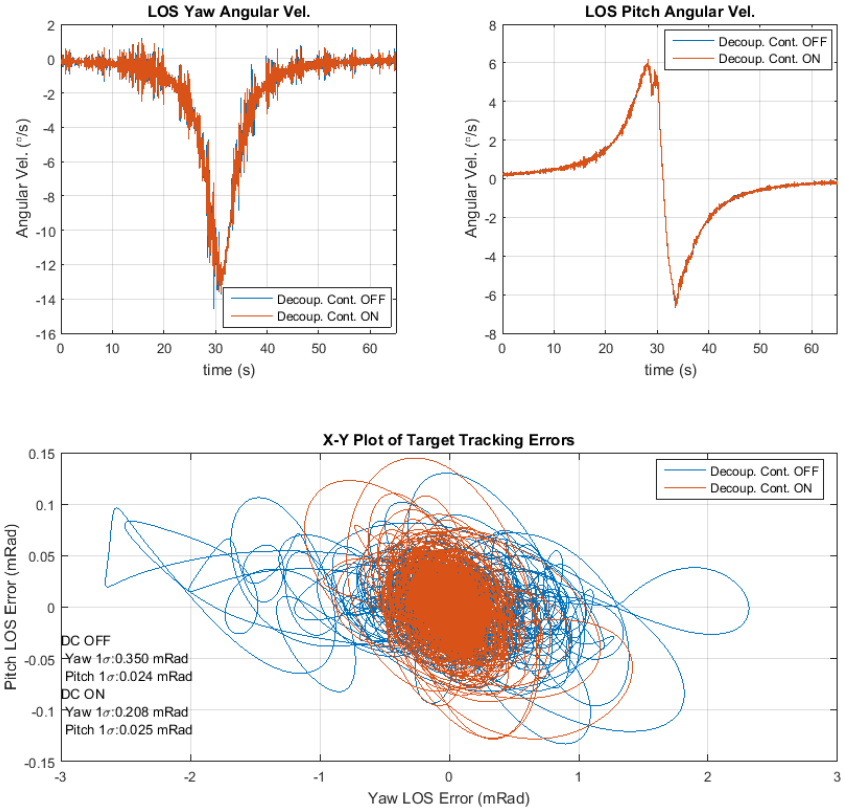

Figure 5-10: Target tracking simulation result for 10 km/h vehicle speed

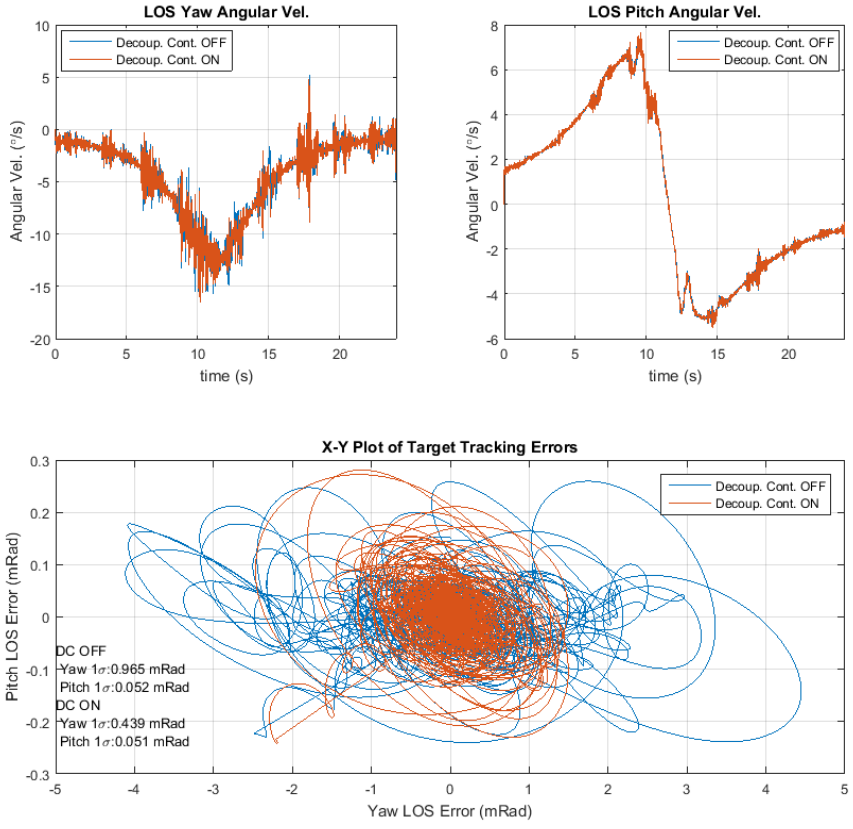

Figure 5-11: Target tracking simulation result for 20 km/h vehicle speed

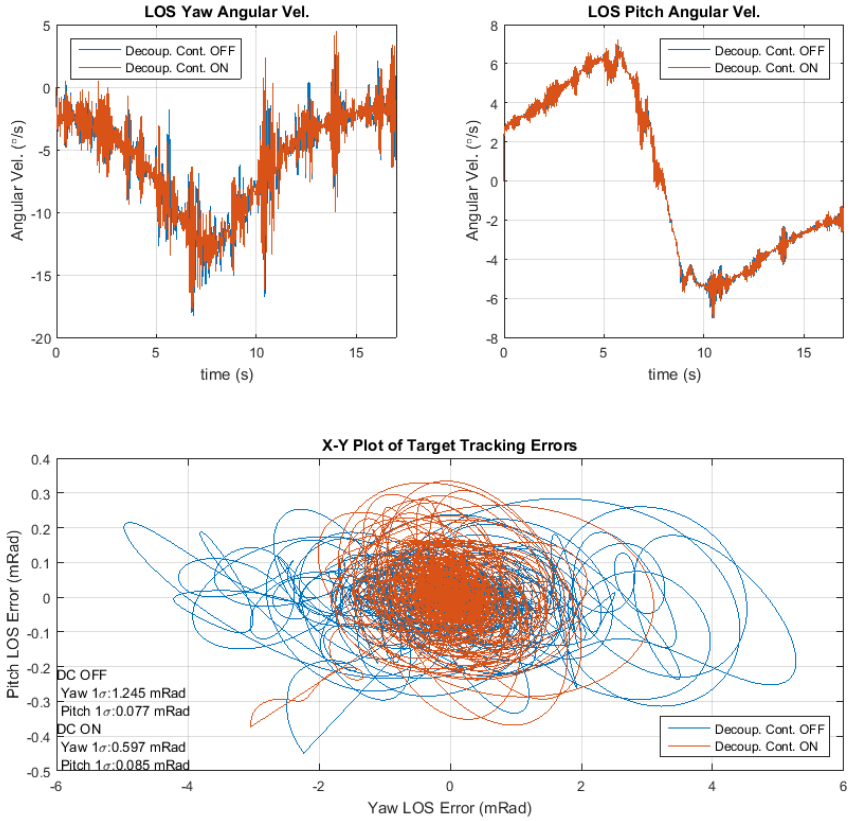

Figure 5-12: Target tracking simulation result for 30 km/h vehicle speed

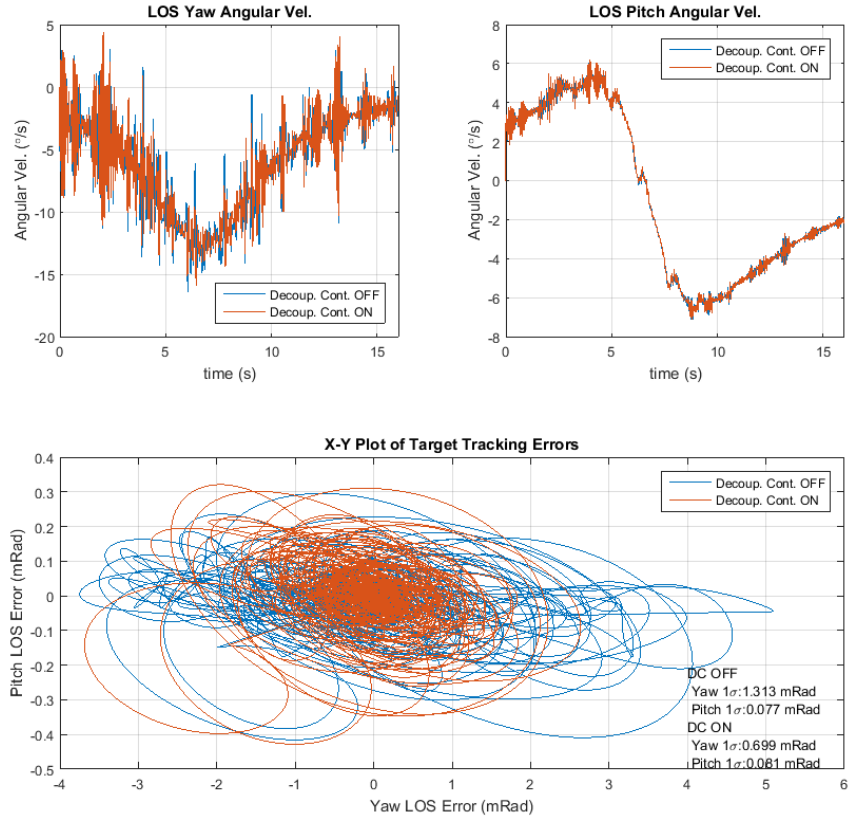

Figure 5-13: Target tracking simulation result for 40 km/h vehicle speed

CHAPTER 6

SUMMARY AND CONCLUSIONS

This study is concentrated on developing a complete direct control method to overcome kinematic and geometric coupling effects acting on a motion stabilized target tracking gimbal assembly. Backbone of the constructed decoupling controller is calculating torque requirements through nonlinear kinematic and dynamic equations using outputs of inertial sensors placed on platform and relative angle sensors on gimbal assembly. The objective behind conducted work is to increase overall performance of the system through increased stabilization and target tracking accuracy in the event of platform motion.

6.1. Summary

In the first step of the study, complete set of angular kinematic relations for the two axis gimbal system is derived. LOS stabilization is imposed on the system as additional kinematic constraints over platform motion and obtained equations are solved accordingly to obtain body angular velocity and acceleration components of gimbal frames for utilization in decoupling controller. A complete and a simplified representations of kinematic coupling acceleration requirement are presented which demonstrate asymptotical increase in torque requirement in outer gimbal axis as system approaches gimbal lock condition. In addition, kinematic relations regarding target tracking and resolution of platform motion over gimbal axis angles are also included in the study as they are indispensable for conducting system simulations. Additional sensor requirements for obtaining full angular kinematic state of the system are also stated with methods on calculating required kinematic quantities. These additional sensors are chosen to be placed on platform, since required torque values are to be calculated for an ideally operating gimbal assembly and later be fed to the system in order to make it behave likewise in a similar manner to command feed forward control method.

After kinematic relations are obtained, the next step is to obtain governing dynamic relations of the system which is accomplished by utilizing Euler equations for both gimbal bodies. Through these equations and torque interactions between bodies, geometric coupling torques acting on the system are identified in terms of body angular kinematic quantities. A two axis gimbal model is constructed based on derived equations which represent coupled behavior of the two axis gimbal system. An additional system identification process in frequency domain is included in order to match forward torque path dynamics of the real system and constructed model which is essential in this study, since such dynamics play a critical role in obtainable disturbance rejection characteristics.

Kinematic and dynamic relations in hand, the next step is to construct a control method to decouple described kinematic and geometric coupling effects. The decoupling controller is constructed as to calculate torque values required to overcome coupling effects when platform undergoes an angular motion. The idea behind this construction is to aid existing feedback controllers by supplying system with additional torque values required to overcome coupling effects without the need of error accumulation in control outputs. This way of overcoming disturbances without allowing error accumulation undoubtedly improves overall disturbance rejection characteristics when compared to a system solely depending on error based controllers. Decoupling controller is constructed as to calculate additional torque requirements only in the state of LOS stabilization, and the purpose of this construction is to supply feedback controllers a working environment as if the platform is stationary. In other words, disturbances due to coupling effects originated from platform motion are overcome by decoupling controller, and rest of the command tracking workload is left to feedback controllers. One important aspect to emphasize about implementation of the decoupling controller is its outputs being fed to the system through torque output filters which reduces its performance but is necessary in order not to excite resonances of the system.

The final step of this study is to elaborate effectiveness of developed decoupling controller through simulations. Developed method is tested under a high number of scenarios incorporating both LOS stabilization and target tracking. In these

scenarios, artificial and realistic platform motion are fed to the system and LOS stabilization and target tracking accuracy values obtainable at different scenarios are examined. In all these different simulations, decoupling controller is found to improve overall system performance in different proportions as scenarios change.

6.2. Conclusions

Main challenge in this study is to construct a well defined method to obtain required kinematic components for producing required corrective action which is accomplished by inverse solution of governing nonlinear kinematic equations with LOS stabilization constraint. The calculation of required torque values in order to cancel out coupling effects is rather a more straightforward process of carefully identifying each disturbance torque in Euler equations.

After decoupling controller is constructed and tested with simulations, considerable performance improvements are found in a number of different scenarios which justifies the aim of this work and paves the way for actual system implementation and extensive field testing. The amount of work devoted to obtain a realistic model and obtained results combined together also gives hope that actual system implementation may be a smooth transition from simulation environment to real life and not be a problematic process.

Although a direct method to calculate coupling effects is developed, the method's performance is degraded by utilized torque output filters as expected, which cannot be altered unless a method of applying exact corrective action without exciting structural resonances is further developed. However satisfactory results are obtained when compared to a system solely depending on performance of feedback controllers.

Another conclusion made in this study is that amount of coupling effects acting on different axes strictly depend on used gimbal configuration and mass properties of gimbal frames. However, simplifications are avoided in the design process in order to constitute a generic method in order to alleviate future applications of developed method in different systems.

6.3. Future Work and Recommendations

The most essential future work for this study is to conduct a real system implementation and perform tests to evaluate realistic performance of the developed method as also mentioned in previous section.

Another future work awaiting to be done is to find a method to enhance performance of developed method by eliminating output filters on corrective action paths as also stated in conclusions section.

One another future work that can be performed is to extend developed method to command tracking since most of the required governing equations are derived already for the presented method. One challenge in such a work is to estimate LOS angular acceleration and velocity requirements from given two axis velocity commands.

REFERENCES

[1] P. J. Kennedy and R. L. Kennedy, “Direct versus indirect line of sight (LOS) stabilization,” *IEEE Trans. Control Syst. Technol.*, vol. 11, no. 1, pp. 3–15, 2003.

[2] J. M. Hilkert, “Inertially stabilized platform technology: Concepts and principles,” *IEEE Control Syst. Mag.*, vol. 28, no. 1, pp. 26–46, 2008.

[3] A. K. Rue, “Precision Stabilization Systems,” *IEEE Trans. Aerosp. Electron. Syst.*, vol. AES-10, no. 1, pp. 34–42, 1974.

[4] S. Yoon and J. B. Lundberg, “Equations of motion for a two-axes gimbal system,” *IEEE Trans. Aerosp. Electron. Syst.*, vol. 37, no. 3, pp. 1083–1091, 2001.

[5] J. M. Hilkert, “Kinematic algorithms for line-of-sight pointing and scanning using INS/GPS position and velocity information,” *Proc. SPIE*, vol. 5810, pp. 11–22, 2005.

[6] K. L. Sorensen, W. Singhose, and S. Dickerson, “A controller enabling precise positioning and sway reduction in bridge and gantry cranes,” *Control Eng. Pract.*, vol. 15, no. 7, pp. 825–837, Jul. 2007.

[7] Y. Han, Y. Lu, and H. Qiu, “An Improved Control Scheme of Gyro Stabilization Electro-Optical Platform,” *2007 IEEE Int. Conf. Control Autom.*, vol. 00, pp. 346–351, 2007.

[8] M. K. Masten, “Inertially stabilized platforms for optical imaging systems,” *IEEE Control Syst. Mag.*, vol. 28, no. 1, pp. 47–64, 2008.

[9] J. M. Hilkert and B. Pautler, “A reduced-order disturbance observer applied to inertially stabilized Line-of-Sight control,” *Proc. SPIE*, vol. 8052, pp. 1–12, 2011.

[10] Q. Zhang, Z. Tan, and Y. Liang, “Gyro Stabilized System Based on Auto-Disturbance Rejection Controller,” *2008 Isecs Int. Colloq. Comput. Commun. Control. Manag. Vol 2, Proc.*, vol. 11, no. 2, pp. 34–38, 2008.

[11] J. M. Hilkert and D. A. Hullender, “Adaptive control system techniques applied to inertial stabilization systems,” *Proc. SPIE*, vol. 1304, pp. 190–206, 1990.

[12] C. Perez and F. R. Rubio, “Implementation of an Inertial Controller for a 2 DOF platform,” *Proc. 2001 IEEE Int. Conf. Control Appl.*, pp. 668–673, 2001.

[13] A. P. Trueba and J. R. L. García, “Nonlinear Optimal Line-Of-Sight Stabilization with Fuzzy Gain-Scheduling,” *World Acad. Sci. Eng. Technol. Int. J. Comput. Electr. Autom. Control Inf. Eng.*, vol. 5, no. 8, pp. 807–814, 2011.

[14] “Selex SASS.” [Online]. Available: http://www.selex-es.com/-/sass. [Accessed: 08-May-2015].

[15] “Sea Zenith CIWS.” [Online]. Available : http://www.buquesdeguerra.com/en/photo-gallery/equipos-armas-ciws-sea-zenith/ciws-sea-zenith-913.html. [Accessed: 15-Jun-2015].

[16] J. M. Hilkert and M. Jonas, “A unique three-axis gimbal mechanism,” *Proc. SPIE*, vol. 6971, pp. 69710E(1–8), 2008.

[17] W. J. Bigley and F. Schupan, “Wideband Base Motion Isolation Control for a Mobile Platform,” *Proc. Am. Control Conf.*, pp. 1483–1490, 1987.

[18] X. Zhou, G. Gong, J. Li, H. Zhang, and R. Yu, “Decoupling control for a three-axis inertially stabilized platform used for aerial remote sensing,” *Trans. Inst. Meas. Control*, vol. 37, no. 9, pp. 1135–1145, 2015.

[19] X. Zhou, H. Zhang, and R. Yu, “Decoupling control for two-axis inertially stabilized platform based on an inverse system and internal model control,” *Mechatronics*, vol. 24, no. 8, pp. 1203–1213, 2014.

[20] Z. M. Zhao, X. Y. Yuan, Y. Guo, F. Xu, and Z. G. Li, “Modelling and simulation of a two-axis tracking system,” *Proc. Inst. Mech. Eng. Part I J. Syst. Control Eng.*, vol. 224, no. 2, pp. 125–137, 2010.

[21] V. Sangveraphunsiri and K. Malithong, “Control of Inertial Stabilization

Systems Using Robust Inverse Dynamics Control and Sliding Mode Control," in *The 6th International Conference on Automotive Engineering (ICAE-6)*, 2010, pp. 1–10.

[22] S. J. Ovaska and S. Väliviita, "Angular acceleration measurement: a review," *IEEE Trans. Instrum. Meas.*, vol. 47, no. 5, pp. 875–880, 1998.

[23] T. R. Williams, D. W. Raboud, and K. R. Fyfe, "Minimal Spatial Accelerometer Configurations," *J. Dyn. Syst. Meas. Control*, vol. 135, no. 2, p. 021016, Feb. 2013.

[24] P. Cardou and J. Angeles, "Linear Estimation of the Rigid-Body Acceleration Field From Point-Acceleration Measurements," *J. Dyn. Syst. Meas. Control*, vol. 131, no. 4, p. 041013 (1–10), 2009.

[25] P. D. Groves, *Principles of GNSS, Inertial, and Multisensor Integrated Navigation Systems*, First Edit. Artech House, 2008.

[26] J. H. Ginsberg, *Advanced engineering dynamics*, Second. Cambridge University Press, 1998.

[27] H. Yang, Y. Zhao, M. Li, and F. Wu, "The Static Unbalance Analysis and Its Measurement System For Gimbals Axes of an Inertial Stabilization Platform," *Metrol. Meas. Syst.*, vol. 22, no. 1, pp. 51–68, Jan. 2015.

[28] D. R. Otlowski, K. Wiener, and B. a. Rathbun, "Mass properties factors in achieving stable imagery from a gimbal mounted camera," in *Proceedings of SPIE*, 2008, vol. 6946, pp. 69460B(1–13).

[29] Ö. Gökhan, "System Identification and Modeling of Gyro-Stabilized IR/EO Gimbal System in Frequency Domain," Middle East Technical University, 2014.

[30] G. Ellis and R. D. Lorenz, "Comparison of motion control loops for industrial applications," in *Conference Record of the 1999 IEEE Industry Applications Conference. Thirty-Forth IAS Annual Meeting (Cat. No.99CH36370)*, 1999, vol. 4, pp. 2599–2605.

[31] G. Ellis and R. D. Lorenz, "Resonant load control methods for industrial servo drives," *Conf. Rec. 2000 IEEE Ind. Appl. Conf.*, vol. 3, pp. 1438–1445, 2000.

APPENDICES

A.1. VRML Model to Animate Simulations

An animation model is constructed using MATLAB Simulink 3D Animation to further visualize results given in Chapter 5. The embedded virtual reality modeling language file is constructed as a modification performed for camera placements, zoom adjustment and environment variables on readily available "Plane Take-Off" example which is a copyrighted product of Humusoft S.r.o. and The MathWorks Inc. Overview of the model can be seen in Figure A-1 and a screenshot for the animation can be seen in Figure A-2.

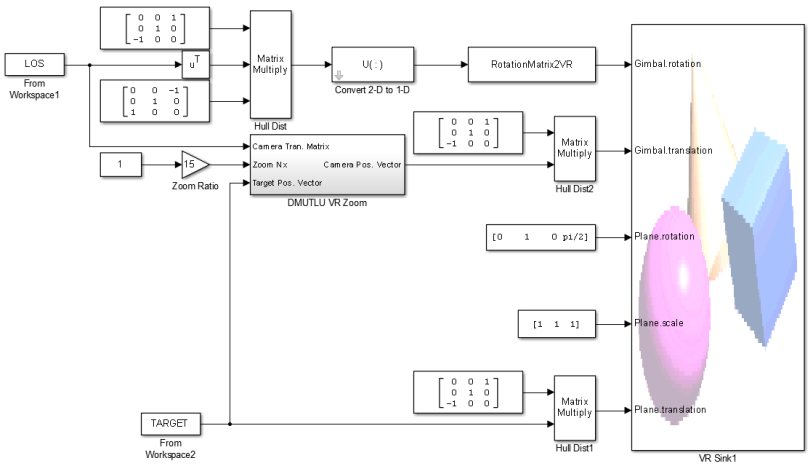

Figure A-1: Overview of animation model constructed in MATLAB Simulink

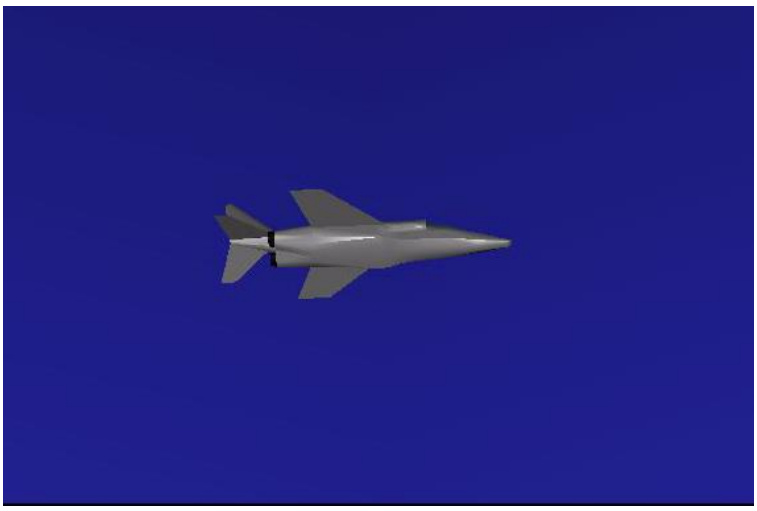

Figure A-2: A screenshot from simulation result animations